Electrochemical Energy Reviews (2024) 7:3
https://doi.org/10.1007/s41918-023-00196-4

REVIEW ARTICLE

Research Progress on the Solid Electrolyte of Solid-State Sodium-Ion Batteries

Shuzhi Zhao[1] · Haiying Che[2] · Suli Chen[3] · Haixiang Tao[2] · Jianping Liao[2] · Xiao-Zhen Liao[1] · Zi-Feng Ma[1,4]

Received: 16 April 2022 / Revised: 7 January 2023 / Accepted: 29 June 2023

Abstract

Because sodium-ion batteries are relatively inexpensive, they have gained significant traction as large-scale energy storage devices instead of lithium-ion batteries in recent years. However, sodium-ion batteries have a lower energy density than lithium-ion batteries because sodium-ion batteries have not been as well developed as lithium-ion batteries. Solid-state batteries using solid electrolytes have a higher energy density than liquid batteries in regard to applications with sodium-ion batteries, making them more suitable for energy storage systems than liquid batteries. Due to their low ionic conductivity, solid electrolytes are currently unable to achieve comparable performance to liquid electrolytes at room temperature. In this review, we discuss the advancements in SSEs applied to sodium-ion batteries in recent years, including inorganic solid electrolytes, such as Na–β-Al_2O_3, NASICON and Na_3PS_4, polymer solid electrolytes based on PEO, PVDF-HFP and PAN, and plastic crystal solid electrolytes mainly composed of succinonitrile. Additionally, appropriate solutions for low ionic conductivity, a narrow electrochemical stability window and poor contact with electrodes, which are the significant flaws in current SSEs, are discussed in this review.

Keywords Energy storage · Sodium-ion batteries · Solid-state electrolyte · Ionic conductivity · Electrochemical stability window

1 Introduction

In recent years, renewable energy issues have been raised because of the well-known limitations of fossil fuels. Thus, it is imperative to develop green energy, especially electric energy, to replace traditional energy. However, renewable power generation energy, such as solar power, is characterized by unstable output, which results in a great deal of interest in energy storage [1–5]. Proton exchange membrane fuel cells (PEMFCs) are devices that convert fuel energy to electric energy smoothly and conveniently [6–10]. Lithium-ion batteries (LIBs) are also one of the most promising energy sustainable storage technologies because of their excellent electrochemical performance and recyclable nature, thereby maintaining a dominant position as a form of energy storage for electric vehicles (EVs) and energy storage systems (ESSs) at present [11–13]. These systems, however, suffer from a lack of precious metal resources and a high cost, which makes them unsuitable for use as grid energy storage systems [8, 13–16]. Alternative energy storage devices have been explored as replacements for the current devices. Sodium-ion batteries (SIBs) are the most promising alternative because of the abundance of sodium resources, the low production costs, and the similar charge/discharge principles with LIBs [17–23]. Although the theoretical energy density of SIBs is considered lower than that of LIBs because the relative atomic mass of sodium is much higher than that of lithium, safety and cost are primarily considered in situations such as large-scale energy

✉ Haiying Che
chysyx@sjtu.edu.cn

✉ Zi-Feng Ma
zfma@sjtu.edu.cn

1 Shanghai Electrochemical Energy Devices Research Center, Department of Chemical Engineering, Shanghai Jiao Tong University, Shanghai 200240, China

2 Zhejiang Natrium Energy Co., Ltd., Shaoxing 312300, Zhejiang, China

3 School of Chemical and Materials Engineering, Jiangnan University, Wuxi 214122, Jiangsu, China

4 Shaoxing Research Institute of Renewable Energy and Molecular Engineering Shanghai Jiao Tong University, Shaoxing 312300, Zhejiang, China

Published online: 11 January 2024

storage devices, which explains the wide variety of applications of SIBs [24–28]. SIBs have a limited capacity for these applications, primarily due to their short development time compared with LIBs. Because LIBs have been developed for nearly 30 years, their specific capacities are close to their theoretical capacities, whereas this is not the case with SIBs [25, 27, 29]. In light of the research conducted on the positive and negative materials for SIBs, there are several potential areas for improvement in terms of capacity and cycle life. To facilitate the application of SIBs, researchers have enhanced their energy density from a variety of aspects. New "anode-free technologies" have been developed, for example, to eliminate the defect of low energy density in SIBs [30]. In this technology, the anode active material is removed from the battery, and instead, a sodium metal layer is formed on the surface of the anode side current collector through the first cycle of charge and discharge. As a result, the energy density is significantly increased. It is also likely that some new problems may arise as well, such as the formation of sodium dendrites and the reaction between the electrolyte and the sodium metal [31]. Overall, SIBs are still in need of innovation in each component of the battery to increase their capacity.

The electrolyte plays an essential role in SIBs. By transferring sodium ions between the positive and negative electrodes, it greatly influences the energy density and rate capability. Generally, electrolyte systems can be divided into three categories: water-based systems, organic solvent systems, and solid-state systems [18, 32–35]. Even though the water-based electrolyte provides SIBs with stable cycling performance, the maximum voltage typically does not exceed 2 V due to the low electrochemical window of water, which results in a low energy density. Voltages exceeding 2 V can only be achieved when the salt concentration is high, for example, 17 mol kg^{-1} $NaClO_4$ [32, 36–39]. Similar to LIBs, organic liquid electrolytes, such as carbonates and ethers, are increasingly used in SIBs. The commonly used carbonate organic solvents of liquid electrolytes in SIBs, such as ethylene carbonate (EC) [17, 18, 40, 41], propylene carbonate (PC) [18, 42–44], and ethyl methyl carbonate (EMC) [18, 44–46], have a strong ability to dissolve salt. EC and PC have been gaining attention during the period of traditional liquid electrolytes because they possess a high dielectric constant and broad electrochemical window, preventing liquid electrolytes from reacting with electrodes and forming a stable solid electrolyte interface (SEI [43, 44, 47]. Due to the evolution of energy density, it is not possible to satisfy both the requirements of stability and electrochemical performance with a single kind of liquid electrolytes. To achieve higher performance, different liquid electrolytes have been mixed. There have been numerous studies utilizing EC and PC together as the electrolyte for SIBs to enhance their performance [48–50]. Carbonate electrolytes, however, did not form suitable binary co-intercalation compounds with sodium ions, making graphite ineligible for use in SIBs. Instead, ether electrolytes allow the effective use of graphite and other negative electrodes in SIBs, providing stable intercalation and desorption of sodium, although ethers have a lower electrochemical window [51–53]. Sodium metal anodes have been proposed as an effective means of improving the practical capacity of SIBs [54]. The use of organic solvent electrolytes, as described above, may cause sodium dendrites during the charging and discharging cycles, resulting in short circuits and accidents. There is a limited electrochemical window for those electrolytes as well as for sodium metal anodes [55–58]. Apart from the defects mentioned above, liquid electrolytes and organic solvents also have the well-known disadvantages of being flammable, toxic, and volatile. Liquid electrolytes are unable to be applied and developed further due to safety concerns that are either difficult or costly to overcome. It is believed that ionic liquids (ILs), which typically contain organic cations and anion ions, are a safer and stabler electrolyte than carbonate and ether liquid electrolytes [59]. The benefits of ILs include their low volatility, high boiling point, wide electrochemical window, good thermal stability, and ease with which they can be designed. They are generally preferred as an electrolyte because they can improve the safety of batteries [60–63]. Nevertheless, their high cost and high viscosity hinder the application of ILs as electrolytes [64]. Accordingly, optimizing and balancing the performance, cost, and safety of liquid electrolytes remains a major challenge. Solid-state electrolytes (SSEs) have been considered a possible alternative to liquid electrolytes in this situation [11, 21, 35, 55]. Compared with liquid electrolytes, SSEs have the advantages of good processability and good safety. As a result of the compatibility with sodium anodes, it was expected that SIBs with SSEs would have a higher energy density than those with liquid electrolytes. Some SSEs that apply polymers as the base material can have even lower costs. These remarkable characteristics of SSEs have gradually attracted the attention of researchers [56, 65–67]. According to a study of the number of publications related to solid electrolytes of SIBs, the number of publications has increased over the period 2010–2022, as shown in Fig. 1.

Different research groups have highlighted the following characteristics of SSE: electrochemical stability, mechanical strength, and increased energy density [68–70]. Specifically, Fig. 2a shows that different varieties of electrolytes have different calculated theoretical energy densities, of which the SSE has the highest [18]. This is due to the compatibility of SSEs with sodium metal anodes. A higher electrochemical window is claimed for SSEs, resulting in compatibility with high-voltage cathodes as well. Additionally, the design of the battery assembly could be simplified because the SSE serves the same purpose as the separator, which is required

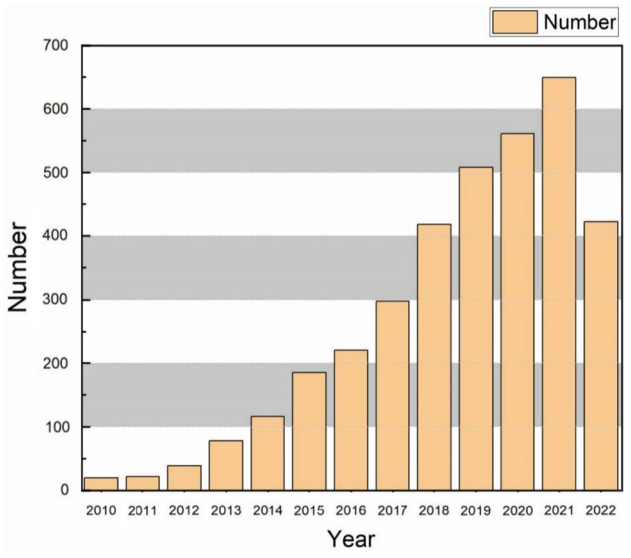

Fig. 1 A trend of publication numbers for solid electrolytes of sodium-ion batteries in recent years. (*Note* datas from Web of Science on 21/09/2022)

when using liquid electrolytes [71]. The commercialization of SSEs is, however, still hindered by some shortcomings. It has been pointed out that one of the main defects of the SSE is that its ionic conductivity is too low to meet the requirements of applications at room temperature. In Fig. 2b, the ionic conductivity of illustrative SSEs is summarized, which indicates that at room temperature, the ionic conductivity of SSEs is inferior to that of a liquid electrolyte [55]. The contact between the electrolyte and the positive and negative electrodes must also be improved, as it is difficult and complex to form a low-impedance interface [19, 55, 57, 70, 72, 73]. The solid−solid interface between the electrodes and solid electrolytes is also a key factor that determines the electrochemical performance of solid-state batteries. Moreover, the electrochemical window and mechanical strength of SSEs play an important role in assessing the stability of the electrolyte [74–76]. The sodium-ion SSE system reported thus far is unable to overcome all of the shortcomings mentioned above; thus, further research is needed. Essentially, to establish a good SIB-based SSE, it is generally necessary to have a high ionic conductivity of more than 10^{-4} S cm^{-1}, a low electron conductivity to prevent self-discharging, and a high electrochemical stability window to be compatible with the electrodes [77–79]. To supersede Li-ion technology, novel cell systems must utilize a sodium negative electrode, which can significantly increase the specific energy [57]. In addition, the SSE should also be mechanically strong enough not only to facilitate engineering processes but also to prevent dendrite formation. In this article, a review of the recent developments in the areas of the ionic conductivity, electrochemical stability window properties, interface state with electrodes, and electrochemical performance in batteries will be presented. Multiple types of solid electrolytes are included, including inorganic solid electrolytes, polymer solid electrolytes, gel polymer electrolytes, and plastic crystal electrolytes, to determine the future development direction of SSEs.

2 Inorganic Solid Electrolyte

Inorganic solid electrolytes (ISEs) have the advantages of being nonflammable, chemically stable, and mechanically strong [1, 80, 81]. In an earlier study by Famprikis et al.

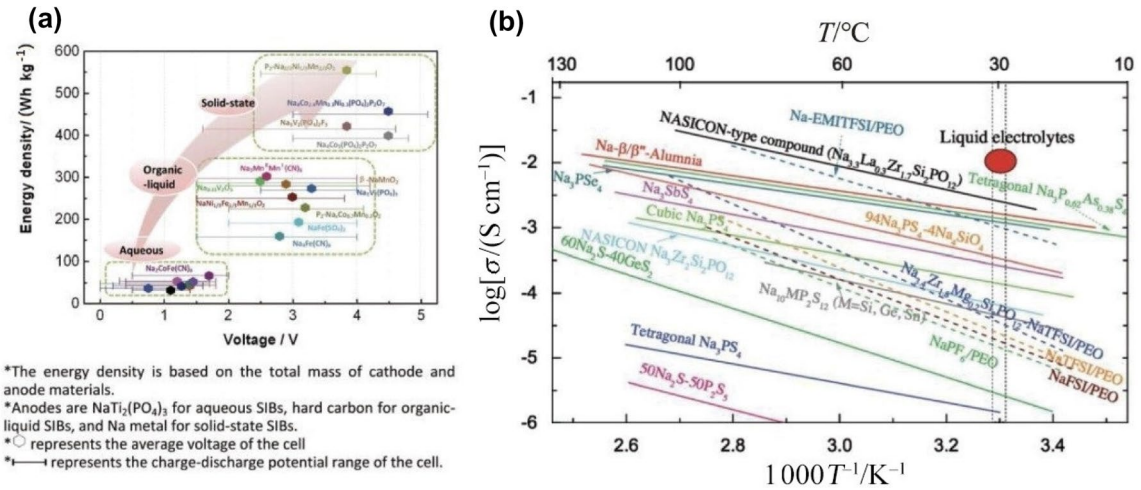

Fig. 2 **a** Theoretical energy density of different varieties of electrolytes. Reprinted with permission from Ref. [18]. Copyright © 2017, Royal Society of Chemistry; **b** ionic conductivity of SSEs and liquid electrolytes at different temperatures. Reprinted with permission from Ref. [55]. Copyright © 2018, John Wiley and Sons

[80], it was concluded that the ion diffusion mechanism of an ISE can be divided into four categories: vacancy migration, interstitial migration, correlated migration, and concerted diffusion. It was found that sodium-ion diffusion was closely related to the activation energy of the material and the number of defects in the vacancies, which indicated that the ion conductivity of the ISE can be enhanced by ion doping. The general electrochemical window of different sodium-based inorganic compounds was studied by Lacivita et al. [82]. Based on density functional theory (DFT) calculations, a wide range of Na SSE chemistries were investigated in terms of their electrochemical stability and chemical reactivity. Sodium compounds exhibit lower reduction limits, as shown in Fig. 3, indicating their increased cathodic stability and the ability to cycle sodium against a variety of oxides with increased stability. In addition to oxidation and reduction reactions against Na metal, some reduction reactions are also depicted in the figure. In general, solid electrolytes can be classified by the anion or anion group, namely oxide-based solid electrolytes, sulfide-based solid electrolytes, and other inorganic solid electrolytes. Below are a few examples of different types of ISEs.

3 Oxide-Based Solid Electrolyte

3.1 Na–β-Al_2O_3

β-Al_2O_3 is a kind of alternate layered accumulation compound. The layered compound of the conductive plane and the spinel block corresponds to two different crystal structures, namely β-Al_2O_3 (the hexagonal crystal system, $Na_2O{\cdot}(8–11)Al_2O_3$) and β″-$Al_2O_3$ (rhombus, $Na_2O{\cdot}(5–7)Al_2O_3$) [83, 84]. The microstructures of β-Al_2O_3 and β″-Al_2O_3 are shown in Fig. 4 [85]. Due to a higher percentage of sodium ions in the crystal lattice and a weaker ionic bond between sodium and oxygen, the ion conductivity of β″-Al_2O_3 is consequently higher [86]. The Na–β-Al_2O_3 SSE was first discovered by Yung Fang et al. in 1967 [87]. It was reported that the diffusion coefficient of sodium ions was up to 1×10^{-5} cm^2 s^{-1} at 593 K and 4.0×10^{-7} cm^2 s^{-1} at room temperature, indicating a high ionic conductivity and thermal stability at high temperature. Commercialized cell systems utilizing sodium as the negative electrode and Na–β-Al_2O_3 as the solid electrolyte have been developed. A well-known example of these batteries is the Na–S battery, which operates at temperatures of 350 °C [88].

Many studies have been conducted to improve the ionic conductivity of Na–β-Al_2O_3 SSE. The methods mainly used in the past are ion doping with other metal ions [89]

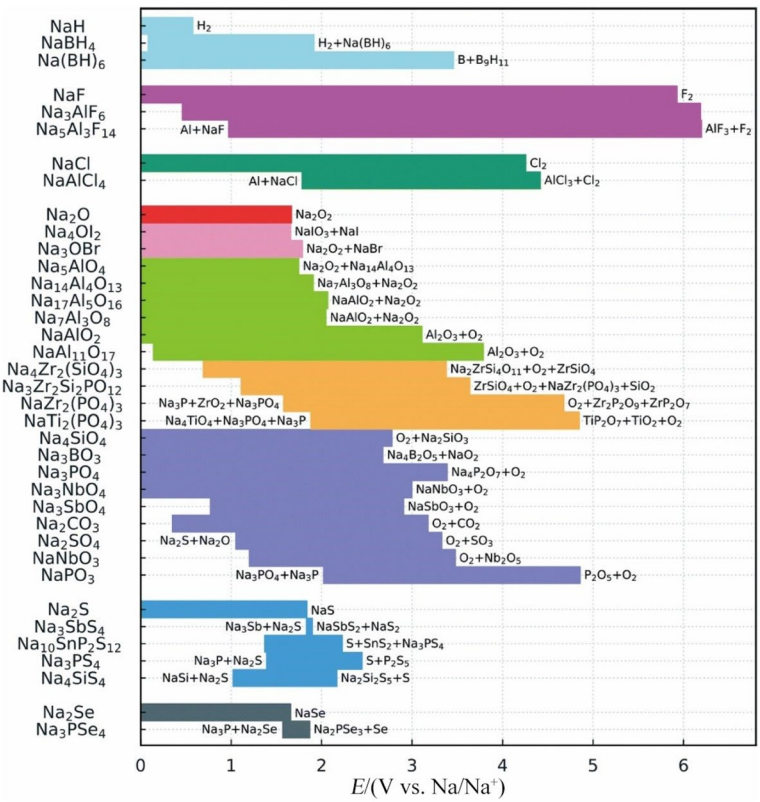

Fig. 3 Calculated electrochemical stability windows of Na inorganic SSEs [82]

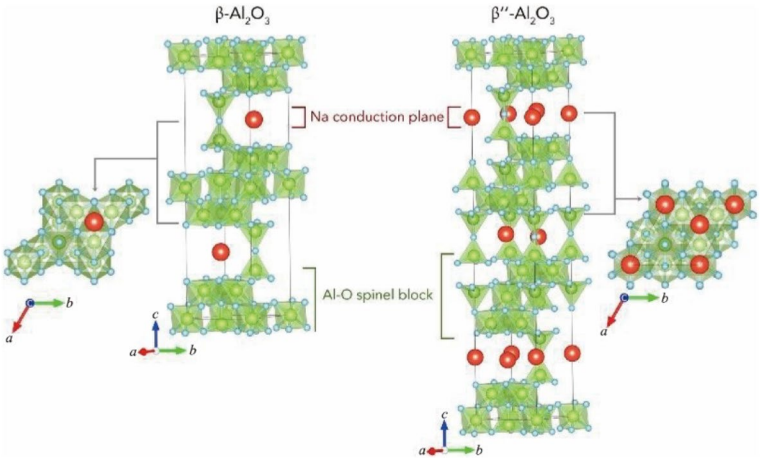

Fig. 4 Microstructure of β-Al_2O_3 and β''-Al_2O_3. Reprinted with permission from Ref. [85]. Copyright © 2018, Elsevier

and adjusting the rate between β-Al_2O_3 and β''-Al_2O_3 [90]. Recently, it has been reported that a high β''-Al_2O_3 content Na–β-Al_2O_3 SSE was synthesized by using boehmite as an alumina source [91]. In this study, the effects of sodium oxide on the SSE were examined from the perspective of phase constituents and ionic conductivity to the point of application. By increasing the content of β''-Al_2O_3 to 95 wt% (wt% means the weight percentage), the newly synthesized Na–β-Al_2O_3 SSE showed a high ionic conductivity of 6.30×10^{-4} S cm^{-1} at room temperature and 1.16×10^{-2} S cm^{-1} at 350 °C. Using the $Na_3V_2(PO_4)_3$ cathode and Na metal anode materials, the battery exhibited an initial discharge capacity of 80.5 mAh g^{-1} at 0.5C. The optimized Na–Al_2O_3 SSE displayed excellent electrochemical stability against sodium metal. According to Fig. 3, the electrochemical stability window of Na–β-Al_2O_3 is between 3 and 4 V, and the reduction limit vs. Na/Na$^+$ is nearly 0 V, indicating that Na–β-Al_2O_3 is suitable for sodium metal anodes.

Ion doping is an effective way to improve the performance of ionic conductivity. Hua et al. [92] reported a novel Na–β-Al_2O_3 SSE composed of β''-Al_2O_3 and an ethylenediaminetetraacetic acid (EDTA)-zirconium$^{(IV)}$/yttrium$^{(III)}$ complex. The manufacture and modification process of the SSE is depicted in Fig. 5. Different characteristics, such as microstructure, were also studied. With the outcome that 5 wt% nano 33 mol% (mol% means the molar percentage) yttrium partial stabilized zirconia (3YSZ) offered a high performance in terms of density and microstructure, the ionic conductivity reached 7.1×10^{-2} S cm^{-1} at 300 °C and 0.33 S cm^{-1} at 600 °C. Although the ionic conductivity of Na–β-Al_2O_3 SSE has been optimized to over 10^{-2} S cm^{-1}, it is the high temperature to which SSEs can only be applied. It is not only the ionic conductivity but also the contact surface with the electrode that produces a high resistance at room temperature.

Substantial effort has been made to apply Na–β-Al_2O_3 SSEs at room temperature to the Na–S battery. Electrochemical cells operated at room temperature do not inevitably prevent dendrite growth when sodium-beta alumina is used since dendrite formation is not solely dependent on the Na–β-Al_2O_3 SSE itself. It is also crucial to consider the properties of the sodium metal negative electrode, in which the solid state and liquid state are different [93]. Spencer et al. [94] investigated the surface between a Na–β-Al_2O_3

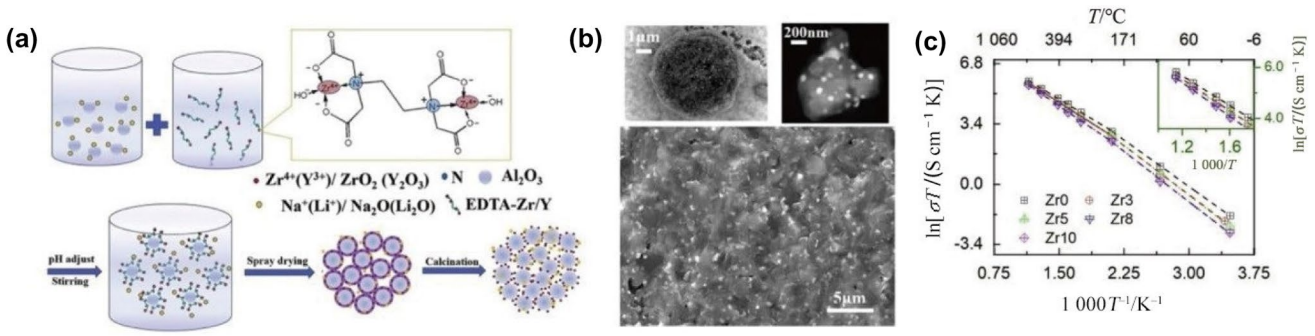

Fig. 5 **a** synthetic route; **b** SEM microstructure and **c** ionic conductivity of SSEs. Adapted with permission from Ref. [92]. Copyright © 2020, Elsevier

SSE and a sodium metal anode at room temperature to understand the failure mechanism of a Na–β-Al_2O_3 SSE at ambient temperature. Using three electrodes and tomographic imaging, it was found that voids form within the Na metal at the interface during stripping and accumulate during cycling, resulting in an increase in interfacial current density, dendritic formation on plating, short circuits, and failures of the batteries, as shown in Fig. 6. It was also investigated that above 9 MPa is required to prevent the formation of dendrites when cycled at current densities lower than 2.5 mA cm^{-2} at room temperature. Clearly, the conditions for stable cycling at room temperature are harsh and impede progress towards commercialization of the Na–β-Al_2O_3 SSE. Currently, optimization of the surface of SSEs is required to be compatible with sodium metal anodes and to apply a lower temperature, such as 60 °C [95].

Although the Na–β-Al_2O_3 SSE exhibits a high ionic conductivity at both high and room temperatures, it still has low kinetics owing to both its thickness and its interfacial properties. Due to the formation of solid polysulfides with slow electrochemical reactivity, reducing the operation temperature of Na–S batteries limits their electrochemical performance as well [96]. Therefore, researchers are focusing on optimizing the interface between Na–β-Al_2O_3 SSEs and electrodes to obtain usable batteries at lower temperatures. The use of ILs with good chemical stability and performance has been, for example, demonstrated. In their study, Wang et al. [97] investigated a dual electrolyte comprising a Na–β-Al_2O_3 SSE and an inorganic IL Na[OTf]–Cs[TFSA] that possesses a high ionic conductivity and a wide electrochemical stability window of 5.1 V, where $[OTf]^-$ is trifluoromethanesulfonate and $[TFSA]^-$ is bis(trifluoromethanesulfonyl)amide. At an operation temperature of 150 °C, the Na–S battery achieves a high reversible capacity of 795 mAh $(g\text{-}S)^{-1}$. Figure 7 shows the electrochemical performance and a schematic illustration of this dual-electrolyte Na–S battery. During a 1 000 cycle test, an average capacity of 381 mAh $(g\text{-}S)^{-1}$ was achieved with an average 100% coulombic efficiency. It was also investigated that the usage of an electrolyte based on Na[OTf] is employed as a method of improving the kinetics of inert polysulfides through Na^+ conduction. The presence of a large number of $[OTf]^-$ donors causes polysulfides to dissolve more readily into the electrolytes, thereby improving the electrochemical performance. Efforts should be made to optimize the cell structure and the IL composition to achieve significant improvements in performance. With improved polysulfide reaction kinetics and sodium dendrites at room temperature, Na–S cells with Na–β-Al_2O_3 SSEs are promising for high practical capacity and safety.

3.2 NASICON

NASICON (Na superion conductor) is different from Na–β-Al_2O_3 SSEs, as NASICON has 3D channels for sodium-ion transportation, whereas Na–β-Al_2O_3 SSEs can only transport sodium ions in plane. NASICON was first discovered by Goodenough and Hong in 1976 and consists of $Na_{1+x}Zr_2Si_xP_{3-x}O_{12}$ $(0<x<3)$ (NZSP) [98, 99]. NZSP is composed of $NaZr_2(PO_4)_3$ and $Na_4Zr_2(SiO_4)_3$. The crystal structure of NZSP at 1400 K has been studied and is shown in Fig. 8 [100]. The transport path of sodium ions marked as yellow stripes is simulated by comparison of neutron powder diffraction data, the maximum entropy method (MEM), the bond valence energy landscape (BVEL) approach, and DFT computations.

Zhou et al. indicated that for NZSP without modification, $Na_3Zr_2Si_2PO_{12}$, which retains a monoclinic structure, shows the highest performance in terms of ionic conductivity and physical and chemical stability [1]. NZSP was reported to reach an ionic conductivity of 6.7×10^{-4} S cm^{-1} at room temperature and 2.0×10^{-1} S cm^{-1} at 300 °C. An electrochemical stability window of up to 6 V is typically observed when applying cyclic voltammetry to NASICON-type electrolytes. Despite this, low values have been obtained experimentally due to the restricted electrode/electrolyte contact area [101]. Figure 3 shows that by calculation, the NASICON reduction limit is approximately 1.1 V, while the NASICON oxidation limit is approximately 3.6 V, indicating a stable electrochemical window of 2.5 V. According to

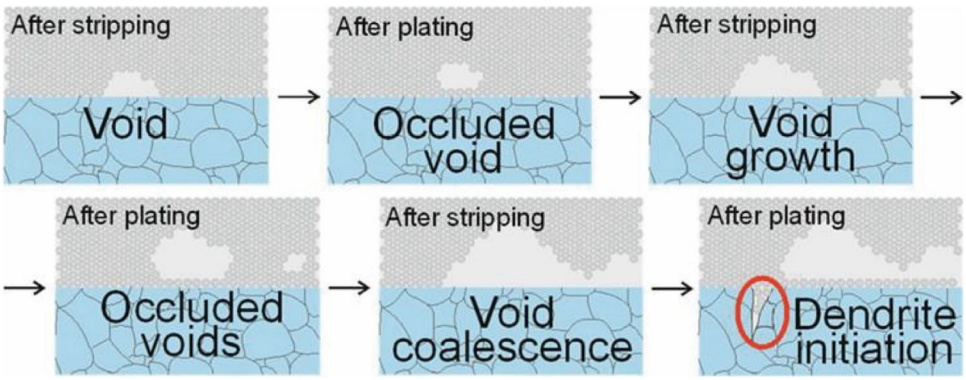

Fig. 6 An illustration of the mechanism that results in the voiding of the cell and subsequent development of dendrites. Grey represents the sodium anode, and blue represents the Na–β-Al_2O_3 SSE. Reprinted with permission from Ref. [94]. Copyright © 2020, American Chemical Society

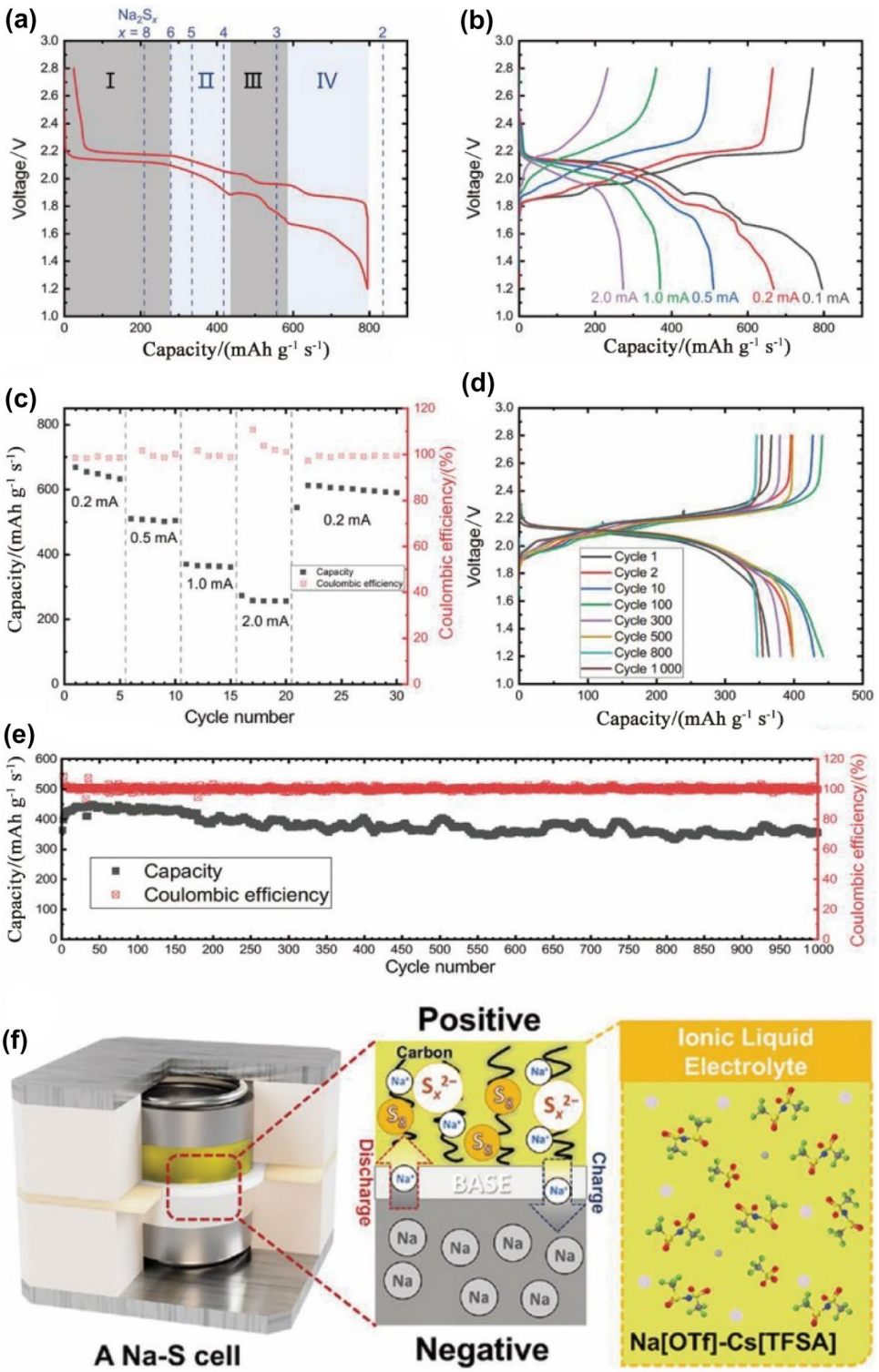

Fig. 7 **a**-**e** Electrochemical performance of a Na–S cell with IL/Na–β-Al_2O_3 electrolytes; **f** Na–S battery operation mechanism diagram with IL/Na–β-Al_2O_3 electrolytes. Adapted with permission from Ref. [97]. Copyright © 2021, John Wiley and Sons

Schwietert et al. [102], the electrochemical stability window of solid electrolytes is significantly larger than predicted for direct decomposition, which rationalizes the observed stability window. The electrochemical stability window depends on the oxidation and reduction potentials of the solid electrolyte, not on the stability of the decomposition products. As a result of this indirect thermodynamic pathway, the electrochemical stability window is generally wider than that based solely on decomposition product stability.

It is possible to increase the ionic conductivity of NASICON from two dimensions. One method involves increasing the concentration of sodium ions. An increased

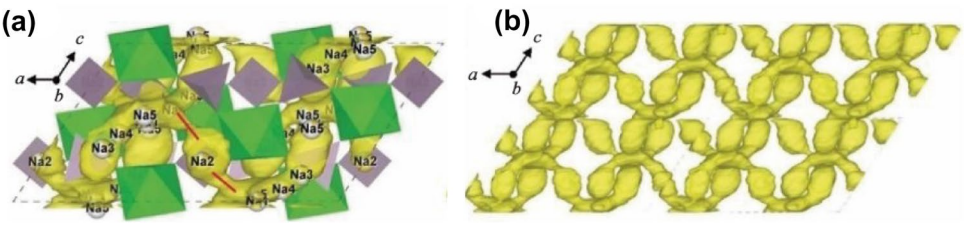

Fig. 8 A simulation of $Na_3Zr_2Si_2PO_{12}$ at 1 400 K. **a** Unit cell; **b** 2*a**1*b**2*c* cells. Adapted with permission from Ref. [100]. Copyright © 2019, John Wiley and Sons

sodium-ion concentration results in an increase in charge carriers. The other method involves the introduction of appropriate substituents. By increasing the size of the bottleneck, substituents can reduce the energy barrier as well as the activation energy [103]. Recently, Sun et al. [104] studied in detail the mechanism of the augmentation of ionic conductivity of scandium doping in sodium-rich NASICON SSEs of $Na_{3+x}Sc_xZr_{2-x}Si_2PO_{12}$ ($x = 0$, 0.1, 0.2, 0.3, 0.4, 0.5, and 0.6) (NSZSP*x*). The microstructure of the general NZSP and X-ray diffraction (XRD) of NSZSP*x* are shown in Fig. 9. It has been discovered that Sc ions are doped into the crystal lattice in place of Zr, which leads to a structural change, enhancing ionic conductivity. According to the results, the highest ionic conductivity of Sc-doped NASICON was $Na_{3.3}Sc_{0.3}Zr_{1.7}Si_2PO_{12,}$ which presented an ionic conductivity of 1.9×10^{-3} S cm^{-1} at room temperature. It was also investigated that with $x < 0.3$, the ionic conductivity was increased by an acceleration of the transference of sodium ions, while for $x > 0.3$, the crystal form of NASICON changed from monoclinic to rhombohedral, which resulted in sluggish sodium-ion transportation. The detailed ion transport mechanism of ion-doped NZSP is still under development, which may result in the progress on a series on NASICON-type SSE materials.

Zhang et al. [105] reported a newly designed NASICON containing lanthanum ions. NASICON was synthesized by $La(CH_3COO)_3$ and NASICON precursors consisting of $NaNO_3$, $ZrO(NO_3)_2$, and $NH_4H_2PO_4$. Scanning transmission electron microscopy (STEM) and electrochemical impedance spectroscopy (EIS) revealed that lanthanum doping enhanced ion transport at grain boundaries, generating new $Na_3La(PO_4)_2$, $La_2O_{3,}$ and $LaPO_4$ phases. With this perfection, the ion conductivity of NASICON reached 3.4×10^{-3} S cm^{-1} at room temperature. According to the authors, the interface impedance between electrodes and SSEs was high due to a relatively low effective contact. Different organic liquid electrolytes (EC–DMC) and ILs ($PP_{13}FSI$) were then added between the electrolyte and $Na_3V_2(PO_4)_3$ (NVP) cathode to adjust the interface contact. The interfacial resistance decreases by dozens of ohm after liquid is added, as shown from Fig. 10e–g, which presents the resistance of NVP/SSE/Na, NVP/LE/SSE/Na, and NVP/IL/SSE/Na, respectively. Through its wetting properties, IL facilitates favorable interface kinetics in SSBs. As shown in Fig. 10d, when IL was introduced between the cathode and SSE, the cell exhibited fantastic electrochemical performance under 10 C at room temperature. When compared to the cycling curve of NVP/LE/SSE/Na in Fig. 10b, the IL is far stabler due to the possible decomposition of the organic liquid electrolyte during cycling. The introduction of ionic

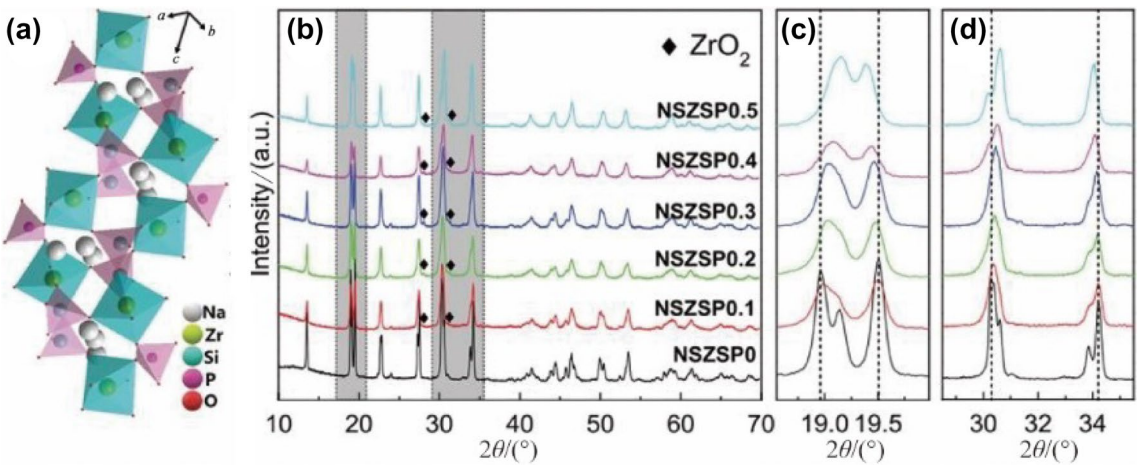

Fig. 9 **a** General microstructure of NZSP; **b** XRD patterns of NZSP and NSZSP*x*; **c**&**d** amplified view of the selected area. Reprinted with permission from Ref. [104]. Copyright © 2021, John Wiley and Sons

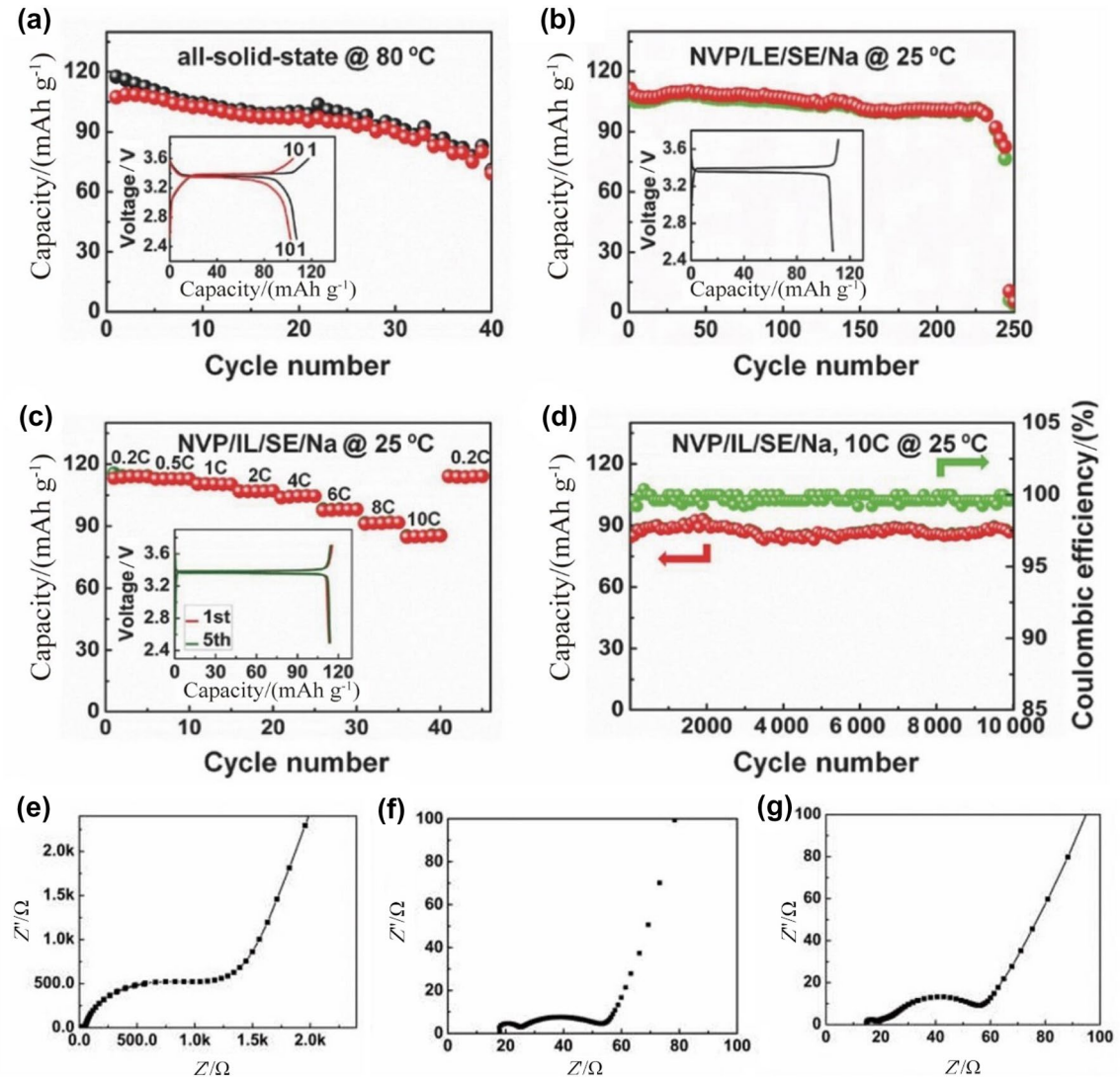

Fig. 10 **a**, **b** and **d** Charge/discharge cycling curves of the marked cell; **c** rate performance of NVP/IL/SSE/Na from 0.2 C to 10 C at 25 °C; **e** to **g** interfacial resistance curve of the cells mentioned in the text. Adapted with permission from Ref. [105]. Copyright © 2016, John Wiley and Sons

liquids may be a new feasible method for ISEs to optimize the interface [106].

It is the electrode/electrolyte interfaces, electrochemical stability windows, and electrolyte variations during long cycling that determine the electrochemical stability of batteries. For enhanced battery performance, intimate contact interfaces with large surface areas and electrode compatibility are the most important factors.

4 Sulfide-Based Solid Electrolyte

The electronegativity of sulfur is smaller than that of oxygen, which reduces the attraction to sodium ions. Under a similar crystal lattice, sulfide-based SSEs have a higher ionic conductivity performance than oxide-based SSEs, which helps form an appropriate transportation channel for sodium ions [81]. Due to their high ionic conductivity, good ability to combine with electrodes, isotropic ionic conduction without grain boundary resistances, and variable composition over a wide range, sulfide-based SSEs have attracted much attention [79]. Sulfide-based SSEs, however, have the drawback of easily becoming bibulous and reacting with airborne water, which increases the difficulty of the product process [107]. Additionally, it should be noted that sulfide-based SSEs have high reduction limits and narrow electrochemical stability windows, as shown in Fig. 3.

4.1 Na_3PS_4

Na_3PS_4 was first synthesized in 1992 and possesses a tetragonal crystal lattice; however, the ionic conductivity was only 4.17×10^{-6} S cm^{-1} at 323 K [108]. Performance in terms of ionic conductivity did not meet the requirements of SSEs. It was then reported by Hayashi et al. in 2012 that a cubic crystal Na_3PS_4 glass–ceramic electrolyte was synthesized [109]. The Na_3PS_4 electrolyte was synthesized by powder compression at room temperature, and the ionic conductivity was 2.3×10^{-4} S cm^{-1}, which revealed the possibility of application.

Ion doping will expand the ionic conductivity of sulfide-based electrolytes, which is the same as oxide-based electrolytes, as the transport channel will be enlarged, and more sodium vacancies will be introduced. Moon et al. reported the synthesis of a new Ca-doped Na_3PS_4 electrolyte ($Na_{3-2x}Ca_xPS_4$ ($0<x\leqslant0.375$)).[110]. According to the XRD spectra, the crystal lattice of the electrolyte changed from tetragonal to cubic with the addition of Ca, and this transformation enhanced the ionic conductivity. The microstructures of the normal Na_3PS_4 crystal and $Na_{3-2x}Ca_xPS_4$ crystal are shown in Fig. 11. According to the complementary analysis thus far, it is rational to conclude that overall conductivity is determined by the interaction between the Na^+ vacancy concentration enhancement caused by Ca doping and the energy barrier impediment caused by Ca^{2+} together. As a result, the impact of vacancies is higher than that of the energy barrier, thereby enhancing the ionic conductivity. The ionic conductivity of the Ca-doped Na_3PS_4 electrolyte reached a maximum of 1×10^{-3} S cm^{-1} at room temperature. Applying the Ca-doped Na_3PS_4 electrolyte to TiS_2/Na–Sn SIBs, the cycling stability performance was significantly improved. The capacity retention of TiS_2/Ca-doped Na_3PS_4/Na–Sn, which was 91.0% after 100 cycles, was higher than that employing the cubic Na_3PS_4 electrolyte of 78.6%. Within the negative (0.0–2.0 V (vs. Na/Na$^+$)) and positive (1.5–5.0 V (vs. Na/Na$^+$)) voltage ranges, a cyclic voltammetry test was applied to the Ca-doped and original Na_3PS_4 electrolytes, as shown in Fig. 11b. The performance of Ca-doped Na_3PS_4 is slightly worse than that of the original Na_3PS_4 in terms of cathodic stability but better in terms of anodic stability. The electrochemical stability window of Ca-doped Na_3PS_4 is still narrow when applied to other electrode systems that possess a high voltage. The method of cation doping displayed an enhancement in ionic conductivity with increasing vacancies, which indicated a technique optimization. Electrochemical stability is still a barrier to the development of high-voltage and high-capacity SIBs.

It has been suggested that the ionic conductivity of tetragonal Na_3PS_4 is much lower than that of cubic Na_3PS_4 [109]. However, it was reported recently by Feng et al. [111] that Cl-doped tetragonal Na_3PS_4 ($Na_{3-x}PS_{4-x}Cl_x$) was produced through a solid-state reaction, which had a persuasive performance. It was demonstrated by the authors that the accelerated and enhanced transportation of sodium ions in $Na_{3-x}PS_{4-x}Cl_x$ was due to functional defects that produced two more sodium transportation channels according to solid-state nuclear magnetic resonance (NMR). As a result, a high ionic conductivity was observed for $Na_{2.9}PS_{3.9}Cl_{0.1}$, which was 1.96×10^{-3} S cm^{-1} at room temperature. According to Fig. 12a, the cyclic voltammetry test of Na|$Na_{3.0}PS_{3.8}Cl_{0.2}$| in cells from -0.5 to 10 V (vs. Na/Na$^+$) showed only sodium deposition at 0 V. No decomposition was found

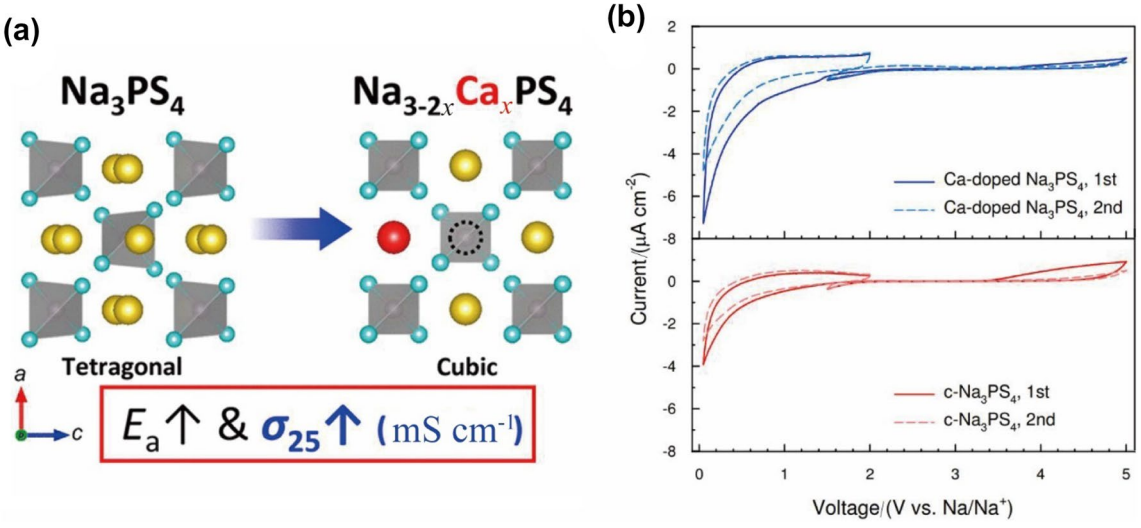

Fig. 11 **a** Microstructure of Na_3PS_4 and $Na_{3-2x}Ca_xPS_4$ with vacancy shown; **b** first two cyclic voltammetry curves for cells in the negative potential range (0.0–2.0 V (vs. Na/Na$^+$)) and in the positive potential range (1.5–5.0 V (vs. Na/Na$^+$)) at 303 K. Adapted with permission from Ref. [110]. Copyright © 2018, American Chemical Society

in the electrolyte even when the voltage was as high as 10 V. It was suggested that the low electron conductivity of $Na_{3.0}PS_{3.8}Cl_{0.2}$ hindered the decomposition. It should be noted that the LSV experiments produce very small currents and large overpotentials due to the slow reaction kinetics of the oxidation reaction, leading to a difference between the experimental oxidation limit and the reality limit [112]. As shown in Fig. 12b, a decrease in specific capacity was observed when the electrolyte was applied to the $Na|Na_{3.0}PS_{3.8}Cl_{0.2}|Na_3V_2(PO_4)_3$ full cell. Possible explanations include interfacial stability during electrochemical cycling. As illustrated in Fig. 12c, impedance measurements before and after cycling provide evidence of this hypothesis. The total interfacial resistance is only 80 Ω before cycling and 1 300 Ω after cycling, resulting from undesirable side reactions between the electrodes and $Na_{3.0}PS_{3.8}Cl_{0.2}$. The anion-doped Na_3PS_4 electrolyte created abundant sodium vacancies in the crystal, which consequently enhanced the ionic conductivity performance. The electrochemical stability window was enhanced due to a high electronic impedance. However, the interfacial resistance during cycling still needs to be solved.

4.2 Na_3SbS_4

Na_3SbS_4 is similar to Na_3PS_4 in that both have tetragonal and cubic crystal lattices, and the ionic conductivity of cubic Na_3SbS_4 is higher than that of tetragonal Na_3SbS_4. Wang et al. [113] first reported that cubic Na_3SbS_4 synthesized based on soft–hard acid-base (SHAB) theory had application prospects for SSEs. Air-conditioning resistance was tested on the product, which overcame the hygroscopicity of Na_3PS_4. The microstructure of cubic Na_3SbS_4 is shown in Fig. 13. It was stated by the authors that this type of SSE has a notable ionic conductivity of 1×10^{-3} S cm^{-1}.

Gamo et al. [114] recently prepared tetragonal Na_3SbS_4 using the liquid phase method. The SSE showed an attractive high ionic conductivity of 3.0×10^{-4} S cm^{-1} at room temperature. Notably, the ionic conductivity of the SSE was enhanced to 3.1×10^{-3} S cm^{-1} at room temperature with ball milling, which proved that the crystal lattice of Na_3SbS_4 changed partially from tetragonal to cubic, forming a multiphase Na_3SbS_4 SSE. An experiment with a TiS_2–$Na_3SbS_4|Na_3SbS_4|$Na–Sn cell was conducted to evaluate the electrochemical characteristics of the prepared Na_3SbS_4. The cell was cycled between 2.50 and 1.50 V at room temperature with a specific capacity of 125 mAh g^{-1} and an average coulombic efficiency of 97%. It was indicated that there were no side reactions between the prepared Na_3SbS_4 and TiS_2.

Ion doping also helps enhance the ionic conductivity of Na_3SbS_4, which has the same purpose of enlarging the transport channel. Yubuchi et al. [115] investigated the use of tungsten instead of antimony, showing that the

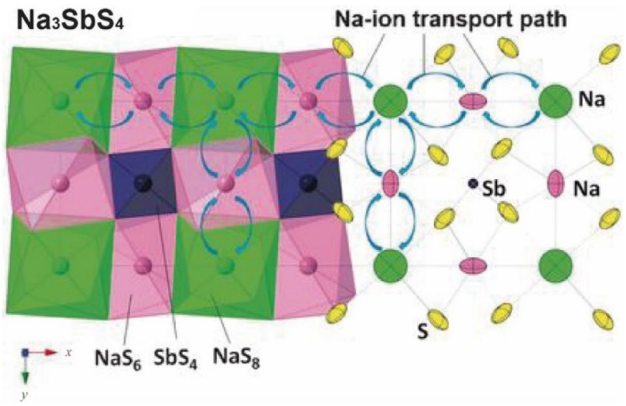

Fig. 13 Microstructure of cubic Na_3SbS_4. Reprinted with permission from Ref. [113]. Copyright © 2016, John Wiley and Sons

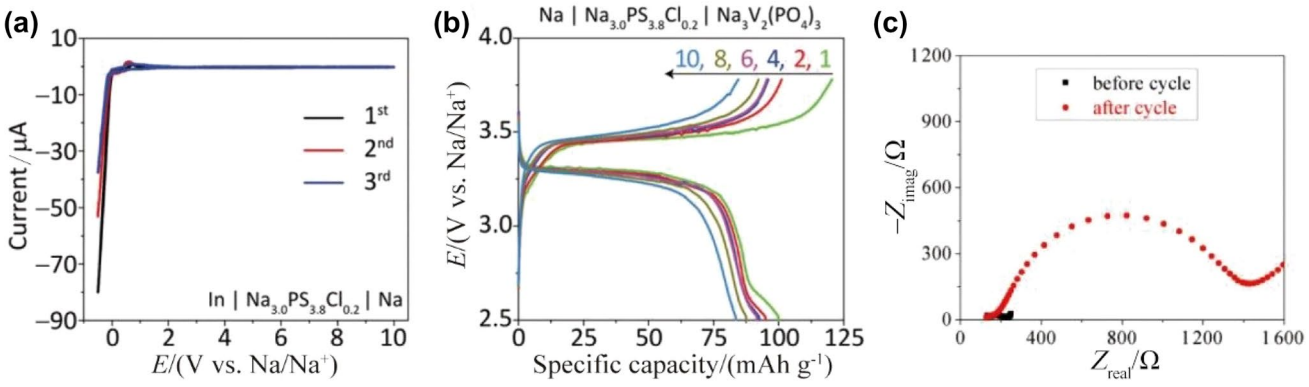

Fig. 12 **a** Cyclic voltammetry test from the 1st to 3rd rounds of the $In|Na_{3.0}PS_{3.8}Cl_{0.2}|Na$ cell; **b** charge/discharge curve from the 1st to 10th cycles of the $Na|Na_{3.0}PS_{3.8}Cl_{0.2}|Na_3V_2(PO_4)_3$ full cell; **c** interfacial resistance of the $Na|Na_{3.0}PS_{3.8}Cl_{0.2}|Na_3V_2(PO_4)_3$ full cell before and after cycling. Adapted with permission from Ref. [111]. Copyright © 2019, John Wiley and Sons

liquid-phase-synthesized Na_3SbS_4 electrolyte upsurged the ionic conductivity from 1.2×10^{-3} to 4.28×10^{-3} S cm^{-1} with the chemical formula of $Na_{2.88}Sb_{0.88}W_{0.12}S_4$. It was suggested that the enhancement of ionic conductivity was due to sodium-ion vacancies from ion doping, which indicated that by introducing doped ions, the ionic conductivity was expanded with the formation of sodium-ion vacancies. Recently, Tsuji et al. investigated the ionic conductivity of cation-doped Na_3SbS_4 with extra sodium, namely $Na_{3+x}Sb_{1-x}M_xS_4$ (M = Si, Ge, Sn), which had lower ionic conductivity than Na_3SbS_4 at room temperature [116]. However, with partial replacement of molybdenum, forming sodium vacancies, $Na_{3-x}Sb_{1-x}Mo_xS_4$ showed attractive ionic conductivity. In particular, $Na_{2.88}Sb_{0.88}Mo_{0.12}S_4$ exhibited an ionic conductivity of 3.9×10^{-3} S cm^{-1} at room temperature. The ionic conductivity at different temperatures is shown in Fig. 14. Accordingly, the author suggests that sodium vacancies, rather than sodium ions, enhance ionic conductivity.

Although Na_3SbS_4 has exhibited exciting ionic conductivity at room temperature and high air stability, its electrochemical stability with sodium metal anodes remains a problem. Na_2S and Na_3Sb can be formed on the interface between Na_3SbS_4 and Na metal [117]. It is likely that a percolating electronic conduction path forms at the interface due to the large fraction of metallic Na_3Sb in the decomposition products, indicating that further decomposition of the Na_3SbS_4 electrolyte will occur. Thus, Tian et al. designed hydration covers on the surface by first-principles computational tools to form an h-Na_3SbS_4 electrolyte [118]. With an acceptable level of ionic conductivity, the hydrated surface ($Na_3SbS_4{\cdot}8H_2O$) formed NaH and Na_2O, which slowed the reaction of the Na_3SbS_4 electrolyte with Na metal compared with the nonhydrated Na_3SbS_4 electrolyte. The formation of the hydrated surface is easy. In ambient air, the Na_3SbS_4 electrolyte was subjected to a humidity of approximately 68% for 10 min. Two different symmetric cells consisting of Na|Na_3SbS_4|Na and Na|h-Na_3SbS_4|Na were cycled at a constant current (0.1 mA cm^{-2}) to evaluate the stability with the Na metal electrode. The result was that the h-Na_3SbS_4 electrolyte showed a stable interface during 25 h of cycling, as shown in Fig. 15a. In contrast, the voltage of the nonhydrated Na_3SbS_4 cell increased continuously due to the polarization of the unstable interface. The synchrotron X-ray diffraction (SXRD) spectra shown in Fig. 15b also show that

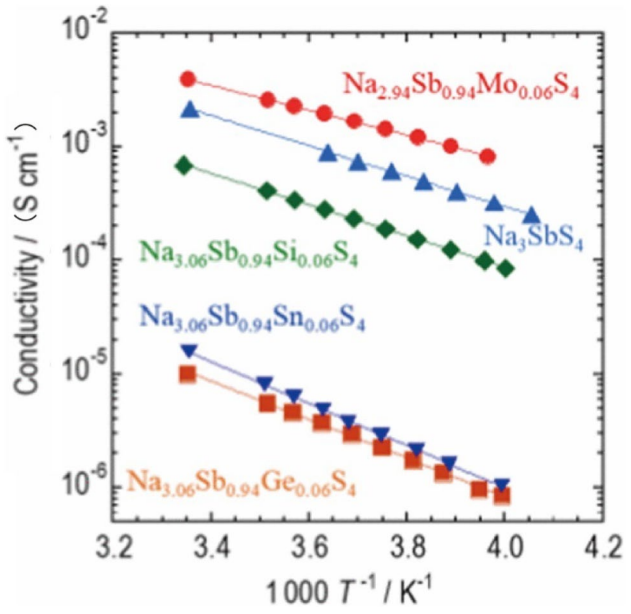

Fig. 14 Temperature dependence of Na_3SbS_4, $Na_{3+x}Sb_{1-x}M_xS_4$ ($x=0.06$) and $Na_{3-x}Sb_{1-x}Mo_xS_4$ ($x=0.06$). Reprinted with permission from Ref. [116]. Copyright © 2020, American Chemical Society

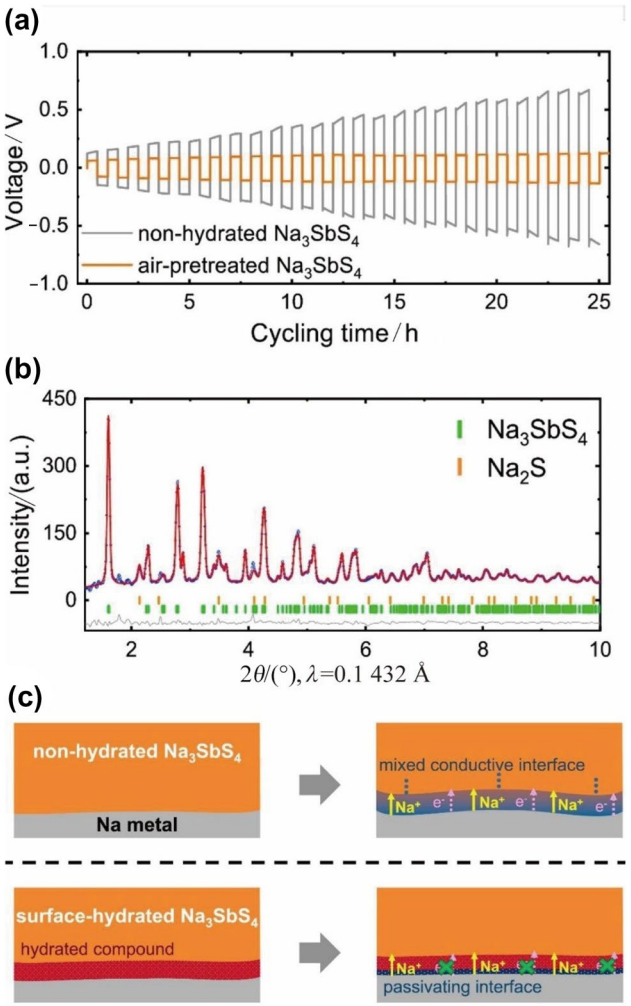

Fig. 15 **a** Symmetric cells consisting of Na|Na_3SbS_4|Na and Na|h-Na_3SbS_4|Na cycled at a constant current (0.1 mA cm^{-2}); **b** SXRD pattern of Na_3SbS_4/Na interface products; **c** schematic diagram of the solid electrolyte-Na metal interface before (left) and after (right) electrochemical cycling. Adapted with permission from Ref. [118]. Copyright © 2019, Elsevier

the reaction product is determined to be NaS of the nonhydrated Na_3SbS_4 electrolyte. The schematic diagram shows a contrast interface between the nonhydrated and hydrated Na_3SbS_4 electrolytes, as shown in Fig. 15c.

Although sulfide-based SSEs show higher performance than oxygen-based SSEs, problems remain. Sulfide-based compounds, especially Na_3PS_4, have the shortcoming of sensitivity to water, which easily forms hydrogen sulfide, causing the collapse of crystals and emission of toxic gases. In addition, elements of high valence, such as phosphorus and antimony, are easily reduced, which leads to a narrow electrochemical stability window. Optimization may focus on the modification of the surface of sulfide-based SSEs to prevent the reactions between the SSEs.

5 Other Inorganic Solid Electrolytes

In addition to oxide- and sulfide-based inorganic solid electrolytes, other inorganic solid electrolytes have also been investigated, such as $Na(BH_4)_x(NH_2)_{1-x}$, NaI, $NaCB_9H_{10}$, and Na_3OBH_4 [119–121]. Composite hydroborate solid electrolytes have unique physical chemistry properties, such as high ionic conductivity, a wide electrochemical stability window, good flexibility, and low density. Sun et al. [121] recently reported that synthesized Na_3OBH_4 demonstrated a high ionic conductivity of 4.4×10^{-3} S cm^{-1} at room temperature. This SSE showed a cubic antiperovskite microstructure, and the BH_4 cluster anion was rotated, which created a fast sodium ion transportation channel. This work revealed the mechanism of cluster anion-based sodium-ion conductors, indicating a new kind of sodium ion super conductor at room temperature.

To develop all-solid-state batteries with high energy and power density, solid electrolytes with a wide electrochemical window and high ionic conductivity are essential. Large cage-like $B_nH_n^{2-}$ anions, namely closo-borates, provide salts with excellent electrochemical performance. However, closo-borates have proven to exhibit an electrochemical stability window in the 3.0–4.0 V range, which is difficult to apply with high-voltage cathodes [122]. Furthermore, according to calculations, hydroborates appear to be reactive with certain oxide-based cathodes, but those results have not yet been demonstrated experimentally [82]. Therefore, it was investigated that the oxidation compound of $B_{10}H_{10}^{2-}$, namely $B_{20}H_{18}^{2-}$, exhibited promising electrochemical stability up to 5.1 V versus Na/Na$^+$ [75]. However, the ionic conductivity of $Na_2B_{20}H_{18}$ has been measured as 2.5×10^{-6} S cm^{-1} at room temperature, which does not meet the requirement of the electrolyte for SIBs. A mixed anion electrolyte was then investigated, namely $Na_2B_{20}H_{18}$–$4Na_2B_{12}H_{12,}$ which exhibited excellent electrochemical performance. The ionic conductivity was improved due to the disordering of the bulk starting materials $Na_2B_{20}H_{18}$ and $Na_2B_{12}H_{12}$. The sodium-ion transference number of this mixed electrolyte was calculated to be 0.976, indicating cation migration for the major proportion. As shown in Fig. 16b, the oxidation limit of $Na_2B_{20}H_{18}/4Na_2B_{12}H_{12}$ was measured to be 4.8 V versus Na/Na$^+$, allowing its application to electrodes of high voltage. The electrochemical performance and stability for the studied closo-borates are listed in Fig. 16c, indicating a balanced high performance of the $Na_2B_{20}H_{18}/4Na_2B_{12}H_{12}$ electrolyte. To investigate the long-term stability and chemical compatibility of electrolytes to metallic sodium, constant-current cycling measurements were taken on the symmetric cell Na|$Na_2B_{20}H_{18}$–$4Na_2B_{12}H_{12}$|Na, which is charged and discharged at a certain current density of 0.1 mA cm^{-2}. An inconspicuous increase in overpotential was observed after 100 h of testing, indicating that a slow parasitic reaction may occur between the electrolyte and sodium metal. An all-solid-state Na|$Na_2B_{20}H_{18}$–$4Na_2B_{12}H_{12}$|TiS_2 cell was established and tested between 1.5 and 2.7 V at 0.1 C. At 25 °C, the cell displayed a reversible charge capacity of 65.2 mAh g^{-1} and a discharge capacity of 64.8 mAh g^{-1}. Unfortunately, the critical current density was shown to be 0.8 mA cm^{-2}, which is possibly due to the formation of sodium dendrites.

A summary of the temperature dependence of the ionic conductivity of some ISEs at approximately room temperature is shown in Fig. 17. Many ISEs have been developed with preferable ionic conductivity at room temperature. Among the above-mentioned sodium ISEs, Na–β-Al_2O_3 is mainly aimed at high-temperature Na–S batteries, and the application of Na–β-Al_2O_3 to lower-temperature Na–S batteries still has problems with the interface with the cathode and dendrites with the anode. Therefore, the optimization of the performance of Na–β-Al_2O_3 at low temperatures should be the focus of future research, especially on surface modification. The ion-doped NASICON shows convincing ionic conductivity at ambient temperature. However, the interface contacts between those sodium ISEs and electrodes remain an urgent problem, which prominently increases the internal resistance of the battery, leading to a reduction in energy density. Thus, the surface needs to be optimized to reduce the resistance by a higher effective contact area. Improving the surface contact can be performed by introducing additives, such as ionic liquids and liquid electrolytes, and high-temperature eutectics. However, a high-temperature eutectic will increase the opportunity for diffusion of elements. In addition to ionic liquids, conductive agents with good electrical conductivity can be considered to increase the contact efficiency between the electrolyte and electrodes [123]. Sulfide-based electrolytes have the obvious problem of a narrow electrochemical stability window in general, which results in limited application to electrodes

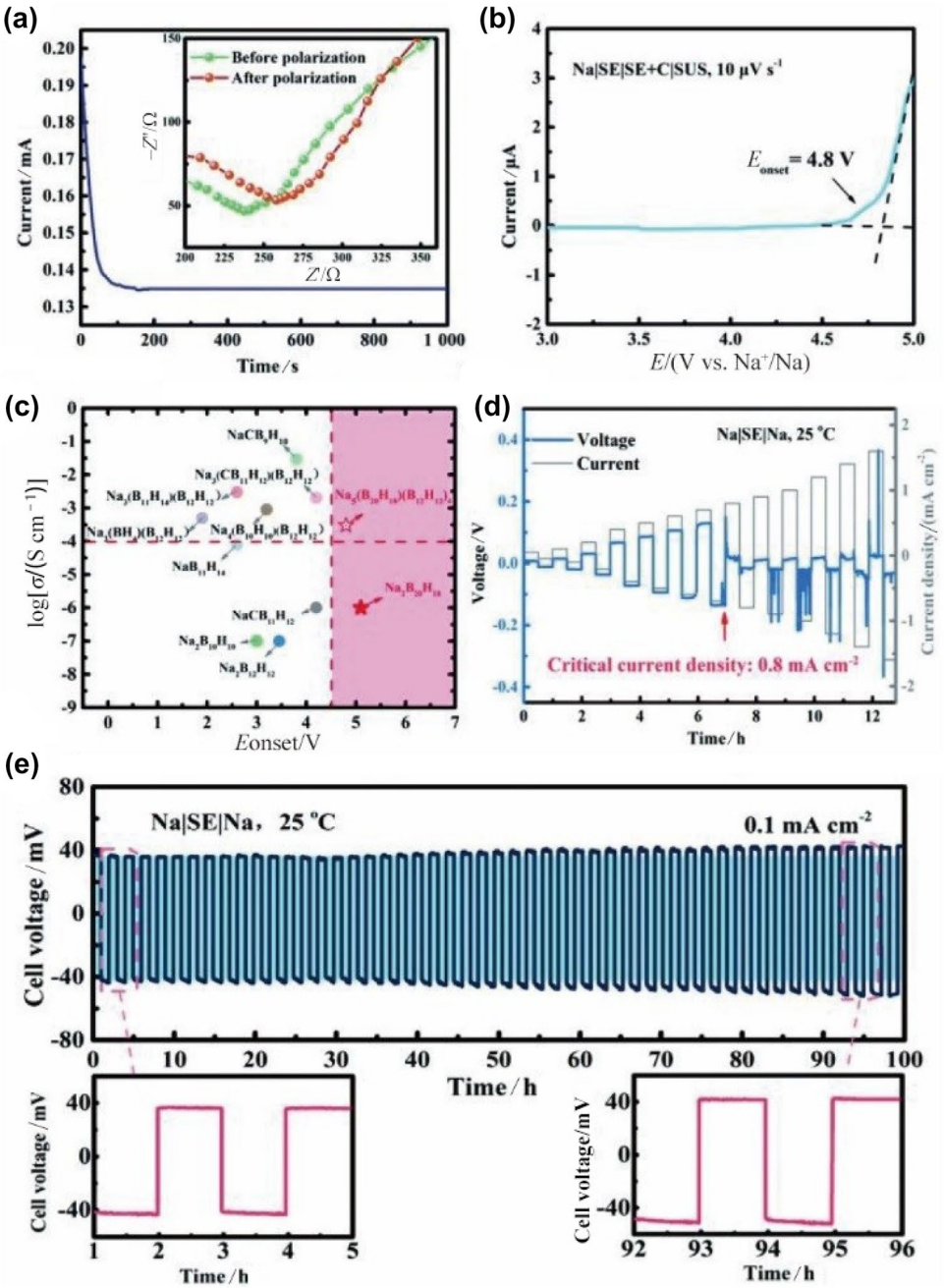

Fig. 16 **a** Current–time curves for Na|$Na_2B_{20}H_{18}$–$4Na_2B_{12}H_{12}$|Na at a polarization voltage of 10 mV. The inset shows the impedance spectra before and after polarization; **b** linear sweep voltammograms (LSVs) of $Na_2B_{20}H_{18}$-$4Na_2B_{12}H_{12}$ measured at a scan rate of 10 μV s^{-1}; **c** summary of the room temperature ionic conductivity and electrochemical stability window of various sodium hydroborate electrolytes; **d** stepped current density galvanostatic cycling of the symmetric Na|$Na_2B_{20}H_{18}$–$4Na_2B_{12}H_{12}$|Na cell; **e** galvanostatic cycling of the symmetric Na|$Na_2B_{20}H_{18}$–$4Na_2B_{12}H_{12}$|Na cell at a current density of 0.1 mA cm^{-2} for 100 h. Reprinted with permission from Ref. [75]. Copyright © 2022, Royal Society of Chemistry

with low voltage, such as TiS_2/Na–Sn. Regarding hydroborate solid electrolytes, research has been limited to date. The results of tests with SIBs have not been as good as those of the other tests. The issue of how to solve the problem with the principle of thermodynamics remains unresolved. Forming an artificial stabilized SEI may help enhance the electrochemical stability. Consequently, the constituent of the SEI that can prevent the decomposition of ISEs and improve the conduction of sodium ions still needs to be certified for each ISE.

6 Organic Solid Electrolyte

The organic solid electrolytes (OSEs) for SIBs generally consist of organic materials and sodium salts [65, 79, 124]. The most studied OSEs are solid polymer electrolytes, gel polymer electrolytes, and plastic crystal electrolytes.

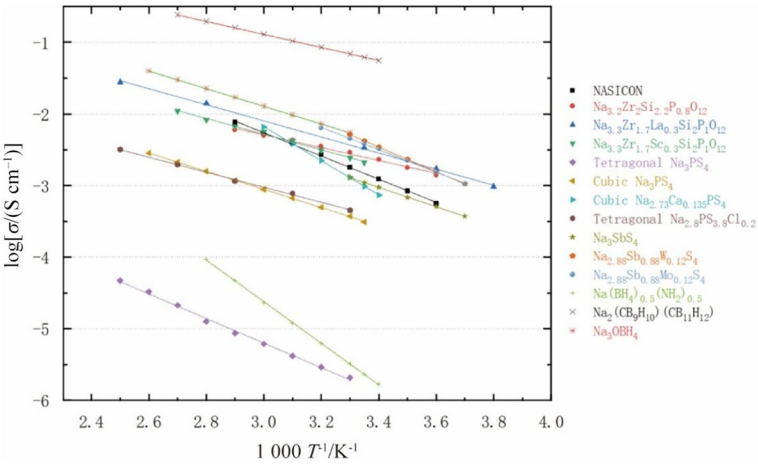

Fig. 17 Summary of the temperature dependence around room temperature of the ionic conductivity of different ISEs [99, 100, 104, 105, 109–111, 114–116, 119–121]

7 Solid Polymer Electrolytes

Solid polymer electrolytes (SPEs) consist of a type of base polymer and an electrolyte salt. It consists of a polymer matrix and alkali metal salts dissolved in the polymer matrix. In comparison with ISEs, SPEs have the advantage of mechanical flexibility, which makes them easier to process, reduces the interface impedance, and eases the expansion of the electrode [125]. In the investigation of SPEs, the ionic conductivity of this material is generally achieved by the movement of chains of base polymer [124]. To date, most research on SPEs has focused on lithium-ion batteries, which provided some guidance in developing SPEs of SIBs.

7.1 PEO-Based SPEs

The polymer poly(ethylene oxide) (PEO) has been an important component of solid electrolytes for a long time. It was first reported by Wright et al. that the compound of NaSCN/PEO and NaI/PEO had the ability for ion conduction, which was deemed to be the beginning of the research on PEO-based solid electrolytes [126]. Xue et al. [127] demonstrated that the mechanism of lithium transportation in the PEO matrix was that the cation was delivered by interchain or intrachain oxygen atoms. In the PEO matrix, sodium behaves in a similar manner to lithium [128]. Occasionally, the electrolyte molecule can assist the cation in being hooped, as shown in Fig. 18.

The ionic conductivity of the PEO-based electrolytes ($< 10^{-6}$ S cm^{-1} at R.T.) is typically lower than that of ISEs, which is due to the high crystallinity of PEO at room temperature. Despite the extensive studies that have been conducted on the solid electrolytes of PEO in solid-state lithium batteries, their ionic conductivity at room temperature is too low, so a higher operating temperature of 50–60 °C is necessary [127, 129]. Based on the ion transport mechanism above, the main strategy to increase conductivity is to reduce the crystallinity of PEO through copolymerization, plasticization, and filler addition. Recently, Devi et al. [128] reported a novel SPE that was synthesized by PEO and polyvinylpyrrolidone (PVP) blended with a sodium

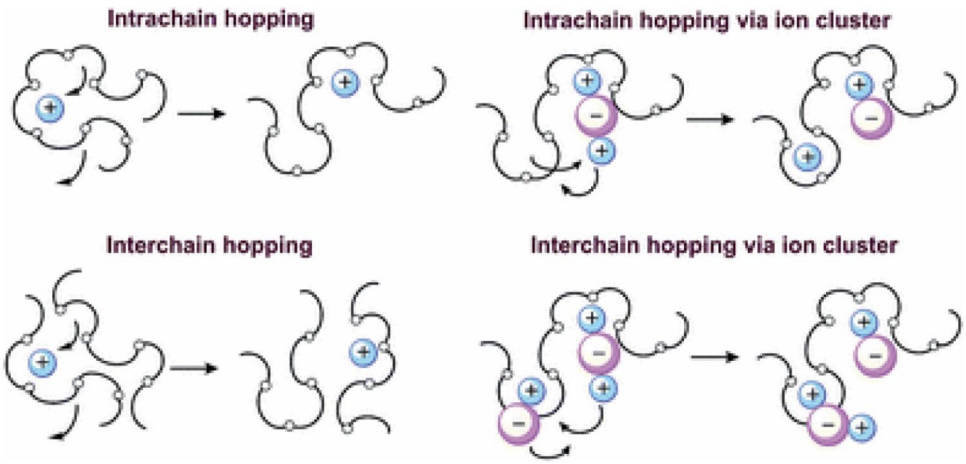

Fig. 18 Mechanism of ion transportation of PEO-based electrolytes. Reprinted with permission from Ref. [127]. Copyright © 2015, Royal Society of Chemistry

hexafluorophosphate ($NaPF_6$) electrolyte in the presence of InAs nanowires. They showed that due to the introduction of InAs, the crystallinity of the copolymer decreased, and the number of flexible chains in the amorphous phase increased. The ionic conductivity was measured to be 1.5×10^{-4} S cm^{-1} at a maximum of 40 °C with 1 wt% InAs. The synthesized PEO–PVP–$NaPF_6$–InAs SPE also showed potential application for lightweight materials. According to the linear sweep voltammetry (LSV) data, the electrochemical stability window was identified as 4.1 V at 40 °C. Although a test with SIBs was not mentioned by the authors, it is convincing that with the addition of InAs nanowires, the PEO-based SPE showed an enhanced electrochemical performance at 40 °C. Similarly, Shenbagavalli et al. [130] reported that SPEs for SIBs based on PEO/PVP and sodium nitrate ($NaNO_3$) with Al_2O_3 added were successfully synthesized. According to the characterization, the PEO–PVP–$NaNO_3$–Al_2O_3 SPE showed a maximum ionic conductivity of 1×10^{-5} S cm^{-1} at room temperature and an electrochemical stability window of approximately 2.69 V, which indicated poor application potential for energy storage devices. The increase in the amorphous phase of PEO was monitored by XRD with the addition of filler concentration. The complexation between the polymer, salts, and filler was observed and detected by Fourier transform infrared spectroscopy (FTIR). The electrochemical performance of the PEO–PVP–$NaNO_3$–Al_2O_3 SPE showed that the enhancement of the electrochemical stability window was also significant.

The use of ISEs as a filler is also possible in addition to the use of inorganic compound fillers for PEO-based SPEs. Yao et al. [131] demonstrated that a PEO-based SPE with the addition of sodium conductive beta-alumina (β''-Al_2O_3) nanoparticles showed promising chemical and electrochemical performance. As shown in Fig. 19a–d, the SPE composed of PEO, $NaClO_4$ and 0–15 wt% beta-alumina was assembled as a $Na_3V_2(PO_4)_3$/SPE/Na system to evaluate the electrochemical performance at 60 °C. With the addition of beta-alumina, the initial capacity, rate performance, and cycling stability of the SPE were better than those without beta-alumina. According to the thermogravimetric analysis (TGA) and differential scanning calorimetry (DSC) results shown in Fig. 19e, f, the thermal stability was enhanced by the addition of beta-alumina, and the glass transition temperature was decreased due to the decreasing crystallinity of the polymer matrix. The ionic conductivity was found to increase with the addition of beta-alumni due to the reduced crystallinity and quick transition of sodium ions at the interface between the active filler and polymer. In addition, SPEs have a stable electrochemical window above 5 V, as determined by LSV measurements, which indicates that the process is stable enough to be used in a practical environment.

ILs are nonflammable and nonvolatile and are safe to apply to batteries, especially electrolytes. ILs can also act as plasticizers of SPEs to reduce the interaction between chains of base polymers so that the crystallinity is reduced, leading to enhancement of ionic conductivity. Chen et al. claimed that a novel PEO-based SPE was synthesized by using sodium perchlorate ($NaClO_4$) and *N*-methyl-*N*-propylpyrrolidinium bis(fluorosulfonyl)imide IL ($Pyr_{13}FSI$) [132]. The composition of this PEO–$NaClO_4$–$Pyr_{13}FSI$ SPE is shown in Fig. 20a, b. As shown in the figure, it was believed that the FSI^- anion was combined with the PEO chain by hydrogen bonding. The combination not only decreased the crystallinity of the base polymer, but more sodium ions were associated with the base polymer. As a result, the SPE with 40 wt% PEO exhibited an improved ionic conductivity of 6.8×10^{-5} S cm^{-1} at room temperature compared with that of ~ 10^{-7} S cm^{-1} for the pure PEO-based SPE. The jumps in ionic conductivity displayed in Fig. 20c indicated that phase transformation occurred between 50 and 60 °C, which was then corroborated by DSC characterization. The electrochemical stability window was also investigated by LSV, and the curve demonstrated that with the addition of $Pyr_{13}FSI$, the electrochemical stability window grew from 3.70 to 4.44 V, as shown in Fig. 20d. The enhanced electrochemical stability of the synthesized SPE made it a viable candidate for use as a solid electrolyte for high-voltage SIBs. $Na_3V_2(PO_4)_3$/SPE/Na solid-state batteries were assembled to evaluate the electrochemical performance. After activation, the enhanced reversibility of the battery was analyzed by using the charge–discharge curve from the first cycle to the tenth, as shown in Fig. 20e. Additionally, from Fig. 20f, a comparison of the retention rate within 70 cycles between the SPEs with IL and without IL showed an influence of the limited ionic conductivity and electrochemical stability window. Finally, the rate performance of the SPE with IL, especially at 1 C and 2 C, was found to show significant progress compared to that of the SPE without IL. The electrochemical performance of the optimized SPE exhibited great potential for application in high-voltage SIBs.

In addition to ILs, liquid crystals (LCs) have been identified as another plasticizer for base polymers because LCs can form a continuous phase with low viscosity for metal ions among the polymer matrices [133]. The characteristics of intermediate crystallization and isotropy can also enhance the transportation ability of metal ions. Koduru et al. [134] claimed that a PEO/E8 LC-based SPE containing sodium meta periodate ($NaIO_4$) was successfully synthesized. According to the results of XRD and micro-Raman spectroscopy, the crystallinity was inhibited by the addition of LCs. The LC-based SPE with 10 wt% $NaClO_4$ showed an ionic conductivity of 1.05×10^{-7} S cm^{-1} at room temperature. Furthermore, the ion transfer number of cations (0.384) was lower than that of anions (0.513), indicating an incompatibility of $NaClO_4$ with the LC-based SPE system. Despite the fact that the ionic conductivity and ion transfer

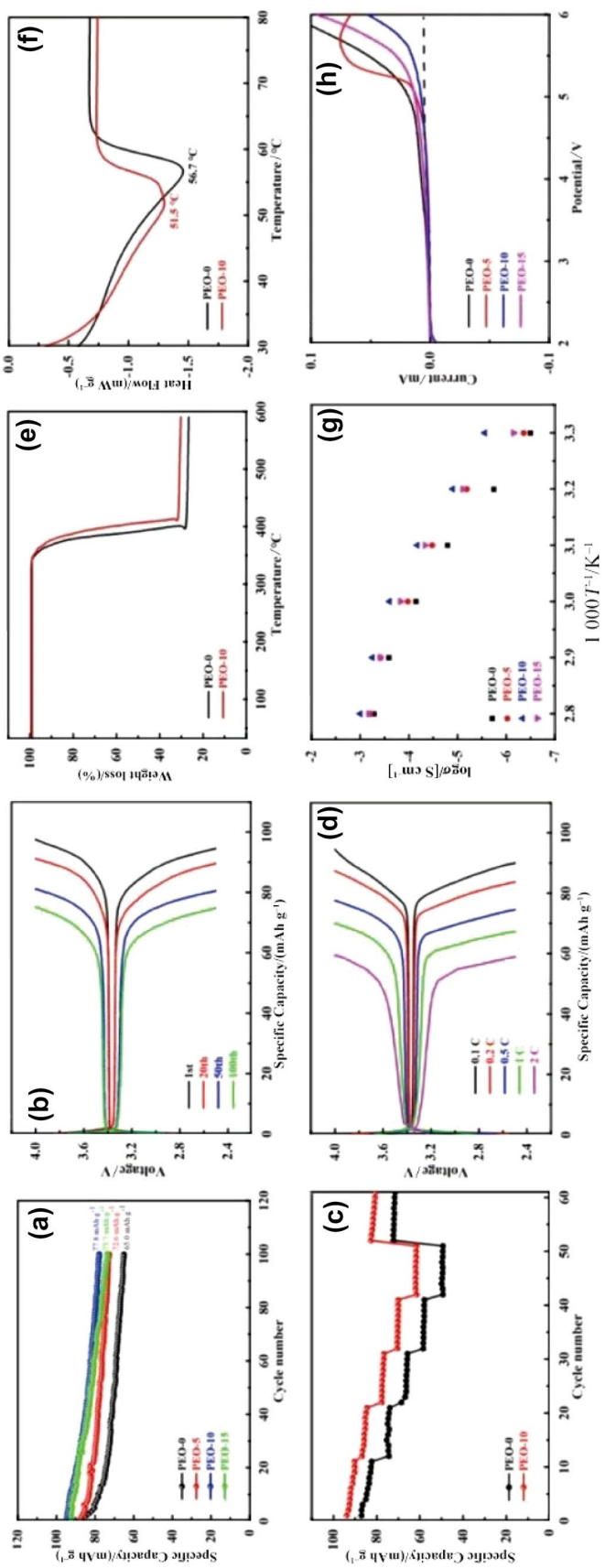

Fig. 19 **a** Cyclic performance; **b** charge/discharge profile; **c** rate performance; **d** charge/discharge curve of different rates of $Na_3V_2(PO_4)_3$/SPEs/Na batteries at 60 °C; **e** TGA curve; **f** DSC curve of PEO-based SPEs; **g** temperature dependence of ion conductivity; **h** LSV curve of synthesized PEO-based SPEs. Adapted with permission from Ref. [131]. Copyright © 2021, Springer

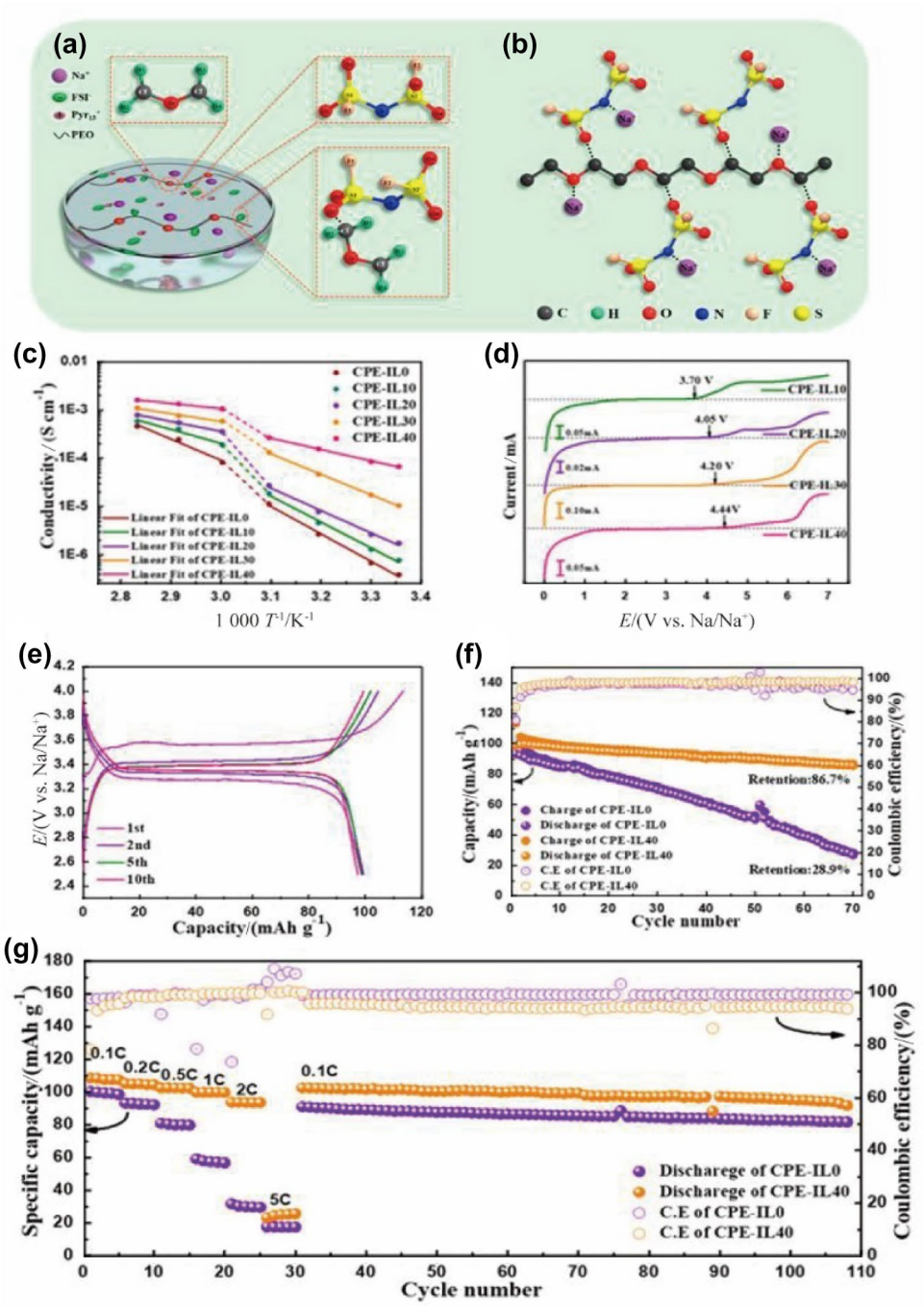

Fig. 20 **a** Composition of PEO-$NaClO_4$-$Pyr_{13}FSI$; **b** schematic illustration of hydrogen bonds between PEO and $Pyr_{13}FSI$; **c** temperature dependence ionic conductivity of SPEs; **d** LSV curves of SPEs with different ILs; **e** charge–discharge curves; **f** cycling performance; **g** rate performance of the $Na_3V_2(PO_4)_3$/SPE/Na cell at 0.1 C and 60 °C. Adapted with permission from Ref. [132]. Copyright © 2019, American Chemical Society

number of LC-based SPEs were not excellent, a new method of enhancing ionic conductivity was developed.

In the field of nanotechnology, metal–organic frameworks (MOFs) are nanoporous materials with high specific surface areas, ordered channels, and stable structures. PEO segment movement can be improved, and salt dissociation can be increased [135, 136]. Similarly, Ge et al. [137] synthesized a flexible PEO–$NaCF_3SO_3$–MIL-53(Al) SPE (PNM–SPE) by the solution casting method. MIL-53(Al) was synthesized by treating aluminum nitrate nonahydrate and 1,4-benzenedicarboxylic acid. Figure 21a illustrates the excellent flexibility of the PNM–SPE, indicating its potential use in flexible foldable batteries. The SPE consisting of 3.24 wt% MIL-53(Al) and an EO 20:Na 1 ratio exhibited the highest ionic conductivity of 6.87×10^{-5} S cm^{-1} at 60 °C. The sodium ion transference number of PNM–SPE was found to be 0.40, which was much higher than that of the SPE without the addition of MIL-53(Al). This is due to the Lewis acidity of MIL-53(Al), which helped to attract the anions of sodium salt. The electrochemical stability window was

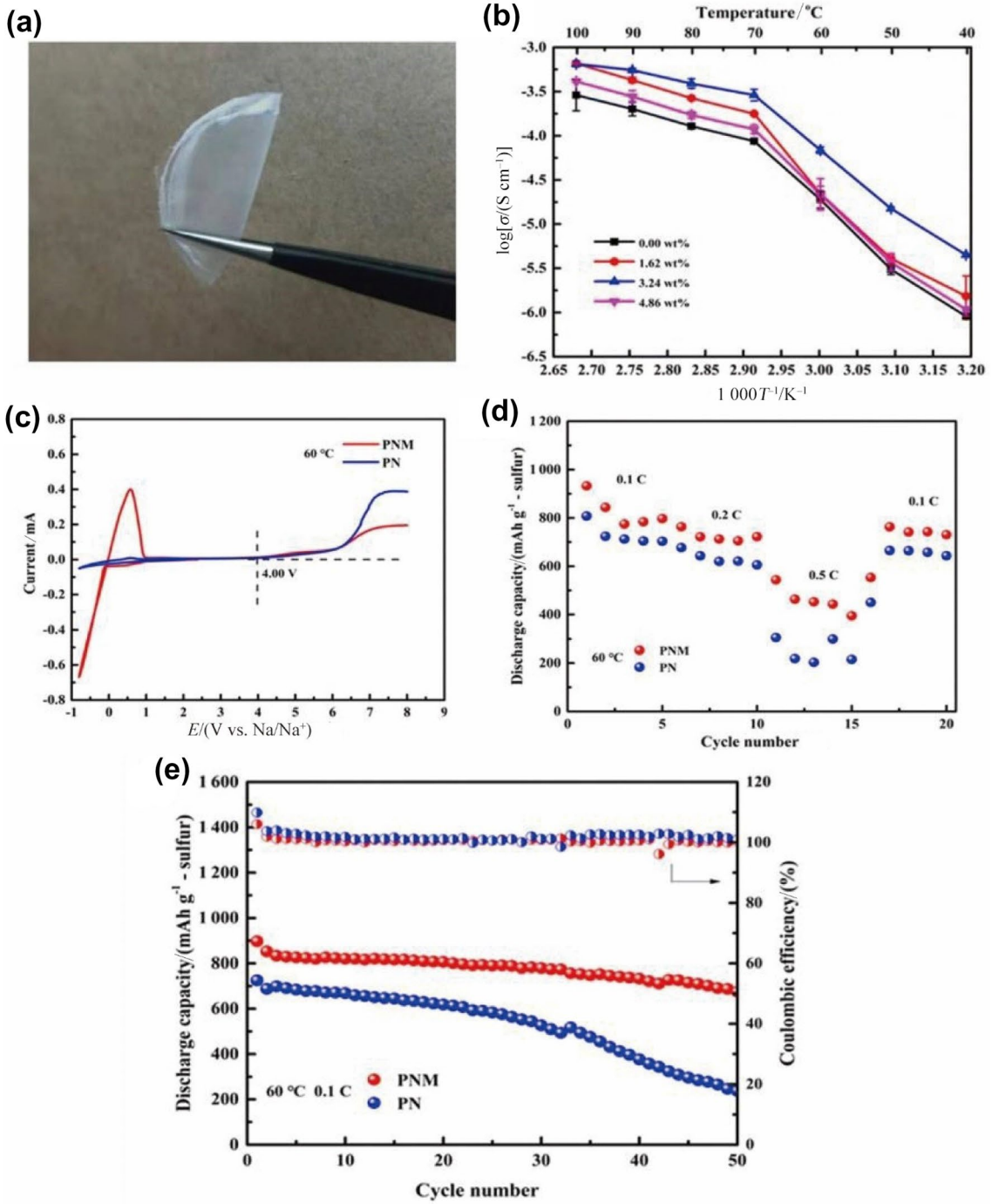

Fig. 21 **a** Photograph of the flexible PNM–SPE; **b** temperature dependence of ionic conductivity of the PNM–SPE with different percentages of MIL-53(Al); **c** cyclic voltammograms curve; **d** rate performance from 0.1 to 0.5 C at 60 °C; **e** cycling performance of the PNM-SPE and PN-SPE at 60 °C. Adapted with permission from Ref. [137]. Copyright © 2020, Springer-Verlag GmbH Germany, part of Springer Nature

determined to be 4.0 V at 60 °C, according to Fig. 21c. There is an electrochemical deposition of sodium on the PNM–SPE electrode at a voltage of 0.07 V and a temperature of 60 °C, which indicates a reversible process of Na plating/stripping. The rate performance of the ASSBs assembled with the PNM–SPE and PN–SPE at 60 °C is shown in Fig. 21d, and the cycling performance is shown in Fig. 21e. A higher capacity and stability were achieved by the application of MIL-53(Al).

7.2 PVDF-Based SPEs

Poly(vinylidene fluoride) (PVDF) is believed to be a fictional material that possesses great chemical and physical properties and has become a kind of commercial product [138]. Bristi et al. [139] reported a novel PVDF, PVP polymer binder, and $NaPF_6$ salt-based SPE. PVDF-based SPEs for SIBs were examined under different $NaPF_6$ salt concentrations, as well as with the SiO_2 nanofiller and PVP binder. For convenience, SPEs of PVDF/$NaPF_6$ (4:1) + PVP (11 wt% of PVDF), PVDF/$NaPF_6$ (9:1) + PVP (11 wt% of PVDF) and PVDF/$NaPF_6$ (17:1) + PVP (11 wt% of PVDF) were recognized as SPE-1, SPE-2, and SPE-3, respectively. The ionic conductivity performance, as shown in Fig. 22a, indicated that SPE-2 possessed the highest ionic conductivity at room and higher temperatures. Most likely, the difference was due to the easier possibility of ion hopping in SPE-2 than in SPE-1 and SPE-3 when $NaPF_6$ salt was present in the amorphous PVDF. In symmetric cell configurations of Na|LE/C|SPE-2|LE/C|Na, where LE was composed of 20 µL of 1 M (1 M = 1 mol L^{-1}) $NaClO_4$ in EC/PC (1:1), Na plating–stripping experiments were conducted to determine the compatibility and stability of the SPE with a Na metal anode. As shown in Fig. 22b, during the 400 cycles of 800 h, good electrochemical stability was achieved for the Na plating-stripping performance. A maximum specific capacity of 105.5 mAh g^{-1} was achieved (Fig. 22c) when assembled as the NVP|LE/C|SPE-2|LE/C|Na battery. With a discharge capacity of 93.20 mAh g^{-1}, a 3.3 V discharge plateau was observed at the same rate for the first cycle, indicating a reduction of $NaV_2^{(IV)}(PO_4)_3$ to $Na_3V_2^{(III)}(PO_4)_3$. The NVP electrode showed excellent cycling performance after 100 consecutive charge–discharge cycles at

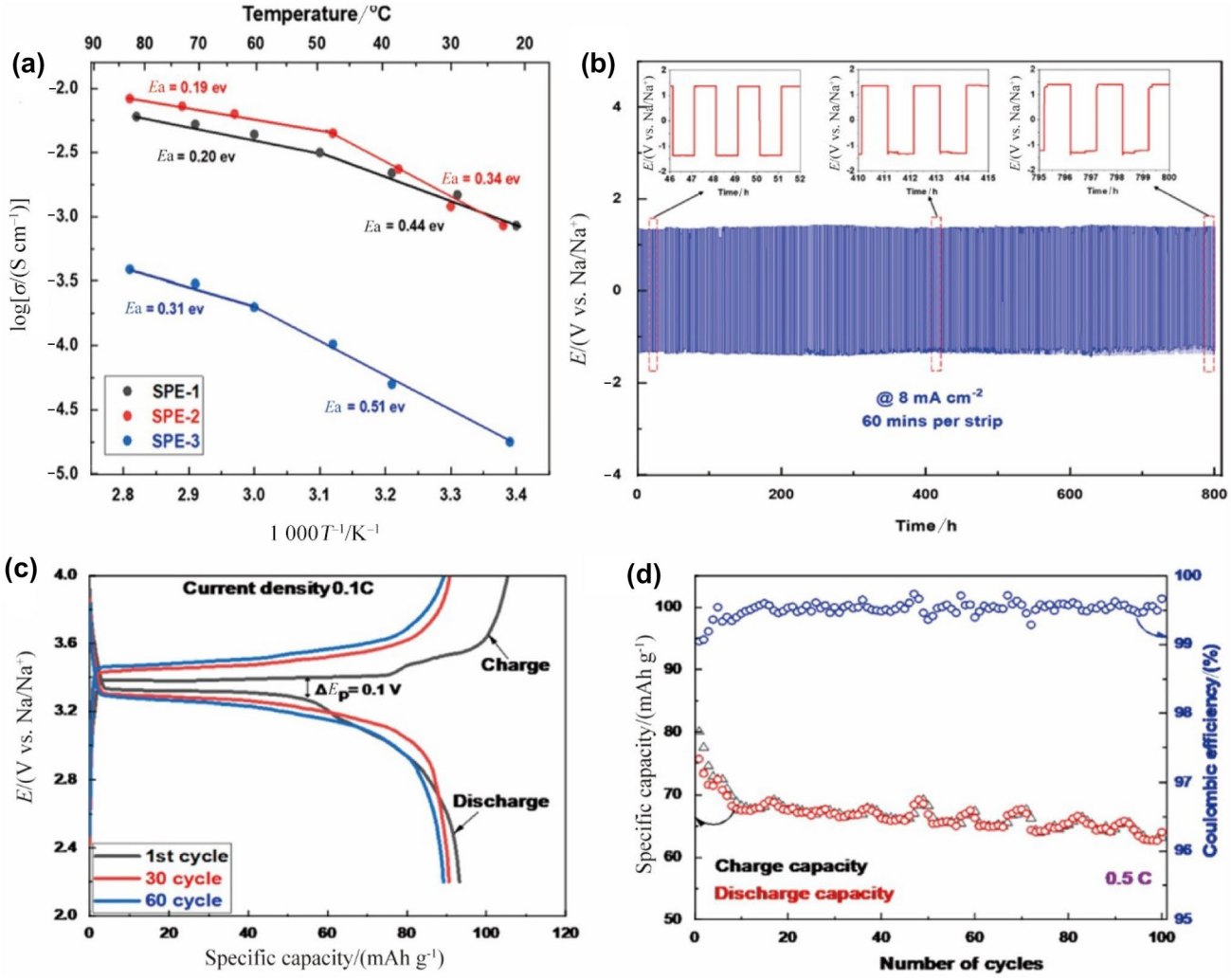

Fig. 22 **a** Temperature dependence of ionic conductivity from SPE-1 to SPE-3; **b** galvanostatic cycling profiles of the symmetric cell Na|LE/C|SPE-2|LE/C|Na; **c** charge–discharge curve of the NVP|LE/C|SPE-2|LE/C|Na battery at 0.1 C; **d** cycling performance of the NVP|LE/C|SPE-2|LE/C|Na battery at 0.5 C. Adapted with permission from Ref. [139]. Copyright © 2022, American Chemical Society

a 0.5 C rate, retaining 86% of its capacity after 100 cycles. It was concluded that PVP binders can contribute significantly to fast Na ion conductivity and excellent Na plating-stripping performance in PVDF-based composite systems.

Bag et al. reported the synthesis and characterization of a novel PVDF-based composite polymer electrolyte (CPE) with the $NaCF_3SO_3$ salt and SiO_2 filler [140]. The CPE was synthesized by casting a slurry of PVDF solution ball milled with SiO_2 powder, as shown in Fig. 23a. Compared to the PVDF–$NaCF_3SO_3$ electrolyte, the ionic conductivity was improved from 2.1×10^{-6} to 6.3×10^{-5} S cm^{-1}. The symmetric sodium cell in Fig. 23c indicated that the synthesized CPE was compatible with sodium. The electrochemical profile of the NVP|CPE|Na cell at 2–4 V and a 0.5 C rate is shown in Fig. 23e, f. A liquid electrolyte of 5 µL was applied to both sides of the CPE. With 86% capacity retention after 250 cycles, the NVP electrode demonstrated outstanding cycling performance. A symmetric NVP full cell was fabricated by using the NVP electrode and the CPE as the electrolyte, as shown in Fig. 23d. It was found to be able to deliver a high specific capacity of 76 mAh g^{-1} with an energy density of 126 Wh kg^{-1} at 0.5 C. As a result, its specific capacity retained 70% of its original value after 100 cycles.

Wang et al. [141] reported the synthesis of an organic ionic plastic crystal (OIPC)-modified PVDF using the electrospinning method. It was demonstrated that the electrolyte of pure PVDF by electrospinning had two phases: an electroactive β phase and a nonactive α phase. With the OIPC added, which was *N*-ethyl-*N*-methylpyrrolidinium tetrafluoroborate [C_2mpyr][BF_4], the prepared composite SPE showed no α phase. The ionic conductivity of the synthesized SPE in different weight percentages of OIPC is shown in Fig. 24. The ionic conductivity of this SPE is detected to be 1.2×10^{-6} S cm^{-1} at room temperature, measured with a single fiber.

Recently, it was stated by Makhlooghiazad et al. [142] that an original electrolyte of PVDF and triisobutyl(methyl) phosphonium bis(fluorosulfonyl)imide ([P_{1i444}][FSI]) OIPC

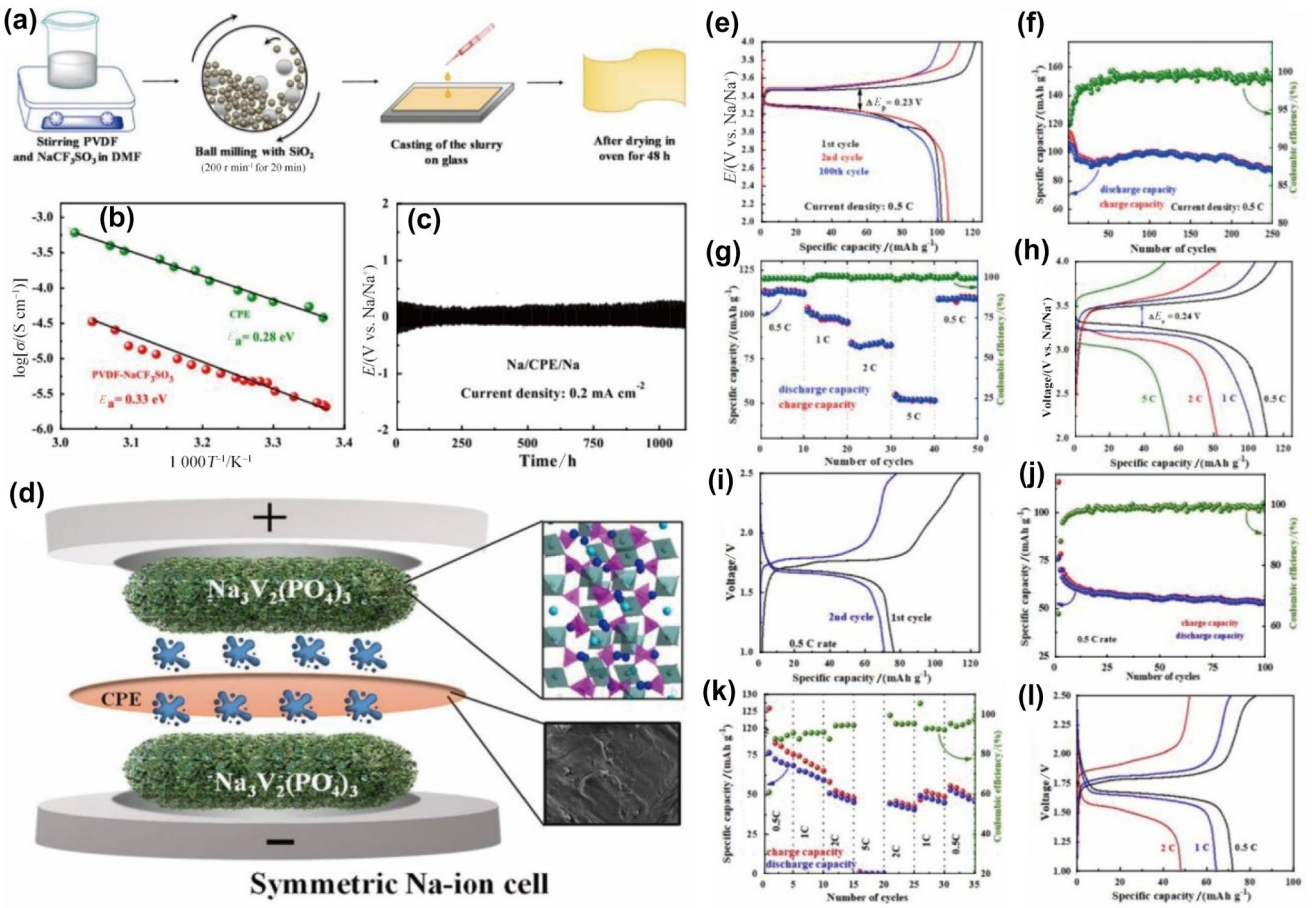

Fig. 23 **a** Schematic illustration of the synthesis process of CPEs; **b** Arrhenius plot for PVDF-$NaCF_3SO_3$ and CPEs; **c** cycling performance of the sodium symmetric cell with CPEs; **d** schematic illustration of the NVP symmetric cell; **e** charging-discharging curve; **f** cycling performance; **g** rate performance; **h** rate charging-discharging curve of the NVP|CPE|Na cell; **i** charging–discharging curve; **j** cycling performance; **k** rate performance; **l** rate charging-discharging curve of the NVP|CPE|NVP symmetric cell. Adapted with permission from Ref. [140]. Copyright © 2020, Elsevier

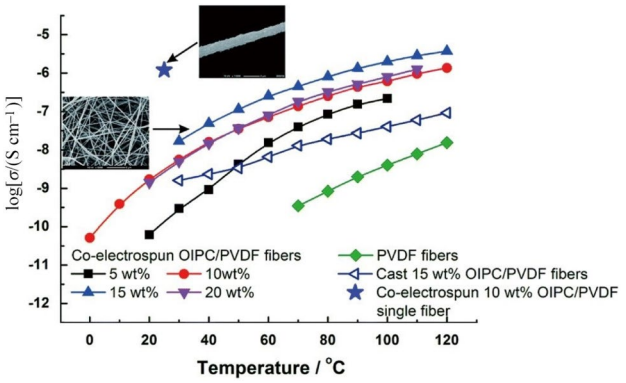

Fig. 24 Ionic conductivity of PVDF/OIPC (5–20 wt%) fibers at different temperatures. Reprinted with permission from Ref. [141]. Copyright © 2016, Royal Society of Chemistry

was prepared with sodium bis(fluorosulfonyl)amide (NaFSI) or sodium bis(trifluoromethanesulfonyl)amide (NaTFSI). The synthesized composite electrolytes showed excellent performance of ionic conductivity of 20 mol% NaFSI of 2.1×10^{-3} S cm^{-1} and 20 mol% NaTFSI of 2.5×10^{-3} S cm^{-1}. The reason for the difference between the NaFSI-based and NaTFSI-based SPEs was that the $TFSI^-$ anion had stronger interactions with PVDF so that a layer possessing higher conductivity for sodium ions formed on the PVDF fibers. Figure 25a, c together introduces the performance of a symmetric Na|SPE|Na cell based on NaFSI and NaTFSI, respectively. For the NaTFSI-based system, a short circuit occurred after two cycles when the current density was increased to 0.5 mA cm^{-2}. It is unclear what caused this behavior, but it is being investigated. In addition, both cells exhibit a very similar high-frequency impedance, which indicates similar ionic conductivity, because high-frequency impedance corresponds to bulk electrolyte resistance, as shown in Fig. 25b, d. Assembled as NVP|SPE|Na solid-state batteries, the electrochemical performance at 50 °C was investigated, as shown from Fig. 25e–h. A remarkable rate capability of the batteries, delivering reversible capacity from 1/20 C to 1 C, was demonstrated for both NaFSI-based and NaTFSI-based systems. Both systems exhibited excellent cycling performance with reversible rates of 98.0% and 98.5% for NaFSI and NaTFSI, respectively. Accordingly, the specific capacity of the NaTFSI-based system was higher than that of the NaFSI-based system. Moreover, the polarization of the mixed anion-based composite cell was lower (20 mV) than that of the cell containing NaTFSI (40 mV), reflecting the higher ionic conductivity of the NaTFSI-based system, as shown in Fig. 25g, h. The combination of PVDF and OIPC provided a new idea to improve the ionic conductivity of SPEs. Further development can be focused on improving the compatibility of polymers with OIPC and reducing the costs of both polymers and OIPC.

Fang et al. [143] reported the synthesis of an ultrathin composite polymer electrolyte consisting of PVDF/sodium β-alumina ceramic electrolyte (SBACE)/$NaPF_6$. The sodium beta-alumina ceramic particles were screened before synthesis to ensure the thickness of the membrane, as shown in Fig. 26a. The highest ionic conductivity of the ultrathin single particle layer (ULSPL) membrane, namely ULSPL-35SBACE, which indicated 35 wt% SBACE of the electrolyte, was tested to be 0.19 mS cm^{-1}. The symmetric Na/Na cells were cycled with different electrolytes to evaluate their compatibility with the sodium anode and to calculate the Na^+ transference number. Similarly, the UTSPL-35SBACE membrane showed a high Na^+ transference number of 0.91, indicating free Na^+ ions in the UTSPL-35SBACE membrane. According to Fig. 26d–f, the ULSPL-35SBACE membrane also showed the best stability at higher current density. An evaluation of the cycling stability and rate performance of cells with the UTSPL-35SBACE membrane was conducted by using potassium manganese hexacyanoferrate (KMHCF) cathodes. With a capacity retention of 95.5% after 100 cycles, Na/KMHCF@CNTs/CNFs cells with the UTSPL-35SBACE membrane displayed good cycling performance.

Although additives and inorganic fillers have been applied to SPEs to increase the performance of ionic conductivity, there is still a giant gap between actual and required performances. The most important part is to determine how to establish a sodium-ion transport channel. In addition, the principle of additives and inactive inorganic fillers is still in doubt, which prevents us from finding a shortcut to select a suitable combination of polymers and additives. A high interfacial resistance is also indicative of difficulties at the interface between SPEs and electrodes.

7.3 Other SPEs

Considering the inspiration from the natural world and the cost, carboxymethyl cellulose (CMC) has been considered a proper polymer to form SPEs. Shetty et al. [144] investigated the biodegradable SPE of poly(vinyl alcohol) (PVA)/sodium salt carboxymethyl cellulose (NaCMC) (PVA/NaCMC with a ratio of 70:30) doped with sodium bromide (NaBr) metal salt. The SEM images of the SPEs based on different mass ratios of NaBr, which were 0 wt%, 5 wt%, 10 wt%, and 15 wt%, indicated that free volumes or voids existed when NaBr was added, as shown in Fig. 27a. In addition, the amorphous phase was enhanced by the increasing free volume. Thus, the ionic conductivity at room temperature of the SPEs based on different ratios of NaBr showed a positive correlation with mass scores, as shown in Fig. 27b.

Similarly, Cyriac et al. [145] studied the effect of the $NaNO_3$ salt concentration (0, 5, 10, 15, 20, 25, and 30 wt%) on the structural, electrical, and mechanical properties of Na-CMC/PVA SPE films. The potential mechanism of the

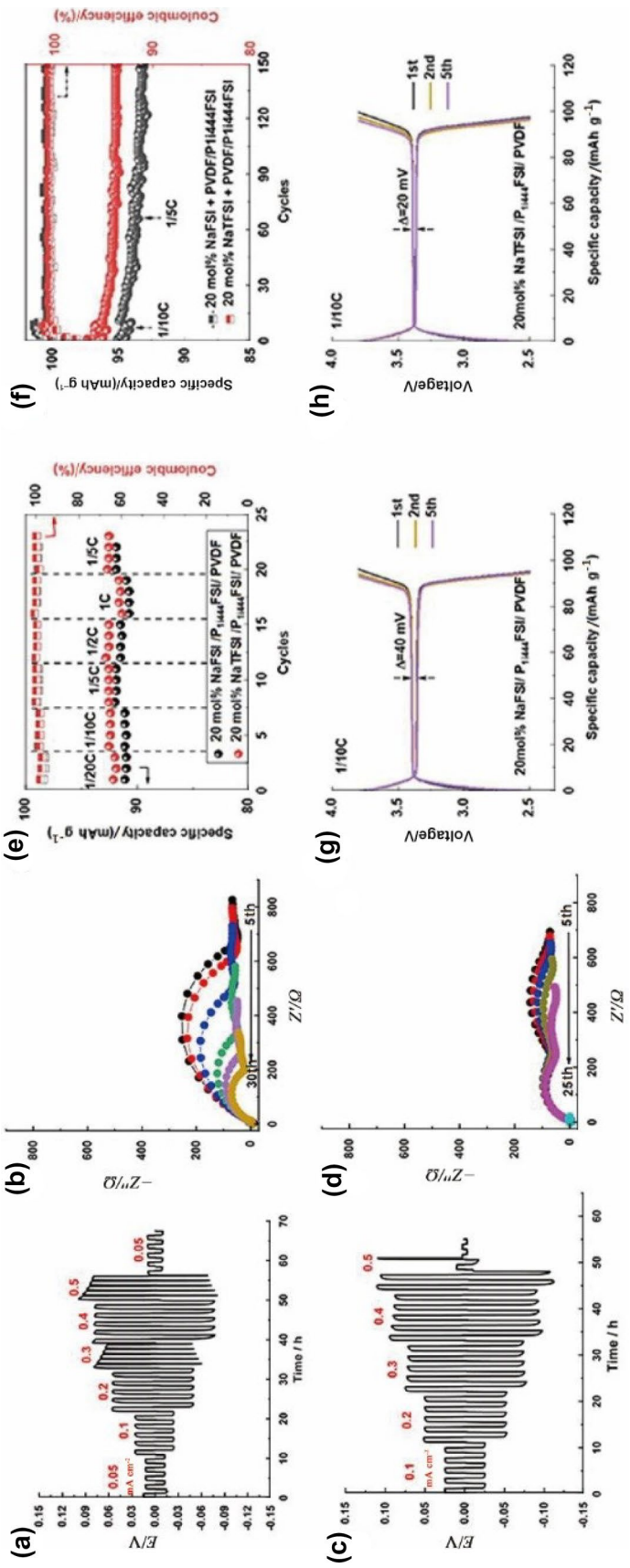

Fig. 25 **a** and **c** Na symmetric cell cycling of NaFSI- and NaTFSI-based SPEs at various current densities; **b** and **d** Nyquist plots of the cell in **a** & **c** every 5 cycles; **e** rate performance from 0.05 to 1 C; **f** cycling performance of NVP|SPE|Na of NaFSI- and NaTFSI-based SPEs; **g** and **h** the cell charge–discharge curve of NaFSI- and NaTFSI-based SPEs at 0.1 C [142]

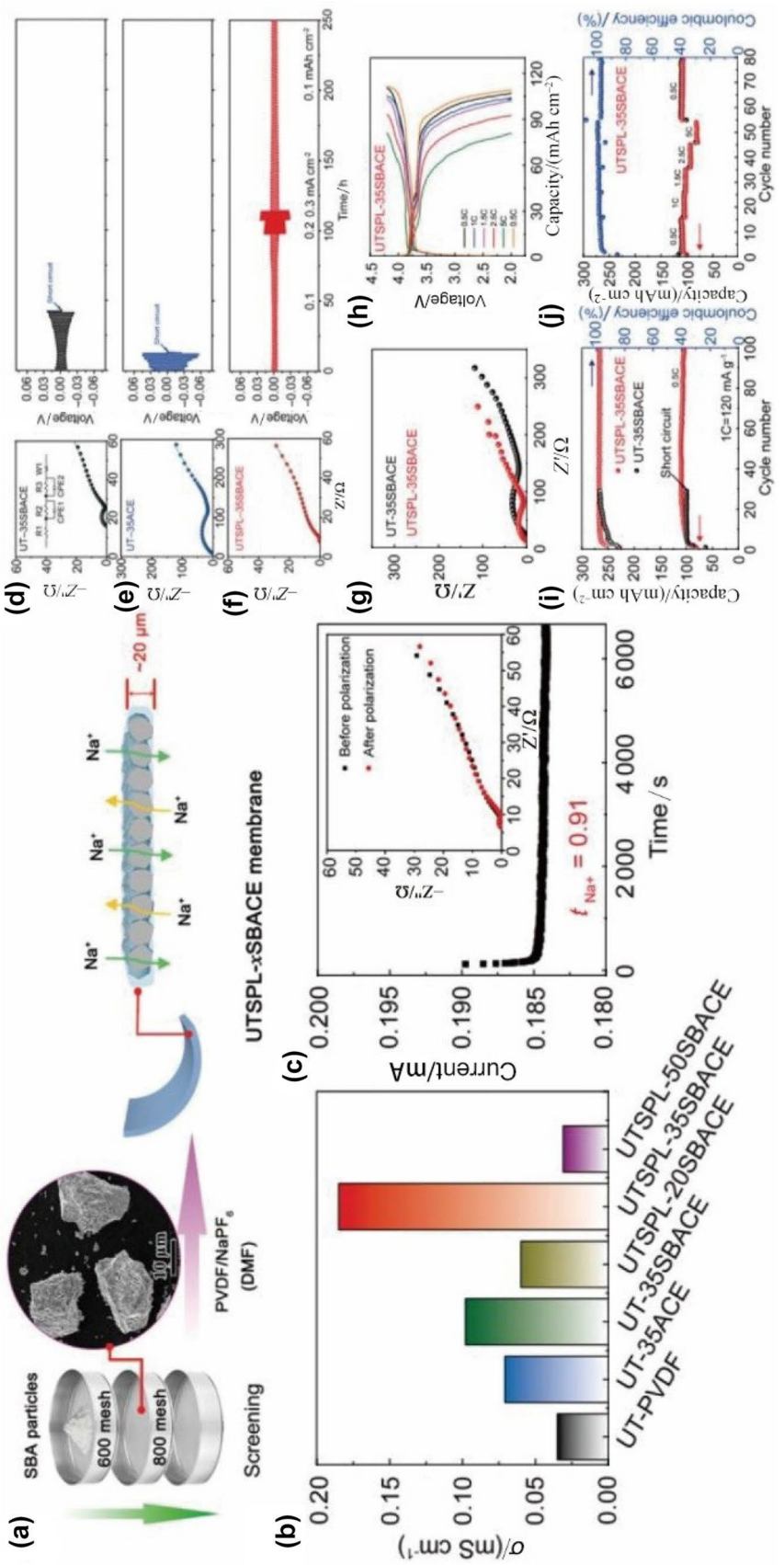

Fig. 26 **a** Schematic illustration of the UTSPL-*x*SBACE membrane structure; **b** ionic conductivity of UTSPL membranes at room temperature; **c** Na^+ transference number test of the UTSPL-35SBACE membrane; **d–f** cycling performance of the sodium symmetric cell applying UT-35SBACE, UT-35ACE and UTSPL-35SBACE, separately; **g** Nyquist plot; **h** charging-discharging curves from 0.5 to 5 C; **i** cycling performance at 1 C; **j** rate performance of Na/KMHCF@CNTs/CNF cells applying UT-35SBACE and UTSPL-35SBACE. Adapted with permission from Ref. [143]. Copyright © 2022, John Wiley and Sons

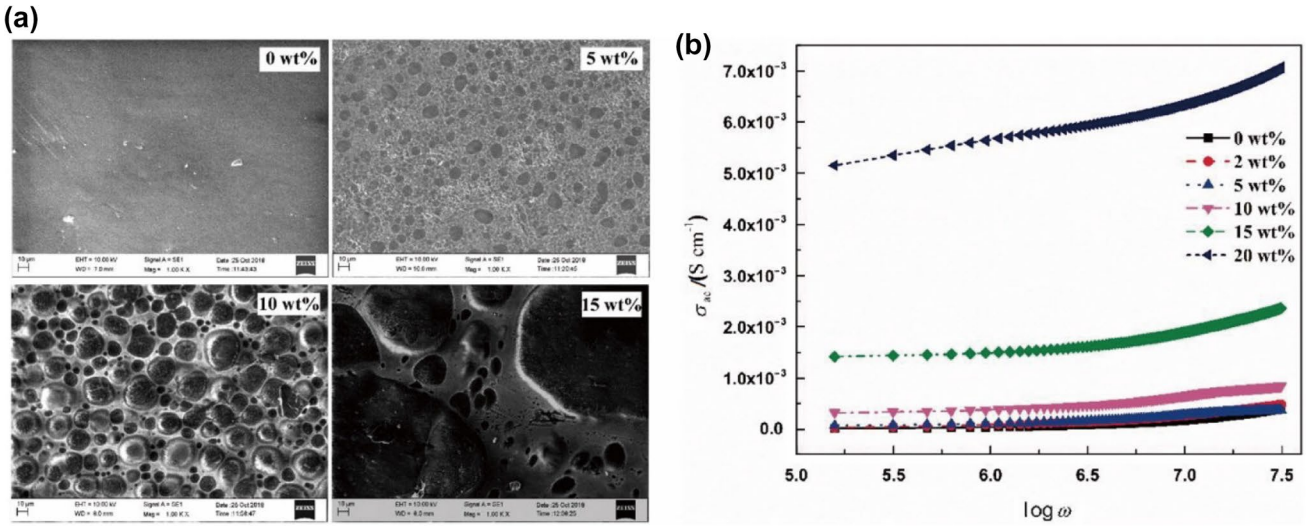

Fig. 27 **a** SEM images and **b** ionic conductivity of pure and NaBr-doped PVA/CMC SPEs. Adapted with permission from Ref. [144]. Copyright © 2021, Taylor & Francis

transportation of sodium ions was studied. Na-CMC and PVA were considered to be connected by hydrogen bonds between the –OH group of Na-CMC and the C=O group of PVA. The formation of hydrogen bonds decreased the crystallinity of the polymer matrix. With the addition and dissociation of $NaNO_3$ salt, the NO_3^- anion was combined with the formation of hydrogen bonds with the Na-CMC chain so that sodium ions could freely transport, as shown in Fig. 28a. Therefore, the ionic conductivity was increased by the addition of $NaNO_3$ salt, which can be observed in Fig. 28b. In the test of the electrochemical stability window, the SPE was tested to have an electrochemical stability window of 3.29 V.

In addition to drug delivery, poly(ethylene glycol) diacrylate (PEGDA) can be used for tissue engineering and

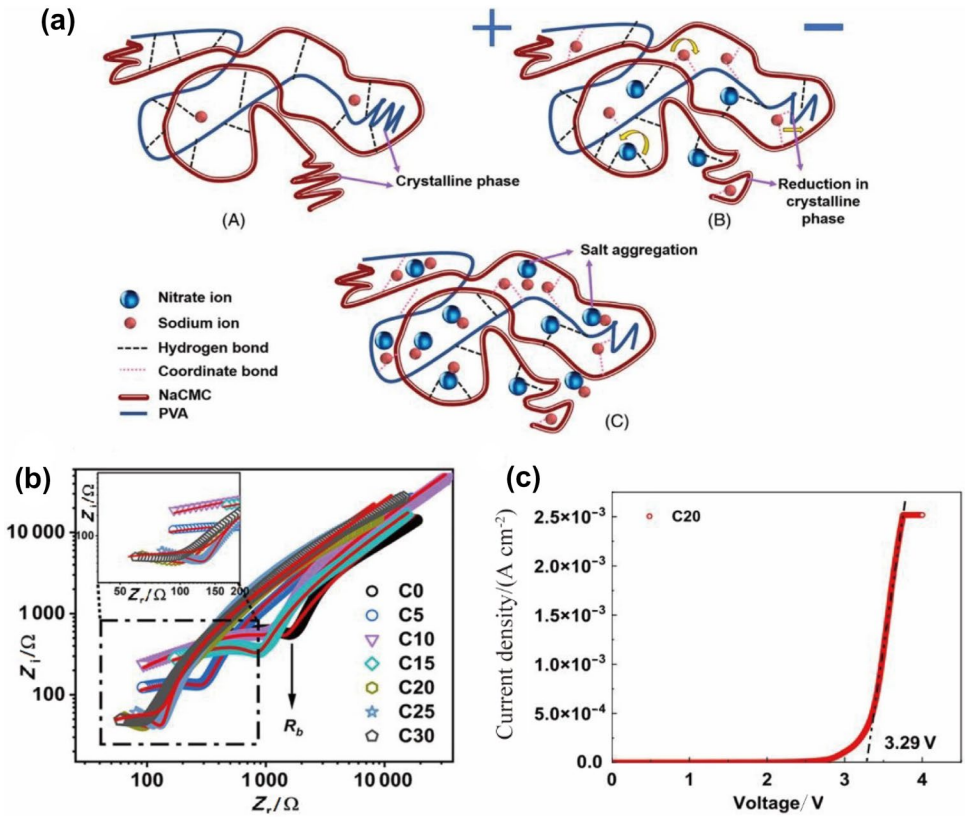

Fig. 28 **a** Schematic illustration of the microstructure of NaCMC/PVA SPEs after the addition of $NaNO_3$ salt; **b** Nyquist plot of SPEs with different mass ratios of $NaNO_3$ salt; **c** electrochemical stability window of SPEs with 20 wt% $NaNO_3$ salt. Adapted with permission from Ref. [145]. Copyright © 2022, John Wiley and Sons

tissue regeneration as a derivative of PEO. Xingwen et al. [146] reported the incorporation of ceramic $Na_3Zr_2Si_2PO_{12}$ nanopowders into a PEGDA polymer matrix to form a novel polymer-ceramic electrolyte. Succinonitrile (SCN) was also utilized to enhance the Na^+ conductivity as a plasticizer. In this work, an investigation of the ionic conductivity of PEGDA/$NaClO_4$ electrolytes with different weight ratios of SCN and $Na_3Zr_2Si_2PO_{12}$ nanopowders was conducted. The composition of the polymer phase of the SSE was selected to be PEGDA:$NaClO_4$:SCN = 52.5:17.5:30. With 30 wt% $Na_3Zr_2Si_2PO_{12}$ nanopowder blended, the ionic conductivity was 4.5×10^{-5} S cm^{-1}. Testing between the sodium working electrode and stainless-steel (SS) counter electrode, the electrochemical stability window was determined to be 5 V. In addition, the sodium-ion transference number was calculated to be 0.41. The reasonable rate capability and high cycling stability performance of Na|PEGDA/$NaClO_4$/SCN/$Na_3Zr_2Si_2PO_{12}$ | $Na_2MnFe(CN)_6$ all-solid-state coin cells were systematically examined and analyzed at ambient temperature.

In addition to NASICONs, sulfide-based ISEs have also been studied in combination with inorganic and organic electrolytes. Ren et al. reported a novel hybrid electrolyte film consisting of pentaerythritol tetraacrylate (PETEA) and Na_3SbS_4 [147]. The cross-linking of liquid PETEA monomer was initiated by Na_3SbS_4 particles, as shown in Fig. 29a. The ionic conductivity of the hybrid solid electrolyte, which was 0.047 mS cm^{-1} at room temperature, was slightly lower than that of the Na_3SbS_4 pellet. However, with the test of sodium symmetric cells, the compatibility of hybrid solid electrolytes with sodium electrodes was found to be much better than that of the Na_3SbS_4 pellet, as demonstrated in Fig. 29c, d. Additionally, the hybrid electrolytes served as an effective barrier between soluble sodium polysulfides (NaPS) in the sulfur cathode and sodium metal, which is critical to the viability of Na-S batteries.

For SPEs, low ionic conductivity at room temperature is still relatively common. Although methods such as copolymerization, adding active inorganic fillers, and adding ionic liquids have been employed to improve the ionic conductivity and electrochemical properties, it is still difficult to meet practical applications. In the presence of low ionic conductivity, both cycling performance and rate performance can be affected. It is not sufficient to reduce the crystallinity of the polymer to improve ionic conductivity. Polymer chains themselves have a slow ion transport rate, making it necessary to add other active inorganic substances or ionic liquids to improve the ion transport rate. For further development, additives can also be considered metal organic frameworks (MOFs). MOFs are a class of compounds consisting of metal ions or clusters coordinated to organic ligands to form dimensional structures [148]. With the metal ions of MOFs introduced, the anion dissociation of sodium salts can easily be attracted and fixed. In addition, the host material of ion transport can be changed from polymers to additives

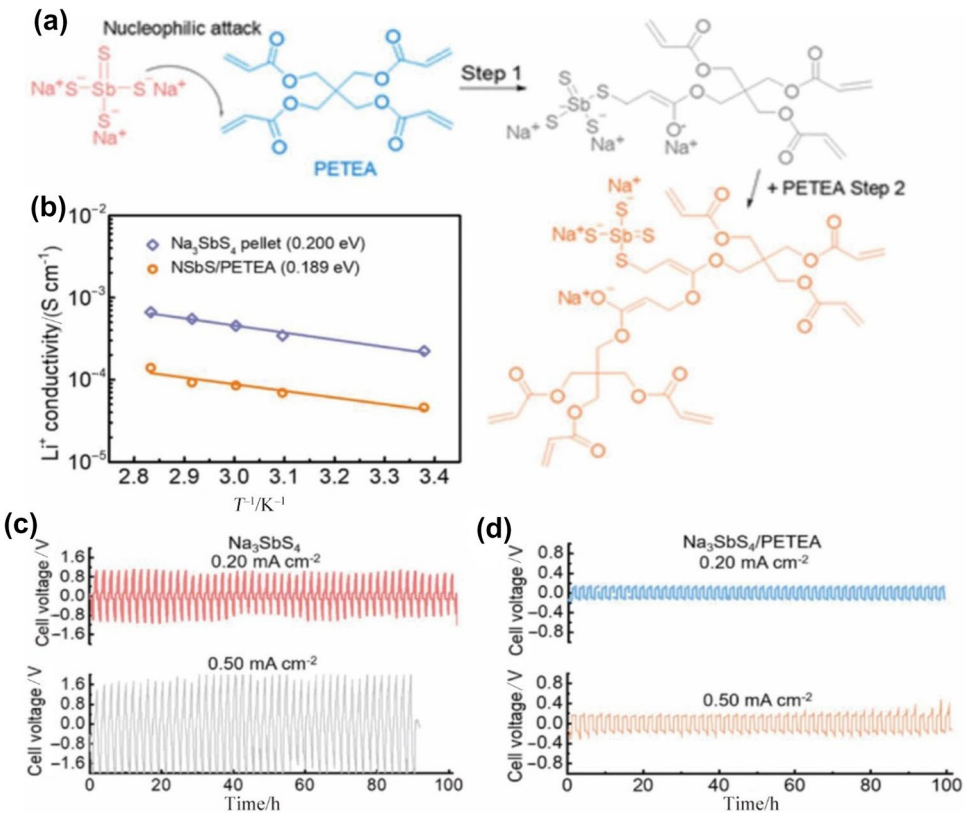

Fig. 29 **a** Schematic illustration of the initiation of PETEA by Na_3SbS_4 particles; **b** comparison of ionic conductivity between hybrid solid electrolytes and Na_3SbS_4 pellets; **c** and **d** comparison of the compatibility with sodium between hybrid solid electrolytes and Na_3SbS_4 pellets. Adapted with permission from Ref. [147]. Copyright © 2021, American Chemical Society

such as extractants. The extractants that may have the ability to transport sodium can be selected or created to construct SPEs. Under the mechanism of ion extraction and transportation, the sodium ions may be transported through SPEs driven by the voltage or the concentration difference.

Not only ion conductivity but also the interface between SPEs and electrodes need attention. Most studies on SPEs have used $Na_3V_2(PO_4)_3$ cathode materials due to the high ionic conductivity of NVP, a NASICON-type material. However, cathode materials, such as $Na_{1.92}Fe[Fe(CN)_6]$ and $Na_{2/3}[Ni_{1/3}Mn_{1/2}Ti_{1/6}]O_2$, have not been adapted for SPEs. The best solution is in situ polymerization, where electrodes are infiltrated while SPEs are still liquid and then polymerized to form the SPEs. This approach has been used in the upcoming gel polymer electrolytes (GPEs), but it is still less used in SPEs and may be a future development trend.

8 Gel Polymer Electrolytes

In addition to SPEs, GPEs have also been investigated in recent years. GPEs consist of base polymers, sodium salts, and liquid solvents [149, 150]. GPEs can be regarded as an intermediate state between solid electrolytes and liquid electrolytes. In 1975, Feuillde et al. [151] investigated GPEs with lithium salts. GPEs were prepared by immersing the synthesized solid electrolytes into liquid electrolytes containing sodium salt. Overall, the electrochemical performance of GPEs was better than that of SPEs because a portion of the safety concern was sacrificed to improve the performance.

8.1 PEO-Based GPEs

Apart from SPEs, PEO is also one of the most commonly used polymers in GPEs. For the development of PEO-based GPEs, Yu et al. [152] reported a newly designed cross-linked poly(ethylene glycol) diglycidyl ether (PEGDE)- and diamino-poly(propylene oxide (DPPO)-based electrolyte. The formed electrolyte consisted of PEO and poly (propylene oxide) (PPO) chains. The electrolyte combined with the supporting glass fiber (GF) material exhibited a high performance in terms of mechanical strength and flexibility. By using compact GF-GPEs, electrolyte solvents can be immobilized tightly during cycling to reduce side reactions with electrodes. The ionic conductivity was confirmed to be 2.18×10^{-3} S cm^{-1} at room temperature, according to Fig. 30a. The electrochemical stability window of the GF–GPE was 4.8 V versus Na^+/Na according to the LSV curves in Fig. 30b, showing the high purity of the GF–GPE. Because SSEs usually show a lower ionic conductivity, the performance at a high rate will obviously decrease. However, this was not observed for GF–GPEs, as shown in Fig. 30c. The cycling performance of GF–GPEs at a rate of 5 C was almost the same as that of GF–LEs. The cycling performance was determined with the assembled NVP|GF–GPE|Na and NVP|GF–LE|Na cells. As a result, the NVP|GF–GPE|Na cell exhibited a discharge capacity of 93.4 mAh g^{-1} after 2 000 cycles at 1 C, retaining its capacity by 96.7%, which was significantly better than that of the NVP|GF–LE|Na cell. The results shown in Fig. 30i illustrate that the GF–LE/Na interface was unstable during cycling in the NVP/GF–LE/Na cell with increased polarization, whereas GF–GPEs promoted the formation of a stable GF-GPE/Na interface. With this robust and compact GF-GPE, Na plating/stripping can be uniformly carried out without Na dendrite penetration, ensuring a very stable Na/GF-GPE interface during cycling.

Menisha et al. also recently showed that EC-, PC-, $NaClO_4$-, PEO-, and $NaClO_4$-based GPEs can be optimized under conditions of immobilization of the rate of EC and PC at 40 wt% for both [150]. It was discovered that the highest ionic conductivity, which pertained to 13 wt% $NaClO_4$ and 7 wt% PEO, was 9.8×10^{-3} S cm^{-1}. The PEO-based GPEs can achieve electrochemical performance similar to liquid electrolytes at room temperature, which is far ahead of PEO-based SPEs. GPEs can be a feasible alternative to liquid electrolytes before the further development of SPEs.

8.2 PVDF-HFP-Based GPEs

Poly(vinylidene fluoride-cohexafluoro-propylene (PVDF-HFP) has been considered a proper material for GPEs because it has the characteristics of high flexibility and dielectric constant [153]. The percentage of amorphous phase in PVDF-HFP is higher, which leads to a higher performance on ionic conductivity. Research on PVDF-HFP-based GPEs has been popular in recent years. Vo et al. [154] synthesized a PVDF-HFP-based GPE consisting of PC and fluoroethylene carbonate (FEC) in a mixture of 98:2. The prepared GPE exhibited a high ionic conductivity performance with $NaClO_4$ or $NaPF_6$ as the sodium salt. The electrolyte of $NaClO_4$ 1 M – PC:2%FEC/PVdF-HFP presented the highest ionic conductivity of 1.91×10^{-3} S cm^{-1}. In addition, the synthesized GPE showed a wide range of electrochemical windows of ~ 4 V, indicating a probable application with a high-voltage electrode pair. A sodium cell with a configuration of Na/GPE/$Na_{0.44}MnO_2$ was evaluated under a constant current density of 0.1 C at room temperature. It was found that PVdF-HFP/$NaClO_4$ PC:2%FEC exhibited nearly no increase in polarization after 20 cycles.

Janakiraman et al. also reported an electrospun PVDF-HFP-based GPE [155]. The liquid electrolyte was selected to be 0.6 M $NaPF_6$ dissolved in EC/PC (1:1). According to the XRD results, PVDF-HFP formed an amorphous electroactive β phase, which indicated an interaction among the

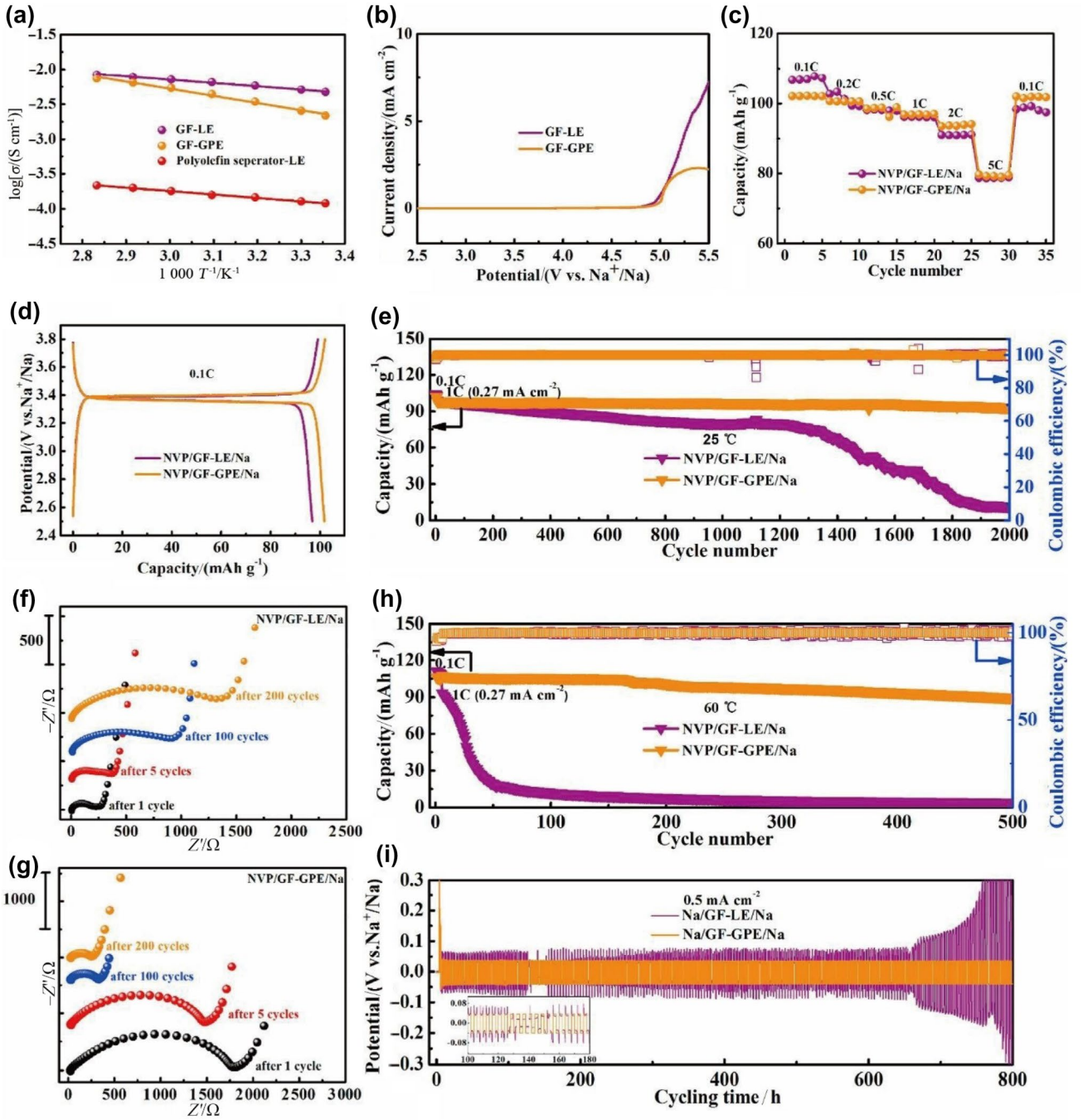

Fig. 30 **a** Temperature dependence of ionic conductivity; **b** LSV curves of GF-GPEs and GF-LEs; **c** rate performance from 0.1 to 5 C; **d** charge–discharge curve of the first cycle; **e** & **h** cycling performance at 25 °C and 60 °C, respectively; **f** and **g** Nyquist plots after cycles of NVP|GF-GPE|Na & NVP|GF-LE|Na cells; **i** cycling performance of the Na-symmetric cell. Adapted with permission from Ref. [152]. Copyright © 2021, American Chemical Society

base polymer, salt, and liquid solvent. The microstructure of the novel GPE was characterized by field emission scanning microscopy (FESEM), as shown in Fig. 31b, giving evidence of the amorphous structure. The ionic conductivity of the synthesized GPE was as high as 1.28×10^{-3} S cm^{-1} at room temperature. The high porosity, amorphicity, and electroactive properties of PVDF-HFP mats were cited as contributing factors to ionic conductivity. Based on Fig. 31c, the PP Celgard membrane was less stable below 4.0 V and started decomposing at 4.0 V, as indicated by an increase in the background current. In contrast, the electrospun GPE with a shallow background current had a stable voltage up

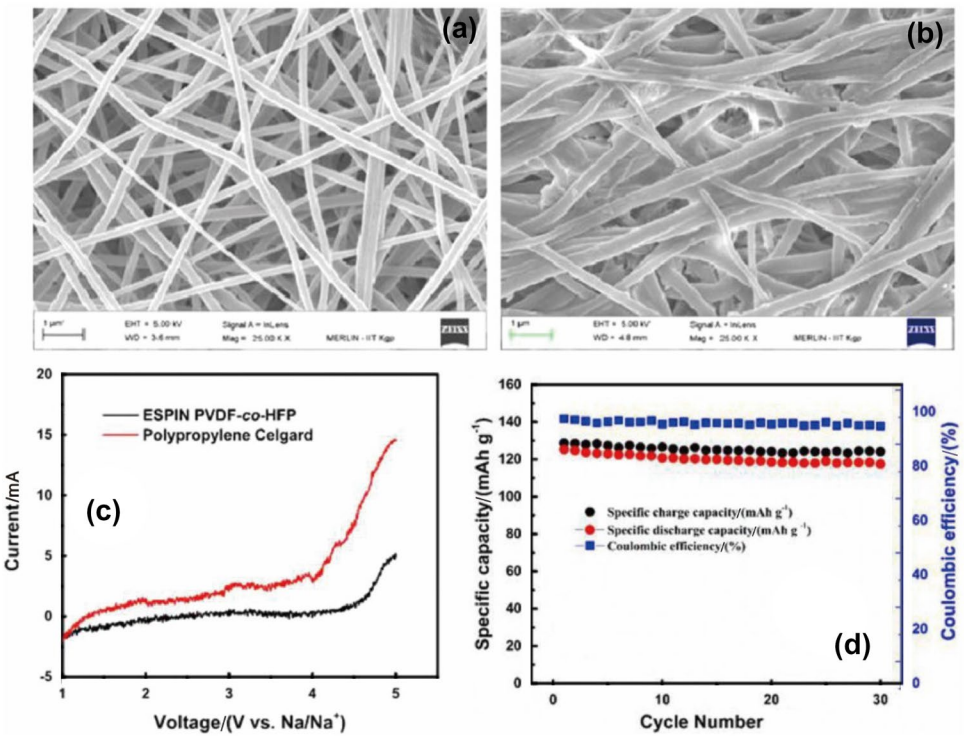

Fig. 31 FESEM image of electrospun **a** PVDF-HFP and **b** GPE. **c** The performance of PP Celgard membrane. **d** The performance of the PVDF-HFP gel electrolyte after 30 cycles Reprinted with permission from Ref. [155]. Copyright © 2021 The Author(s)

to 4.6 V. The performance of the PVDF-HFP gel electrolyte after 30 cycles demonstrated excellent capacity retention of sodium-ion cells, as shown in Fig. 31d.

Chauhan et al. reported a high-performance porous PVDF-HFP-based GPE filled with sodium aluminate ($NaAlO_2$) powder [156]. The composition of the liquid electrolyte applied to the newly prepared GPE was 1 M $NaClO_4$ dissolved in EC/PC (1:1). The $NaAlO_2$ particles initially settled on the PVDF-HFP network, which led to the formation of an amorphous phase. Then, the absorbed liquid electrolyte was also fixed by the $NaAlO_2$ particles, causing multiple pathways for ion transportation. The ion transportation principles of the PVDF-HFP/$NaAlO_2$ GPE are demonstrated in Fig. 32. The ionic conductivity was 6.8×10^{-4} S cm^{-1} maximum at room temperature. The discharge capacity was found to decrease from the first to fourth cycles. At increased discharge currents, the discharge capacity may decrease as a result of a voltage drop caused by a combination of internal resistance and reduced recovery rates as well as a reduction in the active mass contributing to electrochemical

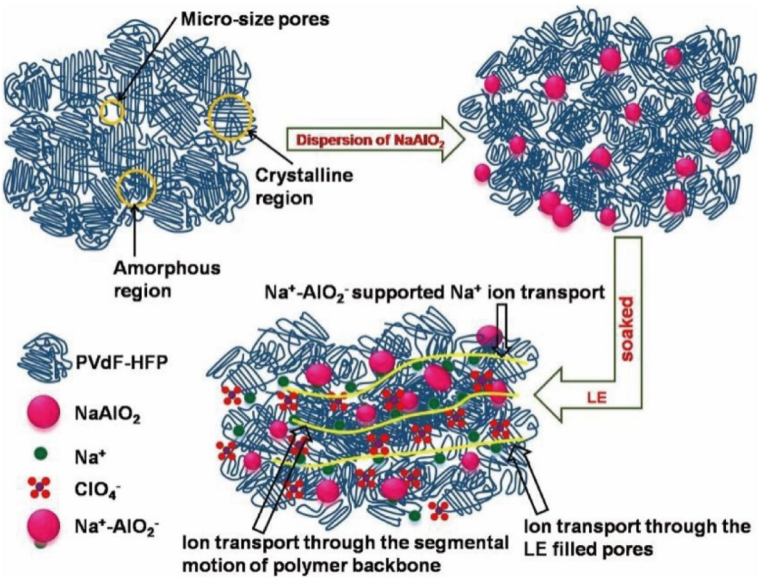

Fig. 32 Illustration of the addition of $NaAlO_2$ particles and ion transport paths in GPEs. Reprinted with permission from Ref. [156]. Copyright © 2021, Elsevier

reactions at high current densities. The insertion of inorganic particles can also increase the mechanical strength of GPEs, which makes up for some shortcomings.

By means of excellent structural control, the sodium-affinity polymer chain can uniformly penetrate PVDF-HFP porous films. Kwon et al. [157] chose sodio-philic gel polymer electrolytes based on poly(ethylene glycol) methyl ether thiol (PEG-SH) and PVDF-HFP(PVH) with a porosity-gradient Janus structure to restrain the formation of sodium dendrites. Capillary action and Marangoni convection joined water vapor into a cluster of hexagonal assemblies spontaneously self-assembling onto the PVH solution. Figure 33a illustrates the creation of an even porous PVH film under the influence of water and KOH solution and the subsequent modification of the PVH–PEG skeleton with PEG–SH solution. With the galvanostatic cycling test of the Na||Na symmetric cell using glass fibers (GFs), a Celgard PP separator, a PVH GPE, and a PVH–PEG GPE, as shown in Fig. 33f, it can be concluded that the insertion of PEG obviously restrained the formation of sodium dendrites. It was also noted that Na electrodeposition can be significantly affected by polymer electrolyte porosity and pore morphology, particularly at the Na/electrolyte interface. GF- and Celgard-based cells were compared with Na|PVH–PEG|NaNFCM ($NaNi_{0.3}Fe_{0.2}Cu_{0.1}Mn_{0.4}O_2$) cells to evaluate their long-term cycling stability, as shown in Fig. 33g. With a similar initial discharge capacity, PVH–PEG showed excellent cycling stability, retaining 68% of its initial discharge capacity after 180 cycles, significantly better than GF (16%) and Celgard (24%). The rate performance of Na|PVH–PEG|NaNFCM was also shown to be the best, according to Fig. 33i. The excellent performance

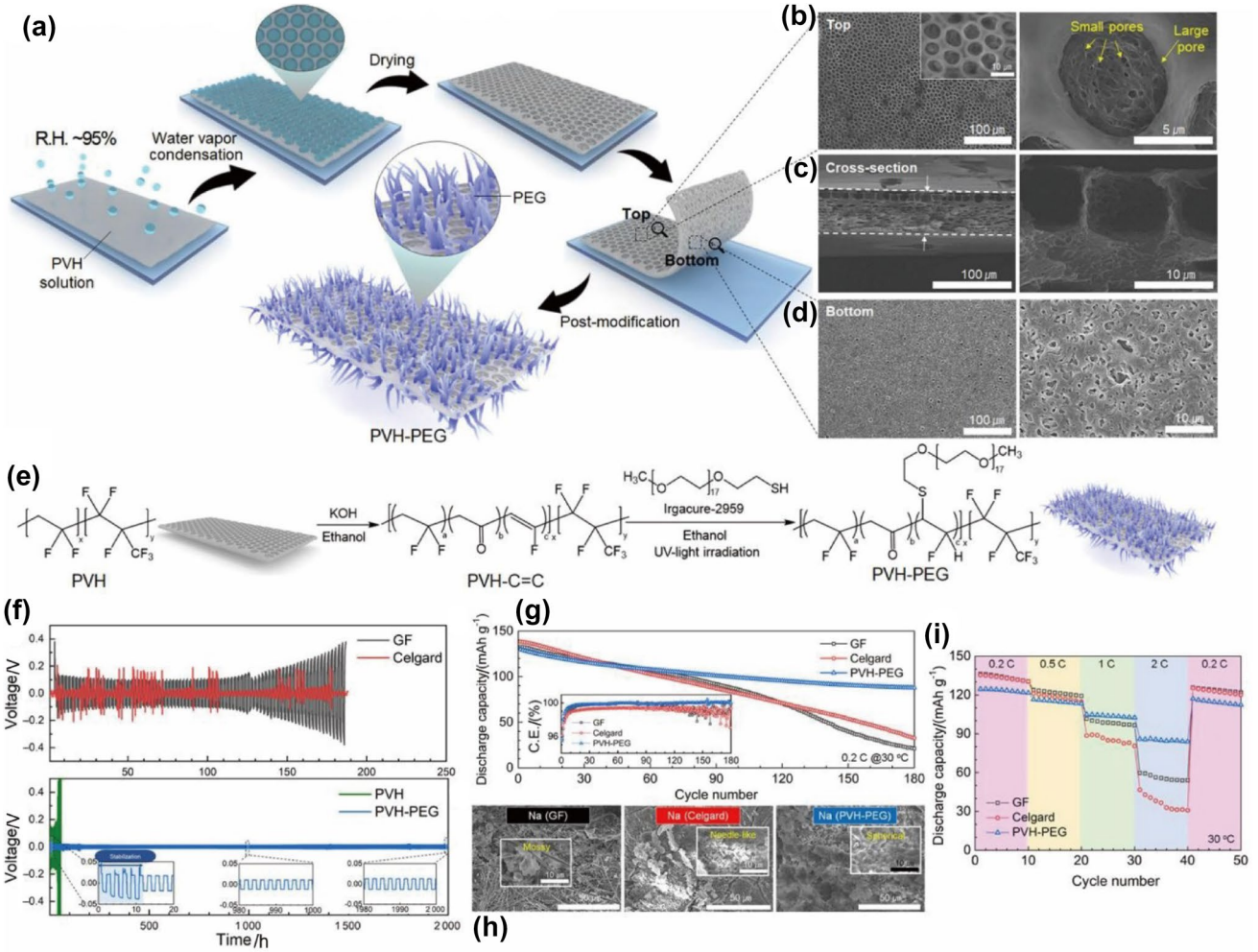

Fig. 33 **a** and **e** Schematic of the preparation progress of the PVH-PEG GPE; **b-d** SEM image of the top surface, cross section and bottom surface, respectively; **f** galvanostatic cycling test of the Na||Na symmetric cell with GF, Celgard, PVH and PVH-PEG; **g** cycling performance of Na|PVH-PEG|NaNFCM compared with cells applying GF or Celgard; **h** SEM image of the cycled Na metal surface of each cell after 180 cycles; **i** rate performance of each cell from 0.2 to 2 C at 30 °C. Adapted with permission from Ref. [157]. Copyright © 2022, American Chemical Society

was attributed to the porosity-gradient Janus structure of the PVH–PEG GPE, which provided a new theory of optimization and enhancement. The formation of dendrites was inhibited by the uniform deposition of sodium ions on the negative electrode under the guidance of the electrolyte.

As PVDF-based GPEs have been well developed, Zhao et al. [158] proposed and investigated a quasisolid-state SIB applying flexible electrodes, utilizing carbon cloth made from commercial cotton cloth for the cathode and flexible anode, combined with a PVDF-based GPE. The PVDF-based GPE (PVDF-HFP–$NaClO_4$) was chosen to achieve the aim of a flexible full cell, according to Fig. 34a. The cathode material was selected as $Na_3V_2(PO_4)_2O_2F$ (NVPOF on a flexible carbon cloth (FCC, which possesses prominent discharging platforms at 3.5 V and 4.0 V. Under the application of the FCC base, the ionic conductivity and electronic conductivity of the NVPOF cathode material were drastically improved. Forming a quasisolid-state battery, the rate performance was as excellent as a nearly 50% retention rate from 0.1 to 15 C, as shown in Fig. 34c. According to the cycling performance in Fig. 34d, the specific capacity retention rate at 5 C after 2 000 cycles was 77.19%, which showed a much higher performance than other studies. A rational configuration of the NVPOF@FCC electrode, using FCC as a substrate, could improve the electrochemical performance of NVPOFs by drastically improving its sodiation/desodiation reaction kinetics.

Vijaya also reported a gel polymer using hydroxyapatite ($Ca_{10}(PO_4)_6(OH_2)$) in PVDF-HFP and a poly(butyl methacrylate) (PBMA) membrane by a simple solution casting technique. The ionic conductivity of freshly prepared GPE was 1.07×10^{-3} S cm^{-1} at room temperature. Under the test with a sodium symmetric cell, the Na^+ transference number was determined to be 0.83. This indicated that ions rather than electrons transported charge in the membrane. The electrochemical stability window of this GPE was observed to be 4.8 V due to its good affinity with liquid electrolytes [159]. The cycling performance of the GPE using NVP as the cathode material was tested between 2.2 and 3.8 V. After 100 cycles, the GPE membrane exhibited an excellent cyclic stability of 92.7%.

8.3 PAN-Based GPEs

A polyacrylonitrile (PAN)-based electrolyte was first investigated in 1975, which was used to form a PAN-based GPE with a high ionic conductivity performance of 1×10^{-3} S cm^{-1} at room temperature [151]. It has been found that polar CN groups can be able to simplify the dissociation of salts added. With the advantage of polar CN groups, PAN-based GPEs have attracted the attention of researchers. In

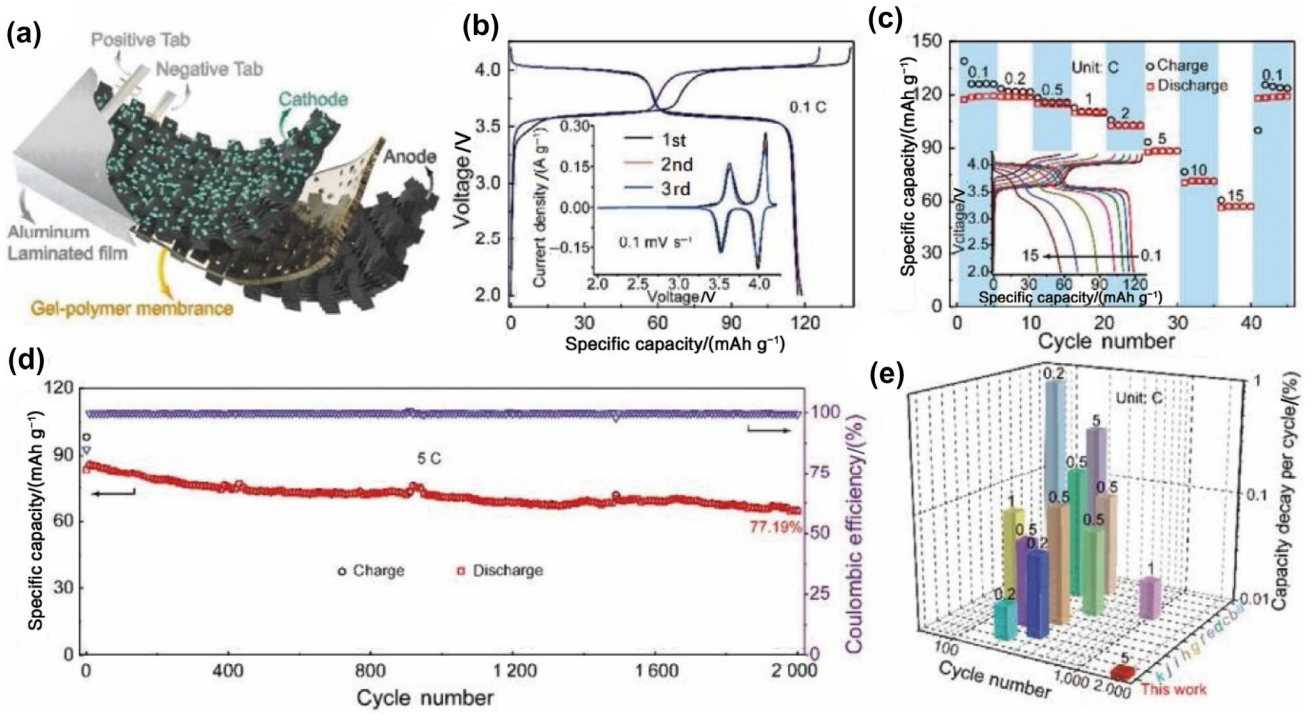

Fig. 34 **a** Schematic illustration; **b** first cycle of charging–discharging curves and CV cycles; **c** rate performance and relative charging–discharging curves; **d** long-term cycling performance of the NVPOF @ FCC|PVDF-HFP-$NaClO_4$|FCC full battery; **e** comparison of stability performance of this work and others. Adapted with permission from Ref. [158]. Copyright © 2021, Springer Nature

2018, Zhang et al. [160] reported the preparation of an aqueous PAN-based GPE for sodium–zinc-ion batteries. The electrospun PAN membrane was immersed in an aqueous solution of 1 M sodium sulfate ($NaSO_4$) and 0.6 M zinc sulfate ($ZnSO_4$). The synthesized aqueous GPE had a high electrochemical performance with a zinc anode and $Na_4Mn_9O_{18}$ cathode material, which still showed a discharge capacity of 64 mAh g^{-1} at 1 C after 200 cycles.

In 2020, Lonchakova et al. [161] claimed that a novel PAN-based GPE was synthesized. The base polymer of the electrolyte was a copolymer poly(acrylonitrile-co-methyl acrylate (PAN-co-PMA), and the plasticizer was selected to be PC. After soaking in $NaClO_4$ or $NaPF_6$ dissolved in PC solution, the prepared GPE showed a high ionic conductivity performance of 1.8×10^{-3} S cm^{-1} at room temperature. As shown in Fig. 35a, the PAN:PC + $NaClO_4$ GPE exhibited wide electrochemical ranges up to 4.5 V versus Na/Na^+. Additionally, PAN-based GPEs and $Na_3V_2(PO4)_3$ cathodes were used to prepare full sodium-ion cells and tested at various charge–discharge rates. Based on these results, it can be concluded that the GPE had no significant defect on the performance of sodium-ion cells compared with liquid electrolytes. Ion transportation occurs in the solvent-rich area of GPEs, with a decoupling effect with the PAN skeleton. PAN-based polymer electrolytes have been investigated for years, which created a series of nanofiber membranes with high electrochemical performance through electrospinning and other technologies. The further development of PAN-based polymer electrolytes may be focused on the enhancement of mechanical strength with SPE formulations.

8.4 Other GPEs

GPEs based on traditional polymers that have been applied to membrane production have gradually developed into a bottleneck in the past few years. Although the GPEs mentioned above possess a high electrochemical performance of ionic conductivity, the higher electrochemical stability and lower amount of liquid electrolytes used have always been the aim of the design of GPEs. Innovative GPEs have been investigated for SIBs to practice the new theories or meet the new requirements.

Constructing a 3D ion diffusion channel through a polymer matrix has been applied to the design of GPEs of SIBs. Zhou et al. reported the development of an in situ 3D ionic conductive GPE based on trihydroxymethylpropyl triacrylate (TMPTA) for SIBs [162]. As a result of heat-triggered in situ polymerization, the GPE was easy to synthesize and exhibited excellent performance characteristics. A schematic illustration and the microstructure of the TMPTA-based GPE are shown in Fig. 36a. With the low interface resistance and high ionic conductivity of the GPE, as shown in Fig. 36b, the GPE exhibited excellent electrochemical performance because the polymer segments in the GPE frameworks could move freely and rotate freely, facilitating Na^+ transport. An investigation of the compatibility of Na/Na symmetrical batteries with Na metal anodes was conducted by using GPEs and LEs. According to Fig. 36e, with LEs in the symmetrical cell, gas bubbles and sodium dendrites were obviously observed, indicating side reactions between the LE and sodium anode. In contrast, when the GPE was applied to the symmetrical cell, no gas bubbles or sodium dendrites were found. Due to a high electrochemical stability window of 4.7 V, the cathode material was chosen as high-voltage P2-$Na_{2/3}Ni_{1/3}Mn_{1/3}Ti_{1/3}O_2$ (NMT) cathodes. Furthermore, the relationship between the calculated energy density based on the cathode value and cycling retention is shown in Fig. 36d. When loaded at 13.01 mg cm^{-2}, the Na|GPE|NMT batteries maintain excellent cycling performance. The rate performance of Na|GPE|NMT batteries indicated that the 3D ionic transport channel and stabilized SEI layer conducted by the GPE successfully resulted in excellent performance in sodium deposition and stripping.

1,3-Dioxolane (DOL) has been studied as an electrolyte, as the polymerization of DOL, namely poly(DOL), possesses a large amount of oxygen atoms on its chains, indicating a potential ability to transport metal ions and in situ polymerization of the electrolyte. Shuai et al. reported the construction of a sodium (fluorosulfonyl) (trifluoromethylsulfonyl) imide (NaFTFSI)/poly(DOL) in situ GPE polymerized by $Sn(OTf_2$ in a Na metal cell [163]. The nuclear magnetic resonance (NMR) spectra of ^1H of poly(DOL) and ^{19}F of NaFTFSI have been selected to prove the successful synthesis progress, as shown in Fig. 37a. The ionic conductivity of the GPE was calculated to be 3.3×10^{-4} S cm^{-1}, which meets the requirement of SIBs. In comparison with $NaPF_6$/diglyme electrolytes, the authors found that the GPE had a larger window for electrochemical stability. The interesting thing about this GPE was that the compatibility between the GPE and different kinds of cathode materials was tested. S@PAN, Prussian blue (PB) and $Na_3V(PO_4)_2$ were chosen as the cathode materials. As shown from Fig. 37e–g, the comparison between cells applying the GPE showed much higher stability and cyclic retention than that with liquid electrolytes.

In addition to having functional properties equivalent to those of natural biomass, renewable macromolecules derived from biomass also offer renewable, biodegradable, and toxicity-free characteristics [164]. Cellulose nanoparticles have gained attention in the field of polymer electrolytes due to their good thermal, mechanical and electrochemical properties [165]. Mittal et al. synthesized cellulose nanofiber (CNF)- and cellulose nanoparticle (CNC)-based GPEs containing $NaClO_4$ in an EC/PC liquid electrolyte. Based on the information presented in Fig. 38d, sodium ions were suggested to move rapidly

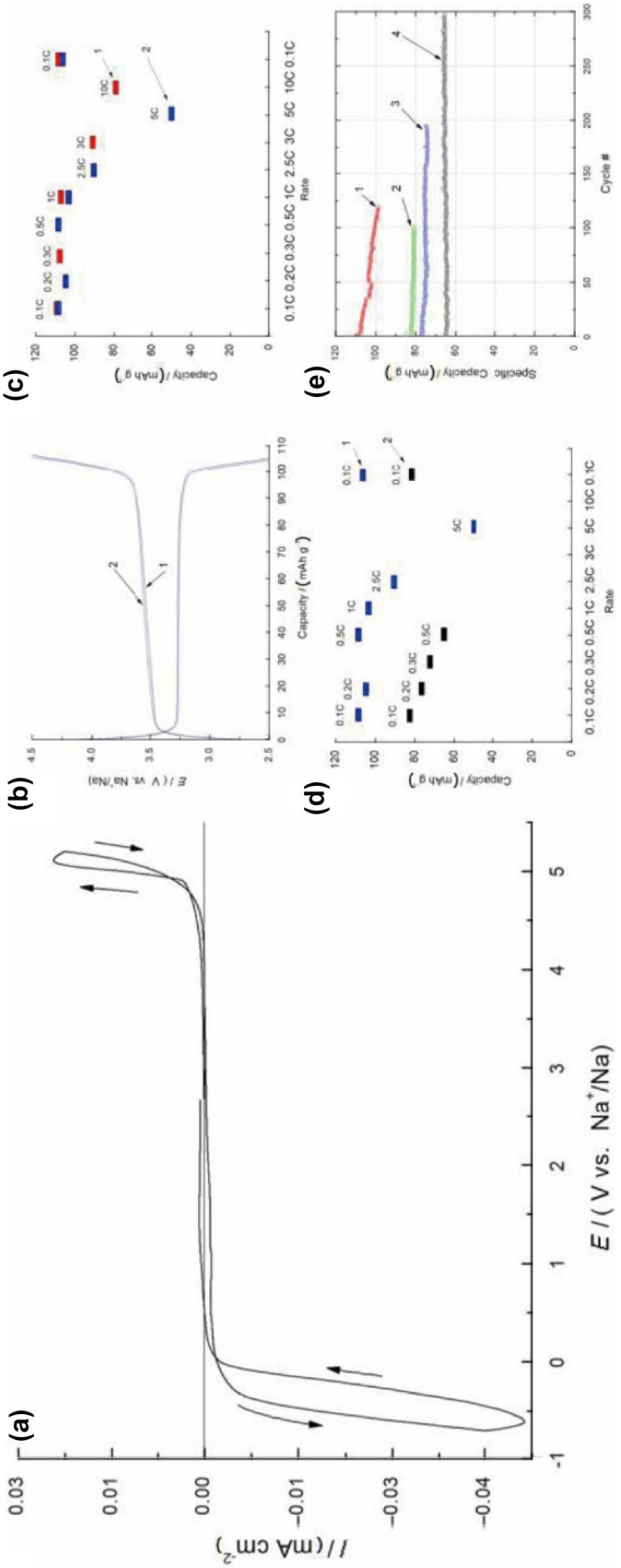

Fig. 35 **a** LSV measurement for a 1:4 PAN: PC + $NaClO_4$ GPE; **b** charge and discharge curve (1, the 1st cycle; & 2, the 10th cycle) at 0.5 C; **c** rate performance from 0.1 C to 10 C (red, the liquid electrolyte; & blue, the GPE); **d** rate performance from 0.1 C to 5 C (blue, the GPE at RT; & black, the GPE at − 20 °C); **e** cycling performance (red, RT at 0.1–0.5 C; & green, − 20 °C at 0.1 C; & blue, − 20 °C at 0.2 C; & black, − 20 °C at 0.5 C) of the NVP|GPE|Na cell. Adapted with permission from Ref. [161]. Copyright © 2020, Elsevier

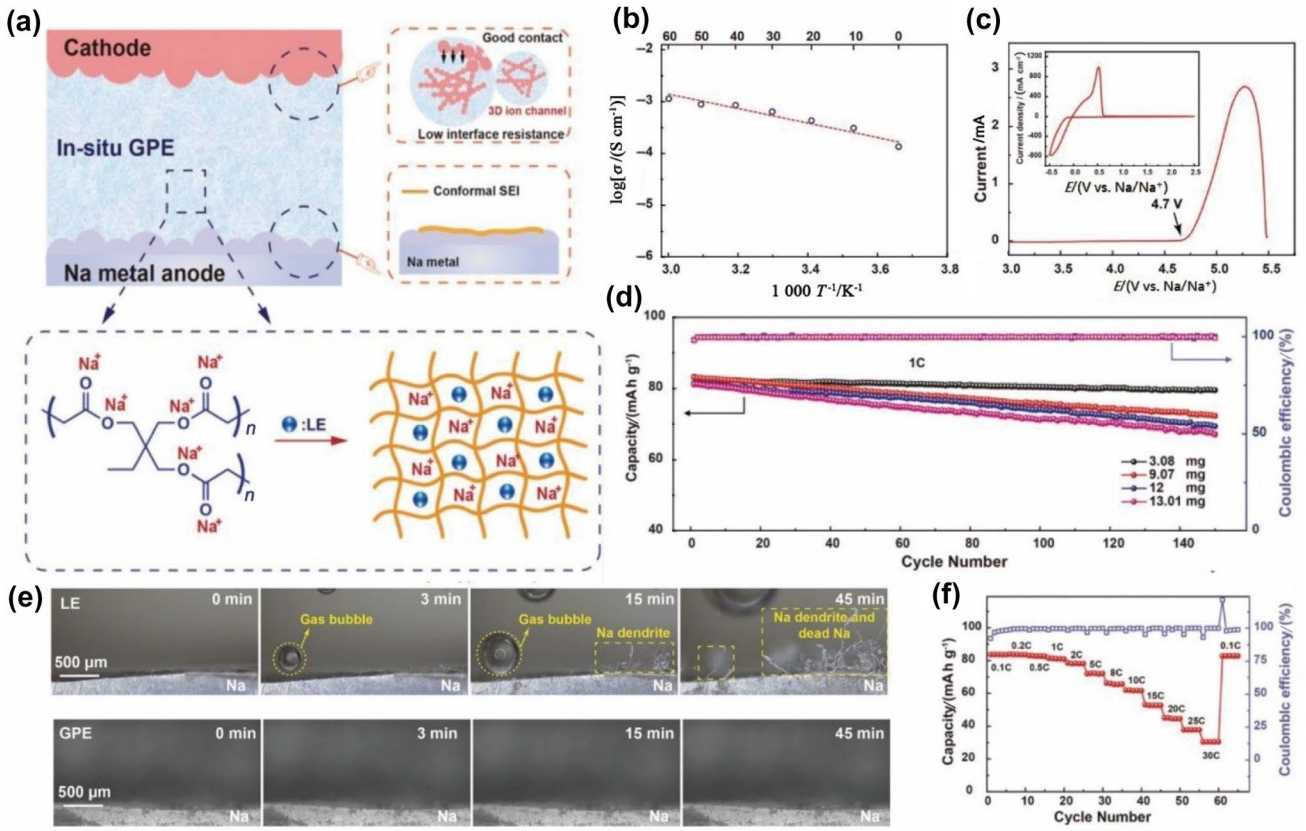

Fig. 36 **a** Schematic illustration of the microstructure of the GPE and in situ formed cell; **b** temperature dependence of the ionic conductivity of the GPE; **c** electrochemical stability window of the GPE; **d** cyclic performance of Na|GPE|NMT batteries with different cathode loading values at 1 C; **e** comparison of the interface between the electrolyte and sodium anode of the LE and GPE; **f** rate performance of the Na|GPE|NMT battery at room temperature. Adapted with permission from Ref. [162]. Copyright © 2022, John Wiley and Sons

between CNFs and CNCs. As a result, the GPE had an ionic conductivity of 2.232 mS cm^{-1} at room temperature with a composition of 50:50 weight ratio of CNFs to CNCs, according to Fig. 38a. A 5.0 V electrochemical stability window was determined for the GPEs, higher than that of many polymer-based electrolytes. It was possible to achieve a maximum Na^+ transference number of 0.860 using the 20:80 GPE. Comparatively, the 80:20 and 50:50 GPEs presented lower Na^+ transference numbers of 0.324 and 0.637, respectively. By dissociating Na^+, the CNF surfaces facilitated Na^+ motion through CNC/CNF gel electrolytes. The interface stability with sodium of CNC/CNF 50:50 was shown by the cycling performance of the sodium symmetric cell, as shown in Fig. 38f. This was attributed to the combination of mechanical ductility provided by CNFs, which ensured an interface without delamination, and inherent mechanical stiffness of CNCs, which prevented dendrite growth.

Nafion membranes, which are highly conductive to protons and chemically stable under strong acidic and oxidizing conditions, are commonly used in low-temperature PEMFCs [167]. Simari et al. [168] reported the first time a sodiated Nafion membrane was used as an electrolyte for SIBs. The solidated Nafion membrane (NNM) was produced by immersing the Nafion membrane in NaOH aqueous solution followed by soaking in an EC/PC anhydrous mixture. The ionic conductivity of NNM was tested to be 0.5 mS cm^{-1} at 20 °C, while it reached 1.5 mS cm^{-1} at 80 °C. The Na^+ transference number of the membrane was also calculated to be (0.82 ± 0.06). An a-$NaMnO_2$|NNM|Na cell has been demonstrated and compared to a liquid electrolyte cell at room temperature.

GPEs have been developed better than SPEs in the existing liquid phase in SSEs. With the higher performance of ionic conductivity, it becomes easier to optimize the electrochemical stability window and the compatibility with different kinds of cathode materials. On the one hand, the liquid phase in GPEs has the ability to infiltrate the cathode materials, which indicates the potential of the application of high-voltage cathode materials, such as PB. On the other hand, in situ polymerized GPEs with a lower amount of liquid phase form better interfaces with both cathodes and anodes. There will be a significant reduction in the total resistance of the cells as a result. Although

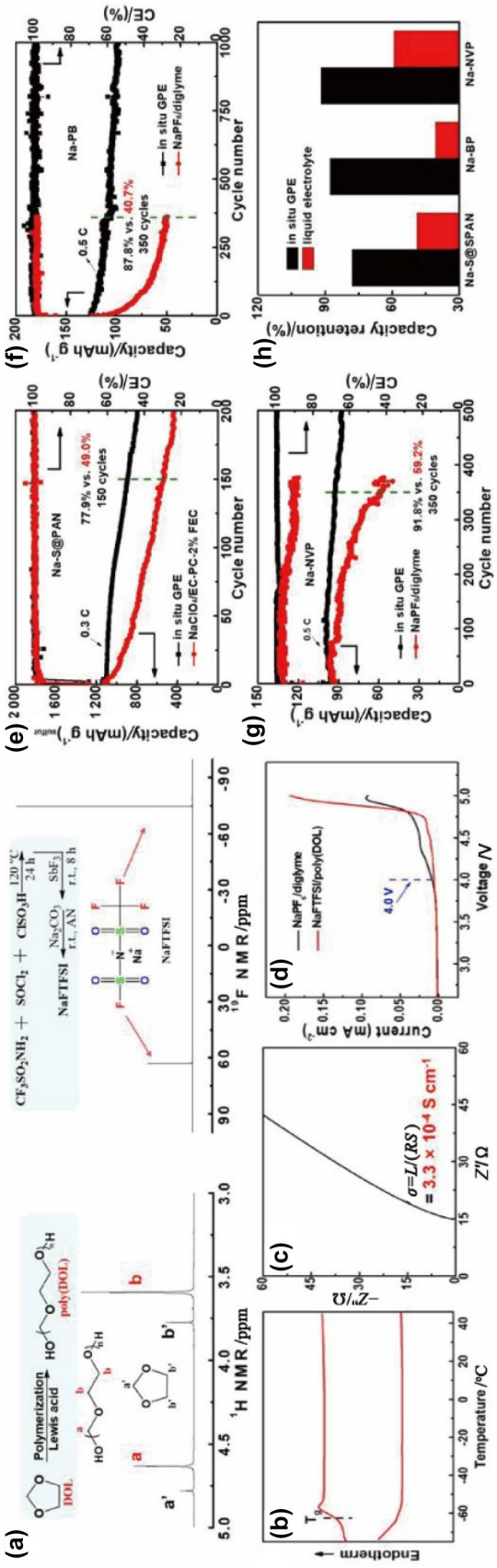

Fig. 37 **a** Schematic illustration of the synthesis of poly(DOL) and NaFTFSI and their NMR spectra; **b** TG and DSC spectra of the GPE; **c** EIS result of the GPE at room temperature; **d** electrochemical stability window of NaFTFSI/poly(DOL) and $NaPF_6$/diglyme; **e**–**h** cycle performance of cells with different electrolytes: **e** Na–S@PAN; **f** Na-PB; and **g** Na-NVP; **h** capacity retention of different systems. Adapted with permission from Ref. [163]. Copyright © 2022, American Chemical Society

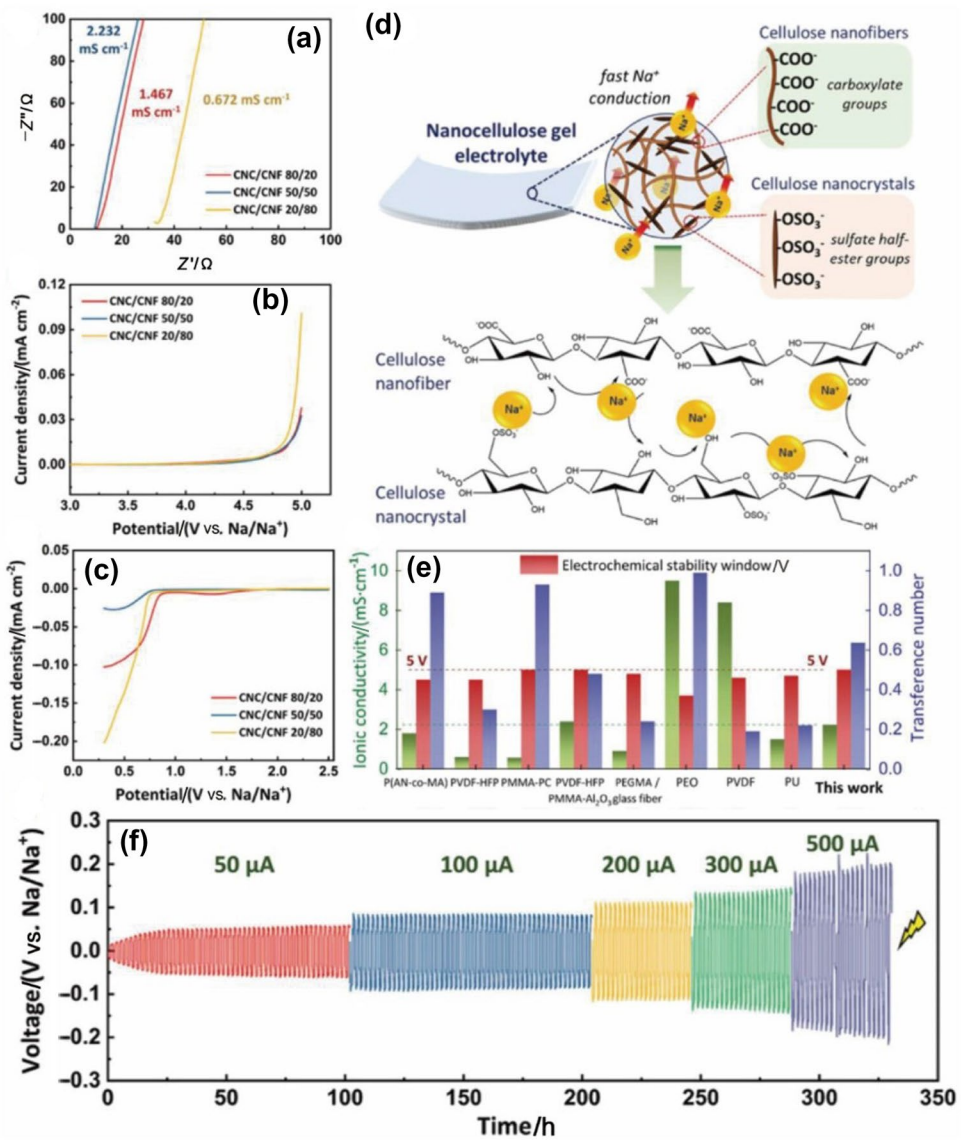

Fig. 38 **a** Nyquist impedance plots of GPEs; **b** anodic scan and **c** cathodic scan LSV curves of GPEs; **d** schematic illustration of sodium ion conduction transport in GPEs; **e** comparison of the 50:50 GPE with state-of-the-art GPEs applied in SIBs; **f** cycling performance of sodium symmetric cells at different current densities [166]

the existence of organic electrolytes has a potential danger, some GPEs optimized by flame-resistant materials or equipped with smaller amounts of liquid electrolytes have proven to be safe as well. In the future, GPEs based on newer theories, such as the 3D polymer skeleton, single-ion transportation or ion exchange, may be constructed. GPEs with a fixed liquid electrolyte phase inside the polymer chain or matrix will be a convincing method to achieve high electrochemical performance and high safety.

9 Plastic Crystal Electrolyte

Plastic crystal electrolytes (PCEs) are a new kind of fast ion-transport OSE. Typically, PCEs consist of polar plastic crystal base materials and metal ion salts. In the past, various kinds of PCEs have been investigated in the field of lithium batteries and fuel cells with impressive ionic conductivity performance [169–171].

Research on PCEs applied to SIBs has just started in recent years. Succinonitrile (SCN) has been selected as a high-performance plastic crystal material for PCEs. The plastic crystal phase of SCN has been pointed out to be suitable as an ion-transporting matrix [172]. Zhu

et al. [173] demonstrated the synthesis of an innovative PCE based on SCN. The PCE was prepared by dissolving sodium salt ($NaClO_4$) into melted SCN and solution casting of the mixture. The preparation process and exterior properties are shown in Fig. 39. The ionic conductivity of the SCN-based PCE was as high as 1×10^{-3} S cm^{-1} at room temperature.

Chen et al. showed in 2019 that SCN-based PCEs were defective in mechanical properties, which prevented the application of SCN-based PCEs to SIBs [76]. They provided a novel plastic crystal polymer electrolyte (PCPE) that combined a PCE with a polymer matrix to enhance the mechanical strength, with a boron-base anion acceptor mixed, namely B-PCPE. The anion of sodium salt was attracted by boron introduced according to SHAB theory, resulting in B-PCPE delivering higher t_{Na^+} values of 0.62, indicating partial sodium-ion conductivity behavior. The B-PCPE was prepared with the method of in situ UV-curing on porous polypropylene-cellulose composite nonwoven (PCN) by SCN-based PCE containing $NaClO_4$ salt and boron-containing cross-linker (B-HEMA), which consisted of trimethyl borate (TMB) and 2-hydroxyethyl methacrylate (HEMA). The synthesis process of B-PCPE is demonstrated in Fig. 40a. Despite the fact that 1 M $NaClO_4$ in SN is liquid, it solidifies completely when UV-cross-linked with B-PCPE or ETPTA. The produced B-PCPE exhibited a high performance in terms of mechanical strength, such as maximum stress and tensile stress. As a result of its superior flexibility and deformability, the B-PCPE was able to bend, twist, and even bend around a glass rod. In addition, the ionic conductivity of the B-PCPE was as high as 3.6×10^{-4} S cm^{-1} at room temperature. A good rate capability is also a critical factor for the practical application of all-solid-state SIBs consisting of $NaNi_{1/3}Fe_{1/3}Mn_{1/3}O_2$ (NFM), B-PCPE and hard carbon (HC), as shown in Fig. 40b. SCN-based solid electrolytes have extremely promising electrochemical performance as an alternative to polymer-based solid electrolytes.

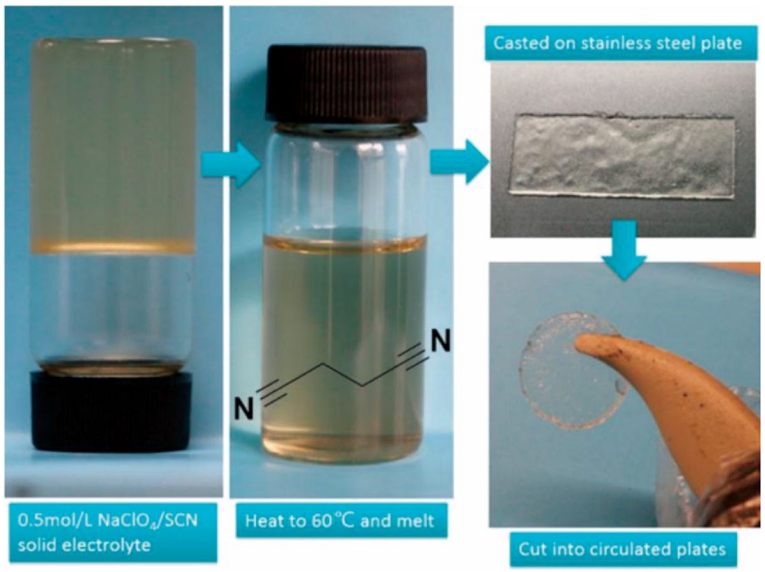

Fig. 39 Preparation process and exterior properties of SCN-based PCE. Reprinted with permission from Ref. [173]. Copyright © 2015 Elsevier Ltd. All rights reserved

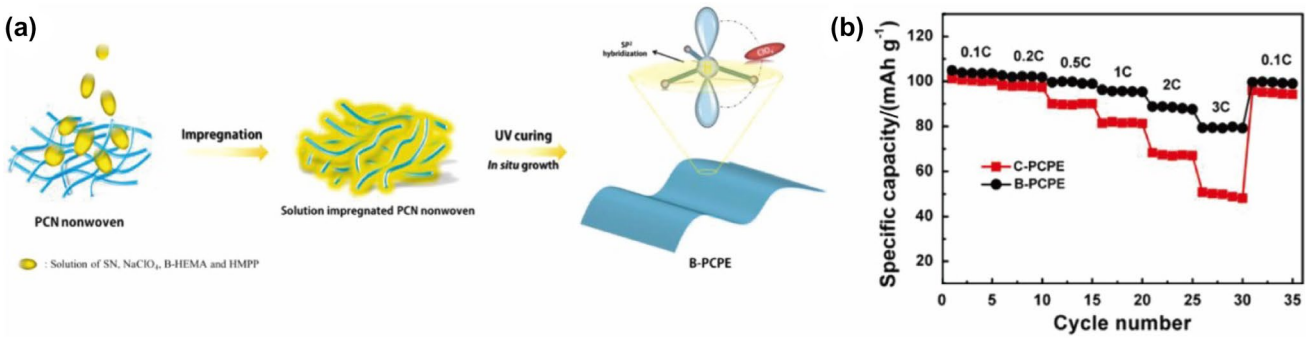

Fig. 40 **a** Schematic demonstration of the synthesis process of the B-PCPE; **b** rate performance comparison of NFM|B-PCPE|HC from 0.1 to 3 C at room temperature. Reprinted with permission from Ref. [76]. Copyright © 2019 Elsevier Ltd. All rights reserved

The main drawback of SCN-based solid electrolytes is their low mechanical strength. In addition to combining with a polymer skeleton, the mechanical strength may be improved with the insertion of inorganic materials.

Another case of combining polymer with SCN was reported by Xingwen et al. [174] in which a laminated polymer/ceramic-polymer SSE was synthesized. To improve the room-temperature ionic conductivity, PEO was used as a negative electrode-benign polymer matrix into which SCN was integrated at the negative electrode. On the positive electrode side, the cathode-friendly PAN served as a matrix for NASICON-type ceramic solid electrolytes ($Na_3Zr_2Si_2PO_{12}$), thereby improving ionic conductivity and preventing Na dendrites from penetrating through the electrolyte. The ionic conductivity of the laminated polymer electrolyte reached 1.36×10^{-4} S cm^{-1} at room temperature. The electrochemical stability window was also determined to be 4.8 V versus Na/Na$^+$. The Na$^+$ transference number was calculated based on the sodium symmetric cell test to be 0.42, which could be further developed.

In addition to SCN, another kind of PCE has been reported. OIPC can be used not only as a plasticizer but also as a plastic crystal [141, 142]. Makhlooghiazad et al. [175] synthesized an OIPC-based PCE, namely an organic ionic plastic crystal electrolyte (OIPCE. The OIPCE was prepared by a mixture of trimethylisobutylphosphonium bis(trifluoromethylsulfonyl)amide ($P_{111/4}NTf_2$) and sodium bis(trifluoromethylsulfonyl)amide ($NaNTf_2$). The thermal phase behavior was studied in detail, and the structures of the mobile phase and crystalline phase were determined by both the temperature and composition. The ionic conductivity of the OIPCE of variable composition was shown to increase sharply at 40 °C to a maximum of 5.01×10^{-3} S cm^{-1}. Recently, Biernacka et al. [176] synthesized a novel OIPC-based PCE, and the thermal phase behavior and ionic conductivity were studied. The electrolyte material was prepared by a mixture of NaFSI and hexamethylguanidinium bis(fluoromethanesulfonyl)imide, [HMG][FSI], in various molar ratios. The contrast in ionic conductivity between pure [HMG][FSI] PCE and 5 mol % NaFSI-OIPCE is shown in Fig. 41. At low temperature, 5 mol % NaFSI-OIPCE exhibited higher ionic conductivity performance, and when reaching the melting point, the ionic conductivities of the two PCEs became similar. As a result, the ionic conductivity of 5 mol % NaFSI-OIPCE reached 2.1×10^{-4} S cm^{-1} [177]. The OIPC-based solid electrolyte has the advantage of high electrochemical performance compared with SPEs. However, there is still little research on OIPC applied as the electrolyte of SIBs, and the theoretical basis is still immature. The feasibility of OIPC-based electrolytes in SIBs still needs to be verified. In addition, the cost of OIPCs is also higher than that of commonly used polymers, and the application of OIPCs will increase the cost of SIBs.

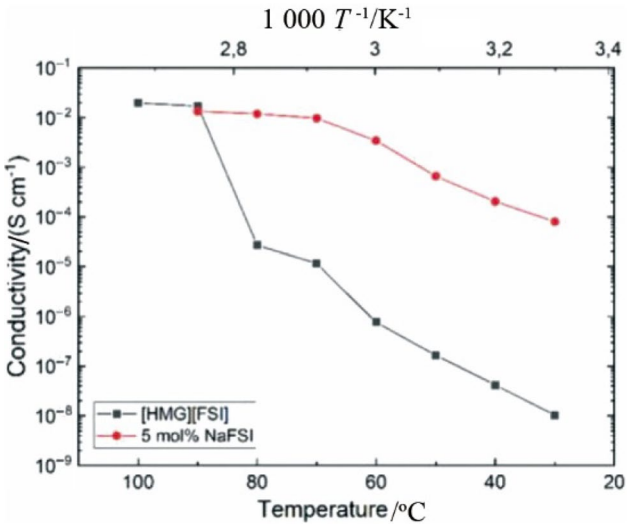

Fig. 41 Comparison of ionic conductivity at different temperatures of pure [HMG][FSI] PCE and 5 mol % NaFSI-OIPCE. Reprinted with permission from Ref. [176]. Copyright © 2021, American Chemical Society

Over the past few years, PCEs have received increasing attention. At room temperature, plastic crystals are able to transfer metal ions, which results in a high ionic conductivity due to their special crystal structure. Its fantastic electrochemical performance has attracted researchers to consider it as an alternative to SPEs. It must be noted, however, that these plastic crystals are characterized by a low mechanical strength, a narrow range of electrochemical stability, and a low thermal stability. Combining polymers with plastic crystals is required to meet these requirements. The polymer elastomer is one of the polymers that perfectly conceal a defect in plastic crystals. The characteristics of elastomers are high mechanical strength and stability but low ionic conductivity. It is anticipated that PCEs will have excellent performance as a high-voltage electrolyte for SIBs as a result of the design of their structure and the ratio between elastomers and plastic crystals. As a result, further research on the compatibility of PCEs with SIBs remains to be conducted.

In organic solid electrolytes, the research direction of GPEs has already developed high ionic conductivity, which satisfies the requirements. Compared with organic liquid electrolytes, the safety has been significantly improved, which indicated some commercial feasibility. Thus, the following research focuses on GPE materials with lower costs, proper electrochemical windows and simple preparation processes. However, to evaluate a certain electrolyte, other physical properties, such as mechanical strength, energy density and even flammability, are essential. From the perspective of safety issues, SPEs are obviously better choices than GPEs, although the ionic conductivity of SPEs is lower. The ionic conductivity of organic solid electrolytes is shown

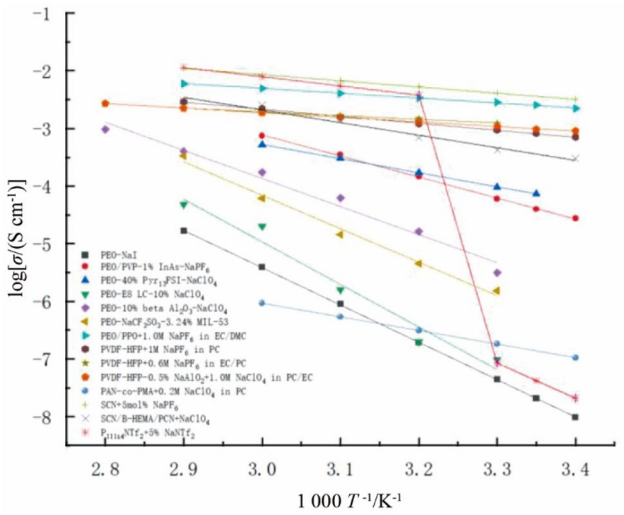

Fig. 42 Summary of the temperature dependence around room temperature of the ionic conductivity of different organic solid electrolytes [76, 128, 131, 132, 134, 137, 152, 154–156, 161, 173, 175]

in Fig. 42. In the future, the promotion of the ionic conductivity of SPEs will be the top priority. Because ISEs usually have higher ionic conductivity at room temperature, a composite electrolyte composed of ISEs and OSEs together may lead to high-performance electrolytes. In addition, the development of a new evaluation system for organic solid electrolytes can be established to rapidly estimate the performance of a kind of electrolyte, which can greatly contribute to screening for the best solution. Apart from the study of the electrochemical performance of OSEs and their batteries, little attention has been given to the SEI and cathode electrolyte interface (CEI) layers. Between the sodium anode and the electrolyte, the SEI layer is responsible for sodium ion transport. Additionally, the CEI layer plays a significant role in the transport of sodium ions between the cathode material and the electrolyte. Without a stabilized CEI and SEI, the cells will not be able to perform well during cycling.

The current SSEs of SIBs have made great progress. At present, the development progress of SSEs can be described in Fig. 43. For ISEs, the sodium ion transport efficiency has been improved by means such as ion doping, and thus, the ionic conductivity is enhanced. At room temperature, the ionic conductivity of those ISEs is sufficient for their application to SIBs. However, the current common shortcoming is that due to the high hardness of ISEs, the flexibility and effective contact with the electrodes is poor, resulting in performance degradation, especially for NASICON-type materials. The Na–β-Al_2O_3 SSE has the problem of forming sodium voids and dendrites at room temperature, preventing the application of Na/S batteries at room temperature. Additionally, SSEs based on sulfides have an electrochemical stability window that is too narrow for their application. Researchers have proposed improved methods for interfacial defects by adding interlayer ionic liquids or surface modification to reduce surface tension. There may still be a problem of the stability of interlayer additives and the modified surface under an external potential. Additionally, the Na–Sn alloy anode material has been applied to sulfide-based SSEs to avoid the reaction between sodium. Additionally, the introduction of an artificial SEI may help with ISEs with low electrochemical stability windows. For ISEs, the solution of the problem of effective contact will be the focus of further development in the future. The potential solution of the interfacial resistance can be optimizing the constituents of the solid electrolyte or electrode composition or introducing an artificial interface layer to reduce the interface impedance. To develop new sodium ion-based ISEs, the sodium ion transportation pathway needs to be designed.

For OSEs, GPEs currently have a relatively high commercial viability due to their superior electrochemical performance in comparison with SPEs and their superior safety performance in comparison with liquid electrolytes.

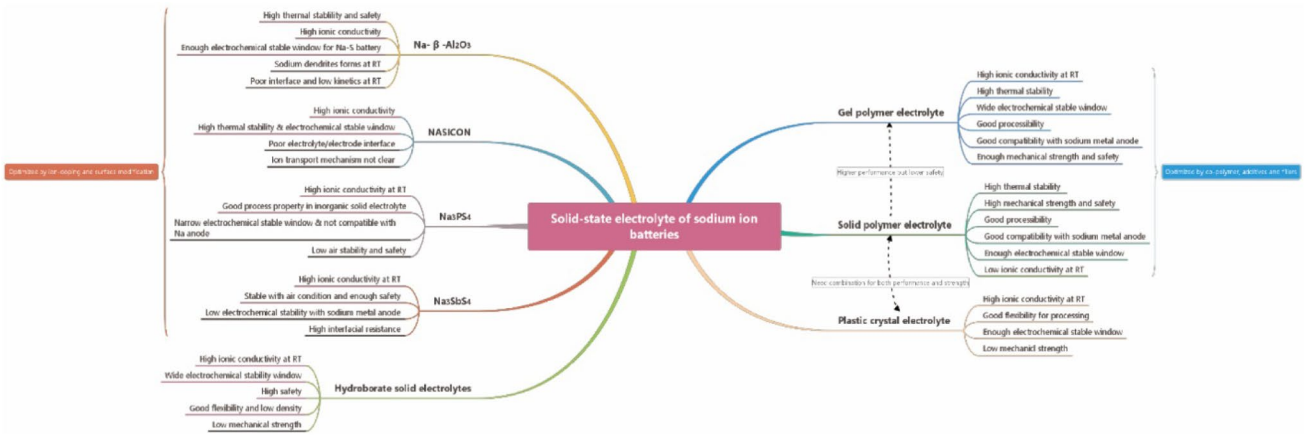

Fig. 43 Summary of the essential characteristics of different SSEs

However, there are still some problems hindering the development of GPEs. For example, poor mechanical strength and safety issues still exist. These problems can be solved by forming a 3D polymer matrix, reducing the proportion of the liquid phase and replacing small-molecule organic solvents with ionic liquids. Currently, GPEs possess sufficient ionic conductivity and electrochemical stability for SIBs. It remains a challenge to ensure that GPEs are compatible with various types of cathode materials. In addition, there are two methods for developing GPEs. It is possible to select GPEs to serve as the first commercial product of SSEs. Therefore, pilot production and industrial design have become the next research areas. Consequently, it is necessary to take into account the cost as well as the technological process involved in GPEs. On the other hand, GPEs may be designed close to SPEs, thereby reducing the amount of solvent required to achieve a balance between electrochemistry, safety, and mechanical performance.

As a result of the removal of organic solvents, SPEs have an extremely high level of safety and mechanical strength. In comparison with ISEs, it has greater flexibility because of polymers and better contact with electrodes. However, a major disadvantage of SPEs is their low ionic conductivity. SPEs are currently the subject of a large number of research studies aimed at improving ionic conductivity at room temperature. However, the gap between them and liquid electrolytes remains insurmountable, and it is not sufficient to achieve commercialization. To improve the ionic conductivity of SPEs, further research must be conducted. Materials with a Lewis acid property, such as MOFs, may enhance ionic conductivity, particularly the sodium-ion transference number. Additionally, new methodologies for ion transport need to be investigated. SPEs can also benefit from the extraction and transportation of ions. Furthermore, in the future, researchers will be able to screen materials using theoretical calculations and big data modelling, allowing them to select appropriate polymers and other materials under the guidance of theory. Through the screening of the materials, new combinations of polymers and additives with proper interactions will be discovered, which will lead to new sodium-ion transporting materials.

PCEs are a recently emerging organic solid electrolyte that has the advantages of high ionic conductivity at room temperature and relatively good electrochemical performance. The current drawbacks are the lack of sufficient mechanical strength and the high cost of some materials. Therefore, the combination of plastic crystals and elastomers has been an attractive choice. The possibility of combinations of PCEs and ISEs has not been considered before. The mixed electrolyte can be layered or sandwiched. For example, the ISE is sandwiched between two PCE layers so that the PCE has high interfacial resistance performance and the ISE provides mechanical strength and ionic conductivity as well. At present, there are still few studies on PCEs, and further systematic research is needed.

10 Conclusion

Generally, with the large-scale application of lithium-ion batteries, worries about the exhaustion of lithium and drivers to reduce costs have forced research on next-generation batteries. With abundant reserves, low raw material prices, wide distribution and aluminum fluid collection applications, SIBs have been considered to be the most promising batteries. Considering the flammability, volatility, and toxicity of liquid electrolytes and improving the energy density of SIBs, solid electrolytes have been developed to overcome these inadequacies for several years. Substantial progress has recently been made in both inorganic solid electrolytes and organic solid electrolytes. The ionic conductivity of ISEs at room temperature has been enhanced, which even caught up to that of liquid electrolytes in some situations. The main defect of ISEs is their high interfacial resistance, which needs to be addressed with a convenient and low-cost method. Under the deep research of the mechanism, the Na–β-Al_2O_3 SSE has the problem of forming sodium voids and dendrites at room temperature, preventing the room-temperature application of Na/S batteries. A further disadvantage of sulfide-based ISEs is the low electrochemical stability window that they exhibit. From the perspective of development, the performance of OSEs can be improved to be higher than that of ISEs, although the room-temperature ionic conductivity of OSEs has not met the requirements of commercial applications. This is because the optimization of organic compounds or polymers is much easier than that of inorganic compounds. The enhancement of OSEs can be inspired by different techniques, such as the membrane technique and synthesizing technique. In addition, the advantage of polymers is flexibility, which indicates that it is easier to form a higher effective contact area between the electrolyte and electrode. According to research papers in recent years, the focus of novelty has become ionic conductivity enhancement at room temperature, which promotes the application and commercialization of solid electrolytes under normalized conditions. However, there are still problems that were mentioned above for different kinds of SSEs. When regulating SSEs, it can be difficult to take into account most of the necessary properties. SSE mechanical strength and electrode wettability, for example, cannot be controlled simultaneously. Increasing the mechanical strength of SSEs typically results in hardening of its surface and a decrease in electrode wettability. Furthermore, in some circumstances, ionic conductivity and mechanical strength cannot be considered simultaneously in SPEs. A decrease in the crystallinity of the polymer in the electrolyte to increase ionic conductivity also leads to a decrease in mechanical strength, which makes it difficult to

prevent the formation of sodium dendrites and self-supporting effects. A significant consideration in this regard is the future performance balance of SSEs. The development of SSEs is at a threshold when compared with liquid electrolytes. Additionally, it is necessary to establish an SSE testing process and standards for SIBs. Thus, further research directions can be guided by the gap between the characteristics of the present electrolyte and the requirements of room-temperature ionic conductivity, a high electrochemical stability window, good interface contact, and great safety.

Acknowledgements This work was supported by the Natural Science Foundation of China (22005190, 21938005), the Science & Technology Commission of Shanghai Municipality (20QB1405700, 19DZ1205500), and the Zhejiang Key Research and Development Program (2020C01128).

Conflict of interest The authors declare no competing financial interest.

References

1. Zhou, C.T., Bag, S., Thangadurai, V.: Engineering materials for progressive all-solid-state Na batteries. ACS Energy Lett. **3**, 2181–2198 (2018). https://doi.org/10.1021/acsenergylett.8b00948
2. Peng, L.S., Wei, Z.D.: Catalyst engineering for electrochemical energy conversion from water to water: water electrolysis and the hydrogen fuel cell. Engineering **6**, 653–679 (2020). https://doi.org/10.1016/j.eng.2019.07.028
3. Wang, Z.Y., Zhao, Z.J., Baucom, J., et al.: Nitrogen-doped graphene foam as a metal-free catalyst for reduction reactions under a high gravity field. Engineering **6**, 680–687 (2020). https://doi.org/10.1016/j.eng.2019.12.018
4. Cai, Y., Chu, G.W., Luo, Y., et al.: An evaluation of metronidazole degradation in a plasma-assisted rotating disk reactor coupled with TiO_2 in aqueous solution. Engineering **7**, 1603–1610 (2021). https://doi.org/10.1016/j.eng.2020.03.020
5. Huang, X.J., Qb, M., Chen, H.J., et al.: Renewable energy conversion, storage, and efficient utilization. Science **360**, 47–51 (2018)
6. Du, S.F.: Recent advances in electrode design based on one-dimensional nanostructure arrays for proton exchange membrane fuel cell applications. Engineering **7**, 33–49 (2021). https://doi.org/10.1016/j.eng.2020.09.014
7. Mohideen, M.M., Radhamani, A.V., Ramakrishna, S., et al.: Recent insights on iron based nanostructured electrocatalyst and current status of proton exchange membrane fuel cell for sustainable transport. J. Energy Chem. **69**, 466–489 (2022). https://doi.org/10.1016/j.jechem.2022.01.035
8. Marappan, M., Palaniswamy, K., Velumani, T., et al.: Performance studies of proton exchange membrane fuel cells with different flow field designs-review. Chem. Rec. **21**, 663–714 (2021). https://doi.org/10.1002/tcr.202000138
9. Steele, B.C.H., Heinzel, A.: Materials for fuel-cell technologies. Nature **414**, 345–352 (2001). https://doi.org/10.1038/35104620
10. Lim, B., Jiang, M.J., Camargo, P.H.C., et al.: Pd-Pt bimetallic nanodendrites with high activity for oxygen reduction. Science **324**, 1302–1305 (2009). https://doi.org/10.1126/science.1170377
11. Hu, Y.S.: Batteries: getting solid. Nat. Energy **1**, 16042 (2016). https://doi.org/10.1038/nenergy.2016.42
12. Wu, T., Wen, Z.Y., Sun, C.Z., et al.: Disordered carbon tubes based on cotton cloth for modulating interface impedance in β″-Al_2O_3-based solid-state sodium metal batteries. J. Mater. Chem. A **6**, 12623–12629 (2018). https://doi.org/10.1039/c8ta01883a
13. Larcher, D., Tarascon, J.M.: Towards greener and more sustainable batteries for electrical energy storage. Nat. Chem. **7**, 19–29 (2015). https://doi.org/10.1038/nchem.2085
14. Goodenough, J.B.: How we made the Li-ion rechargeable battery. Nat. Electron. **1**, 204 (2018). https://doi.org/10.1038/s41928-018-0048-6
15. Yabuuchi, N., Kubota, K., Dahbi, M., et al.: Research development on sodium-ion batteries. Chem. Rev. **114**, 11636–11682 (2014). https://doi.org/10.1021/cr500192f
16. Service RF: Hydrogen cars: fad or the future? Science **324**, 1257–1259 (2009). https://doi.org/10.1126/science.324_1257
17. Hwang, J.Y., Myung, S.T., Sun, Y.K.: Sodium-ion batteries: present and future. Chem. Soc. Rev. **46**, 3529–3614 (2017). https://doi.org/10.1039/c6cs00776g
18. Che, H.Y., Chen, S.L., Xie, Y.Y., et al.: Electrolyte design strategies and research progress for room-temperature sodium-ion batteries. Energy Environ. Sci. **10**, 1075–1101 (2017). https://doi.org/10.1039/c7ee00524e
19. Kim, H., Kim, H., Ding, Z., et al.: Recent progress in electrode materials for sodium-ion batteries. Adv. Energy Mater. **6**, 1600943 (2016). https://doi.org/10.1002/aenm.201600943
20. Ramesh, A., Tripathi, A., Balaya, P.: A mini review on cathode materials for sodium-ion batteries. Int. J. Appl. Ceram. Technol. **19**, 913–923 (2022). https://doi.org/10.1111/ijac.13920
21. Huang, Q., Chen, G.X., Zheng, P., et al.: NASICON-structured Na ion conductor for next generation energy storage. Funct. Mater. Lett. **14**, 2130005 (2021). https://doi.org/10.1142/s1793604721300005x
22. Palomares, V., Serras, P., Villaluenga, I., et al.: Na-ion batteries, recent advances and present challenges to become low cost energy storage systems. Energy Environ. Sci. **5**, 5884–5901 (2012). https://doi.org/10.1039/C2EE02781J
23. Deng, J.Q., Luo, W.B., Chou, S.L., et al.: Sodium-ion batteries: from academic research to practical commercialization. Adv. Energy Mater. **8**, 1701428 (2018). https://doi.org/10.1002/aenm.201701428
24. Pan, H.L., Hu, Y.S., Chen, L.Q.: Room-temperature stationary sodium-ion batteries for large-scale electric energy storage. Energy Environ. Sci. **6**, 2338–2360 (2013). https://doi.org/10.1039/c3ee40847g
25. Peng, J., Zhang, W., Liu, Q.N., et al.: Prussian blue analogues for sodium-ion batteries: past, present, and future. Adv. Mater. **34**, 2108384 (2022). https://doi.org/10.1002/adma.202108384
26. Chae, M.S., Elias, Y., Aurbach, D.: Tunnel-type sodium manganese oxide cathodes for sodium-ion batteries. ChemElectroChem **8**, 798–811 (2021). https://doi.org/10.1002/celc.202001323
27. Wang, Y.S., Feng, Z.M., Cui, P.X., et al.: Pillar-beam structures prevent layered cathode materials from destructive phase transitions. Nat. Commun. **12**, 13 (2021). https://doi.org/10.1038/s41467-020-20169-1
28. Peters, J., Buchholz, D., Passerini, S., et al.: Life cycle assessment of sodium-ion batteries. Energy Environ. Sci. **9**, 1744–1751 (2016). https://doi.org/10.1039/c6ee00640j
29. Reddy, M.V., Mauger, A., Julien, C.M., et al.: Brief history of early lithium-battery development. Materials **13**, 1884 (2020). https://doi.org/10.3390/ma13081884
30. Zeng, Y.: Sodium metal batteries, electrochemical devices. China Patent CN114824167A, 29 Jul 2022
31. Tian, Y., An, Y.L., Wei, C.L., et al.: Recently advances and perspectives of anode-free rechargeable batteries. Nano Energy **78**, 105344 (2020). https://doi.org/10.1016/j.nanoen.2020.105344

32. Nakamoto, K., Sakamoto, R., Sawada, Y., et al.: Over 2 V aqueous sodium-ion battery with Prussian blue-type electrodes. Small Methods **3**, 1800220 (2019). https://doi.org/10.1002/smtd.201800220
33. Jeong, S., Kim, B.H., Park, Y.D., et al.: Artificially coated $NaFePO_4$ for aqueous rechargeable sodium-ion batteries. J. Alloys Compd. **784**, 720–726 (2019). https://doi.org/10.1016/j.jallcom.2019.01.046
34. Zhang, J., Wang, D.W., Lv, W., et al.: Ethers illume sodium-based battery chemistry: uniqueness, surprise, and challenges. Adv. Energy Mater. **8**, 1801361 (2018). https://doi.org/10.1002/aenm.201801361
35. Mauger, Julien, Paolella, et al.: Building better batteries in the solid state: a review. Materials **12**, 3892 (2019). https://doi.org/10.3390/ma12233892
36. Jin, T., Ji, X., Wang, P.F., et al.: High-energy aqueous sodium-ion batteries. Angew. Chem. Int. Ed. **60**, 11943–11948 (2021). https://doi.org/10.1002/anie.202017167
37. Jiang, P., Lei, Z.Y., Chen, L., et al.: Polyethylene glycol-Na^+ interface of vanadium hexacyanoferrate cathode for highly stable rechargeable aqueous sodium-ion battery. ACS Appl. Mater. Interfaces **11**, 28762–28768 (2019). https://doi.org/10.1021/acsami.9b04849
38. Bin, D., Wang, F., Tamirat, A.G., et al.: Progress in aqueous rechargeable sodium-ion batteries. Adv. Energy Mater. **8**, 1703008 (2018). https://doi.org/10.1002/aenm.201703008
39. Zhang, H., Qin, B.S., Han, J., et al.: Aqueous/nonaqueous hybrid electrolyte for sodium-ion batteries. ACS Energy Lett. **3**, 1769–1770 (2018). https://doi.org/10.1021/acsenergylett.8b00919
40. Li, Q., Cao, Z., Wahyudi, W., et al.: Unraveling the new role of an ethylene carbonate solvation shell in rechargeable metal ion batteries. ACS Energy Lett. **6**, 69–78 (2021). https://doi.org/10.1021/acsenergylett.0c02140
41. Olsson, E., Cottom, J., Alptekin, H., et al.: Investigating the role of surface roughness and defects on EC breakdown, as a precursor to SEI formation in hard carbon sodium-ion battery anodes. Small **18**, 2200177 (2022). https://doi.org/10.1002/smll.202200177
42. Dubois, M., Ghanbaja, J., Billaud, D.: Electrochemical intercalation of sodium ions into poly(*para*-phenylene) in carbonate-based electrolytes. Synth. Met. **90**, 127–134 (1997). https://doi.org/10.1016/S0379-6779(97)81261-1
43. Hofmann, A., Wang, Z.Q., Bautista, S.P., et al.: Comprehensive characterization of propylene carbonate based liquid electrolyte mixtures for sodium-ion cells. Electrochim. Acta **403**, 139670 (2022). https://doi.org/10.1016/j.electacta.2021.139670
44. Subramanyan, K., Lee, Y.S., Aravindan, V.: Impact of carbonate-based electrolytes on the electrochemical activity of carbon-coated $Na_3V_2(PO_4)_2F_3$ cathode in full-cell assembly with hard carbon anode. J. Colloid Interface Sci. **582**, 51–59 (2021). https://doi.org/10.1016/j.jcis.2020.08.043
45. Kamath, G., Cutler, R.W., Deshmukh, S.A., et al.: In silico based rank-order determination and experiments on nonaqueous electrolytes for sodium ion battery applications. J. Phys. Chem. C **118**, 13406–13416 (2014). https://doi.org/10.1021/jp502319p
46. Liu, Q., Wu, F., Mu, D.B., et al.: A theoretical study on Na^+ solvation in carbonate ester and ether solvents for sodium-ion batteries. Phys. Chem. Chem. Phys. **22**, 2164–2175 (2020). https://doi.org/10.1039/c9cp05636j
47. Ponrouch, A., Monti, D., Boschin, A., et al.: Non-aqueous electrolytes for sodium-ion batteries. J. Mater. Chem. A **3**, 22–42 (2015). https://doi.org/10.1039/c4ta04428b
48. Wan, M., Tang, Y., Wang, L.L., et al.: Core-shell hexacyanoferrate for superior Na-ion batteries. J. Power Sources **329**, 290–296 (2016). https://doi.org/10.1016/j.jpowsour.2016.08.059
49. Viet Thieu, Q.Q., Hoang, H., Le, V.T., et al.: Enhancing electrochemical performance of sodium Prussian blue cathodes for sodium-ion batteries via optimizing alkyl carbonate electrolytes. Ceram. Int. **47**, 30164–30171 (2021). https://doi.org/10.1016/j.ceramint.2021.07.195
50. Jang, J.Y., Kim, H., Lee, Y., et al.: Cyclic carbonate based-electrolytes enhancing the electrochemical performance of $Na_4Fe_3(PO_4)_2(P_2O_7)$ cathodes for sodium-ion batteries. Electrochem. Commun. **44**, 74–77 (2014). https://doi.org/10.1016/j.elecom.2014.05.003
51. Ponrouch, A., Marchante, E., Courty, M., et al.: In search of an optimized electrolyte for Na-ion batteries. Energy Environ. Sci. **5**, 8572–8583 (2012). https://doi.org/10.1039/c2ee22258b
52. Jache, B., Adelhelm, P.: Use of graphite as a highly reversible electrode with superior cycle life for sodium-ion batteries by making use of co-intercalation phenomena. Angew. Chem. Int. Ed. **53**, 10169–10173 (2014). https://doi.org/10.1002/anie.201403734
53. Lin, Z.H., Xia, Q.B., Wang, W.L., et al.: Recent research progresses in ether- and ester-based electrolytes for sodium-ion batteries. InfoMat **1**, 376–389 (2019). https://doi.org/10.1002/inf2.12023
54. Slater, M.D., Kim, D., Lee, E., et al.: Sodium-ion batteries. Adv. Funct. Mater. **23**, 947–958 (2013). https://doi.org/10.1002/adfm.201200691
55. Zhao, C.L., Liu, L.L., Qi, X.G., et al.: Solid-state sodium batteries. Adv. Energy Mater. **8**, 1703012 (2018). https://doi.org/10.1002/aenm.201703012
56. Amaral, M.M., Venâncio, R., Peterlevitz, A.C., et al.: Recent advances on quasi-solid-state electrolytes for supercapacitors. J. Energy Chem. **67**, 697–717 (2022). https://doi.org/10.1016/j.jechem.2021.11.010
57. Janek, J., Zeier, W.G.: A solid future for battery development. Nat. Energy **1**, 16141 (2016). https://doi.org/10.1038/nenergy.2016.141
58. Guin, M., Tietz, F., Guillon, O.: New promising NASICON material as solid electrolyte for sodium-ion batteries: correlation between composition, crystal structure and ionic conductivity of $Na_{3+x}Sc_2Si_xP_{3-x}O_{12}$. Solid State Ion. **293**, 18–26 (2016). https://doi.org/10.1016/j.ssi.2016.06.005
59. Monti, D., Jónsson, E., Palacín, M.R., et al.: Ionic liquid based electrolytes for sodium-ion batteries: Na^+ solvation and ionic conductivity. J. Power Sources **245**, 630–636 (2014). https://doi.org/10.1016/j.jpowsour.2013.06.153
60. Kaur, G., Kumar, H., Singla, M.: Diverse applications of ionic liquids: a comprehensive review. J. Mol. Liq. **351**, 118556 (2022). https://doi.org/10.1016/j.molliq.2022.118556
61. Ghandi, K.: A review of ionic liquids, their limits and applications. Green Sustain. Chem. **4**, 44–53 (2014). https://doi.org/10.4236/gsc.2014.41008
62. Hagiwara, R., Matsumoto, K., Hwang, J., et al.: Sodium ion batteries using ionic liquids as electrolytes. Chem. Rec. **19**, 758–770 (2019). https://doi.org/10.1002/tcr.201800119
63. Basile, A., Hilder, M., Makhlooghiazad, F., et al.: Sodium energy storage: ionic liquids and organic ionic plastic crystals: advanced electrolytes for safer high performance sodium energy storage technologies. Adv. Energy Mater. **8**(17), 1870078 (2018). https://doi.org/10.1002/aenm.201870078
64. Xu, C.X., Yang, G., Wu, D.X., et al.: Roadmap on ionic liquid electrolytes for energy storage devices. Chem. Asian J. **16**, 549–562 (2021). https://doi.org/10.1002/asia.202001414
65. Wang, Y.M., Song, S.F., Xu, C.H., et al.: Development of solid-state electrolytes for sodium-ion battery: a short review. Nano Mater. Sci. **1**, 91–100 (2019). https://doi.org/10.1016/j.nanoms.2019.02.007

66. Lian, P.J., Zhao, B.S., Zhang, L.Q., et al.: Inorganic sulfide solid electrolytes for all-solid-state lithium secondary batteries. J. Mater. Chem. A **7**, 20540–20557 (2019). https://doi.org/10.1039/c9ta04555d
67. Hu, C.J., Qi, J.Z., Zhang, Y.X., et al.: Room-temperature all-solid-state sodium battery based on bulk interfacial superionic conductor. Nano Lett. **21**, 10354–10360 (2021). https://doi.org/10.1021/acs.nanolett.1c03605
68. Chen, S.L., Che, H.Y., Feng, F., et al.: Poly(vinylene carbonate)-based composite polymer electrolyte with enhanced interfacial stability to realize high-performance room-temperature solid-state sodium batteries. ACS Appl. Mater. Interfaces **11**, 43056–43065 (2019). https://doi.org/10.1021/acsami.9b11259
69. Chen, S.L., Feng, F., Che, H.Y., et al.: High performance solid-state sodium batteries enabled by boron contained 3D composite polymer electrolyte. Chem. Eng. J. **406**, 126736 (2021). https://doi.org/10.1016/j.cej.2020.126736
70. Yao, X.Y., Huang, B.X., Yin, J.Y., et al.: All-solid-state lithium batteries with inorganic solid electrolytes: review of fundamental science. Chin. Phys. B **25**, 018802 (2016). https://doi.org/10.1088/1674-1056/25/1/018802
71. Schnell, J., Günther, T., Knoche, T., et al.: All-solid-state lithium-ion and lithium metal batteries: paving the way to large-scale production. J. Power Sources **382**, 160–175 (2018). https://doi.org/10.1016/j.jpowsour.2018.02.062
72. Xu, G.L., Amine, R., Abouimrane, A., et al.: Challenges in developing electrodes, electrolytes, and diagnostics tools to understand and advance sodium-ion batteries. Adv. Energy Mater. **8**, 1702403 (2018). https://doi.org/10.1002/aenm.201702403
73. Zheng, S.Y., Yan, J.Y., Wang, K.: Engineering research progress of electrochemical microreaction technology: a novel method for electrosynthesis of organic chemicals. Engineering **7**, 22–32 (2021). https://doi.org/10.1016/j.eng.2020.06.025
74. Duchêne, L., Kühnel, R.S., Rentsch, D., et al.: A highly stable sodium solid-state electrolyte based on a dodeca/deca-borate equimolar mixture. Chem. Commun. **53**, 4195–4198 (2017). https://doi.org/10.1039/c7cc00794a
75. Yang, Z., Jin, M.Y., Cheng, S., et al.: Developing a high-voltage electrolyte based on *conjuncto*-hydroborates for solid-state sodium batteries. J. Mater. Chem. A **10**, 7186–7194 (2022). https://doi.org/10.1039/d1ta09386j
76. Chen, S.L., Feng, F., Yin, Y.M., et al.: Plastic crystal polymer electrolytes containing boron based anion acceptors for room temperature all-solid-state sodium-ion batteries. Energy Storage Mater. **22**, 57–65 (2019). https://doi.org/10.1016/j.ensm.2018.12.023
77. Zhang, Z.Z., Shao, Y.J., Lotsch, B., et al.: New horizons for inorganic solid state ion conductors. Energy Environ. Sci. **11**, 1945–1976 (2018). https://doi.org/10.1039/c8ee01053f
78. Banerjee, A., Park, K.H., Heo, J.W., et al.: Na_3SbS_4: a solution processable sodium superionic conductor for all-solid-state sodium-ion batteries. Angew. Chem. Int. Ed. **55**, 9634–9638 (2016). https://doi.org/10.1002/anie.201604158
79. Kim, J.J., Yoon, K., Park, I., et al.: Progress in the development of sodium-ion solid electrolytes. Small Methods **1**, 1700219 (2017). https://doi.org/10.1002/smtd.201700219
80. Famprikis, T., Canepa, P., Dawson, J.A., et al.: Fundamentals of inorganic solid-state electrolytes for batteries. Nat. Mater. **18**, 1278–1291 (2019). https://doi.org/10.1038/s41563-019-0431-3
81. Bachman, J.C., Muy, S., Grimaud, A., et al.: Inorganic solid-state electrolytes for lithium batteries: mechanisms and properties governing ion conduction. Chem. Rev. **116**, 140–162 (2016). https://doi.org/10.1021/acs.chemrev.5b00563
82. Lacivita, V., Wang, Y., Bo, S.H., et al.: *Ab initio* investigation of the stability of electrolyte/electrode interfaces in all-solid-state Na batteries. J. Mater. Chem. A **7**, 8144–8155 (2019). https://doi.org/10.1039/c8ta10498k
83. Lu, X.C., Xia, G.G., Lemmon, J.P., et al.: Advanced materials for sodium-beta alumina batteries: status, challenges and perspectives. J. Power Sources **195**, 2431–2442 (2010). https://doi.org/10.1016/j.jpowsour.2009.11.120
84. Goodenough, J.B.: Evolution of strategies for modern rechargeable batteries. Acc. Chem. Res. **46**, 1053–1061 (2013). https://doi.org/10.1021/ar2002705
85. Lu, Y., Li, L., Zhang, Q., et al.: Electrolyte and interface engineering for solid-state sodium batteries. Joule **2**, 1747–1770 (2018). https://doi.org/10.1016/j.joule.2018.07.028
86. Birnie, D.P., III.: On the structural integrity of the spinel block in the β"-alumina structure. Acta Crystallogr. Sect. B Struct. Sci. **68**, 118–122 (2012). https://doi.org/10.1107/s0108768112002649
87. Kummer, J.T.: Ion exchange properties of and rates of ionic diffusion in beta-alumina. J. Inorg. Nucl. Chem. **29**, 2453–2475 (1967). https://doi.org/10.1016/0022-1902(67)80301-4
88. Sudworth, J.L.: The sodium/sulphur battery. J. Power Sources **11**, 143–154 (1984). https://doi.org/10.1016/0378-7753(84)80080-4
89. Ghadbeigi, L., Szendrei, A., Moreno, P., et al.: Synthesis of iron-doped Na-β″–alumina + yttria-stabilized zirconia composite electrolytes by a vapor phase process. Solid State Ion. **290**, 77–82 (2016). https://doi.org/10.1016/j.ssi.2016.04.006
90. Viswanathan, L., Ikuma, Y., Virkar, A.V.: Transfomation toughening of β″-alumina by incorporation of zirconia. J. Mater. Sci. **18**, 109–113 (1983). https://doi.org/10.1007/BF00543815
91. Liu, Z.H., Chen, J.J., Wang, X.X., et al.: Synthesis and characterization of high ionic-conductive sodium beta-alumina solid electrolyte derived from boehmite. J. Mater. Sci. Mater. Electron. **31**, 17670–17678 (2020). https://doi.org/10.1007/s10854-020-04321-7
92. Li, H., Fan, H.Q., Chen, G.Y., et al.: Performance of nano-3YSZ toughened β''-alumina solid electrolyte prepared by EDTA-$Zr^{(IV)}/Y^{(III)}$ complex as surface modifier. J. Alloys Compd. **817**, 152717 (2020). https://doi.org/10.1016/j.jallcom.2019.152717
93. Park, R.J.Y., Eschler, C.M., Fincher, C.D., et al.: Semi-solid alkali metal electrodes enabling high critical current densities in solid electrolyte batteries. Nat. Energy **6**, 314–322 (2021). https://doi.org/10.1038/s41560-021-00786-w
94. Spencer Jolly, D., Ning, Z.Y., Darnbrough, J.E., et al.: Sodium/Na β″ alumina interface: effect of pressure on voids. ACS Appl. Mater. Interfaces **12**, 678–685 (2020). https://doi.org/10.1021/acsami.9b17786
95. Lei, D.N., He, Y.B., Huang, H.J., et al.: Cross-linked beta alumina nanowires with compact gel polymer electrolyte coating for ultra-stable sodium metal battery. Nat. Commun. **10**, 4244 (2019). https://doi.org/10.1038/s41467-019-11960-w
96. Medenbach, L., Hartmann, P., Janek, J., et al.: A sodium polysulfide battery with liquid/solid electrolyte: improving sulfur utilization using P_2S_5 as additive and tetramethylurea as catholyte solvent. Energy Technol. **8**, 1901200 (2020). https://doi.org/10.1002/ente.201901200
97. Wang, D., Hwang, J., Chen, C.Y., et al.: A β″-alumina/inorganic ionic liquid dual electrolyte for intermediate-temperature sodium–sulfur batteries. Adv. Funct. Mater. **31**, 2105524 (2021). https://doi.org/10.1002/adfm.202105524
98. Goodenough, J.B., Hong, H.Y.P., Kafalas, J.A.: Fast Na^+-ion transport in skeleton structures. Mater. Res. Bull. **11**, 203–220 (1976). https://doi.org/10.1016/0025-5408(76)90077-5
99. Hong, H.Y.P.: Crystal structures and crystal chemistry in the system $Na_{1+x}Zr_2Si_xP_{3-x}O_{12}$. Mater. Res. Bull. **11**, 173–182 (1976). https://doi.org/10.1016/0025-5408(76)90073-8
100. Zhang, Z.Z., Zou, Z.Y., Kaup, K., et al.: Correlated migration invokes higher Na^+-ion conductivity in NaSICON-type solid

electrolytes. Adv. Energy Mater. **9**, 1902373 (2019). https://doi.org/10.1002/aenm.201902373
101. Benabed, Y., Rioux, M., Rousselot, S., et al.: Assessing the electrochemical stability window of NASICON-type solid electrolytes. Front. Energy Res. **9**, 682008 (2021). https://doi.org/10.3389/fenrg.2021.682008
102. Schwietert, T.K., Arszelewska, V.A., Wang, C., et al.: Clarifying the relationship between redox activity and electrochemical stability in solid electrolytes. Nat. Mater. **19**, 428–435 (2020). https://doi.org/10.1038/s41563-019-0576-0
103. Yang, Z.D., Tang, B., Xie, Z.J., et al.: NASICON-type $Na_3Zr_2Si_2PO_{12}$ solid-state electrolytes for sodium batteries. ChemElectroChem **8**, 1035–1047 (2021). https://doi.org/10.1002/celc.202001527
104. Sun, F., Xiang, Y.X., Sun, Q., et al.: Origin of high ionic conductivity of Sc-doped sodium-rich NASICON solid-state electrolytes. Adv. Funct. Mater. **31**, 2102129 (2021). https://doi.org/10.1002/adfm.202102129
105. Zhang, Z.Z., Zhang, Q.H., Shi, J.N., et al.: A self-forming composite electrolyte for solid-state sodium battery with ultralong cycle life. Adv. Energy Mater. **7**, 1601196 (2017). https://doi.org/10.1002/aenm.201601196
106. Martínez-Cisneros, C.S., Pandit, B., Antonelli, C., et al.: Development of sodium hybrid quasi-solid electrolytes based on porous NASICON and ionic liquids. J. Eur. Ceram. Soc. **41**, 7723–7733 (2021). https://doi.org/10.1016/j.jeurceramsoc.2021.08.001
107. Park, K.H., Bai, Q., Kim, D.H., et al.: Design strategies, practical considerations, and new solution processes of sulfide solid electrolytes for all-solid-state batteries. Adv. Energy Mater. **8**, 1800035 (2018). https://doi.org/10.1002/aenm.201800035
108. Jansen, M., Henseler, U.: Synthesis, structure determination, and ionic conductivity of sodium tetrathiophosphate. J. Solid State Chem. **99**, 110–119 (1992). https://doi.org/10.1016/0022-4596(92)90295-7
109. Hayashi, A., Noi, K., Sakuda, A., et al.: Superionic glass-ceramic electrolytes for room-temperature rechargeable sodium batteries. Nat. Commun. **3**, 856 (2012). https://doi.org/10.1038/ncomms1843
110. Moon, C.K., Lee, H.J., Park, K.H., et al.: Vacancy-driven Na^+ superionic conduction in new Ca-doped Na_3PS_4 for all-solid-state Na-ion batteries. ACS Energy Lett. **3**, 2504–2512 (2018). https://doi.org/10.1021/acsenergylett.8b01479
111. Feng, X.Y., Chien, P.H., Zhu, Z.Y., et al.: Studies of functional defects for fast Na-ion conduction in $Na_{3-y}PS_{4-x}Cl_x$ with a combined experimental and computational approach. Adv. Funct. Mater. **29**, 1807951 (2019). https://doi.org/10.1002/adfm.201807951
112. Han, F.D., Zhu, Y.Z., He, X.F., et al.: Electrochemical stability of $Li_{10}GeP_2S_{12}$ and $Li_7La_3Zr_2O_{12}$ solid electrolytes. Adv. Energy Mater. **6**, 1501590 (2016). https://doi.org/10.1002/aenm.201501590
113. Wang, H., Chen, Y., Hood, Z.D., et al.: An air-stable Na_3SbS_4 superionic conductor prepared by a rapid and economic synthetic procedure. Angew. Chem. Int. Ed. **55**, 8551–8555 (2016). https://doi.org/10.1002/anie.201601546
114. Gamo, H., Phuc, N.H.H., Matsuda, R., et al.: Multiphase Na_3SbS_4 with high ionic conductivity. Mater. Today Energy **13**, 45–49 (2019). https://doi.org/10.1016/j.mtener.2019.04.012
115. Yubuchi, S., Ito, A., Masuzawa, N., et al.: Aqueous solution synthesis of Na_3SbS_4–Na_2WS_4 superionic conductors. J. Mater. Chem. A **8**, 1947–1954 (2020). https://doi.org/10.1039/c9ta02246e
116. Tsuji, F., Masuzawa, N., Sakuda, A., et al.: Preparation and characterization of cation-substituted Na_3SbS_4 solid electrolytes. ACS Appl. Energy Mater. **3**, 11706–11712 (2020). https://doi.org/10.1021/acsaem.0c01823
117. Banerjee, A., Park, K.H., Heo, J.W., et al.: Na_3SbS_4: a solution processable sodium superionic conductor for all-solid-state sodium-ion batteries. Angew. Chem. **128**, 9786–9790 (2016). https://doi.org/10.1002/ange.201604158
118. Tian, Y.S., Sun, Y.Z., Hannah, D.C., et al.: Reactivity-guided interface design in Na metal solid-state batteries. Joule **3**, 1037–1050 (2019). https://doi.org/10.1016/j.joule.2018.12.019
119. Matsuo, M., Kuromoto, S., Sato, T., et al.: Sodium ionic conduction in complex hydrides with $[BH_4]^-$ and $[NH_2]^-$ anions. Appl. Phys. Lett. **100**, 203904 (2012). https://doi.org/10.1063/1.4716021
120. Tang, W.S., Yoshida, K., Soloninin, A.V., et al.: Stabilizing superionic-conducting structures via mixed-anion solid solutions of monocarba-*closo*-borate salts. ACS Energy Lett. **1**, 659–664 (2016). https://doi.org/10.1021/acsenergylett.6b00310
121. Sun, Y.L., Wang, Y.C., Liang, X.M., et al.: Rotational cluster anion enabling superionic conductivity in sodium-rich antiperovskite Na_3OBH_4. J. Am. Chem. Soc. **141**, 5640–5644 (2019). https://doi.org/10.1021/jacs.9b01746
122. Duchêne, L., Remhof, A., Hagemann, H., et al.: Status and prospects of hydroborate electrolytes for all-solid-state batteries. Energy Storage Mater. **25**, 782–794 (2020). https://doi.org/10.1016/j.ensm.2019.08.032
123. Yoon, K., Kim, J.J., Seong, W.M., et al.: Investigation on the interface between $Li_{10}GeP_2S_{12}$ electrolyte and carbon conductive agents in all-solid-state lithium battery. Sci. Rep. **8**, 8066 (2018). https://doi.org/10.1038/s41598-018-26101-4
124. Agrawal, R.C., Pandey, G.P.: Solid polymer electrolytes: materials designing and all-solid-state battery applications: an overview. J. Phys. D Appl. Phys. **41**, 223001 (2008). https://doi.org/10.1088/0022-3727/41/22/223001
125. Long, L.Z., Wang, S.J., Xiao, M., et al.: Polymer electrolytes for lithium polymer batteries. J. Mater. Chem. A **4**, 10038–10069 (2016). https://doi.org/10.1039/c6ta02621d
126. Wright, P.V.: Electrical conductivity in ionic complexes of poly(ethylene oxide). Brit. Polym. J. **7**, 319–327 (1975). https://doi.org/10.1002/pi.4980070505
127. Xue, Z.G., He, D., Xie, X.L.: Poly(ethylene oxide)-based electrolytes for lithium-ion batteries. J. Mater. Chem. A **3**, 19218–19253 (2015). https://doi.org/10.1039/c5ta03471j
128. Devi, C., Gellanki, J., Pettersson, H., et al.: High sodium ionic conductivity in PEO/PVP solid polymer electrolytes with InAs nanowire fillers. Sci. Rep. **11**, 20180 (2021). https://doi.org/10.1038/s41598-021-99663-5
129. Guo, B., Fu, Y.D., Wang, J.N., et al.: Strategies and characterization methods for achieving high performance PEO-based solid-state lithium-ion batteries. Chem. Commun. **58**, 8182–8193 (2022). https://doi.org/10.1039/d2cc02306g
130. Shenbagavalli, S., Muthuvinayagam, M., Jayanthi, S., et al.: Investigations on Al_2O_3 dispersed PEO/PVP based Na^+ ion conducting blend polymer electrolytes. J. Mater. Sci. Mater. Electron. **32**, 9998–10007 (2021). https://doi.org/10.1007/s10854-021-05658-3
131. Yao, Y.W., Liu, Z.H., Wang, X.X., et al.: Promoted ion conductivity of sodium salt–poly(ethylene oxide) polymer electrolyte induced by adding conductive beta-alumina and application in all-solid-state sodium batteries. J. Mater. Sci. **56**, 9951–9960 (2021). https://doi.org/10.1007/s10853-021-05885-3
132. Chen, G.H., Bai, Y., Gao, Y.S., et al.: Inhibition of crystallization of poly(ethylene oxide) by ionic liquid: insight into plasticizing mechanism and application for solid-state sodium ion batteries. ACS Appl. Mater. Interfaces **11**, 43252–43260 (2019). https://doi.org/10.1021/acsami.9b16294

133. Hulvat, J.F., Stupp, S.I.: Liquid-crystal templating of conducting polymers. Angew. Chem. Int. Ed. **42**, 778–781 (2003). https://doi.org/10.1002/anie.200390206
134. Koduru, H.K., Marinov, Y.G., Hadjichristov, G.B., et al.: Characterization of polymer/liquid crystal composite based electrolyte membranes for sodium ion battery applications. Solid State Ion. **335**, 86–96 (2019). https://doi.org/10.1016/j.ssi.2019.02.021
135. Park, S.S., Tulchinsky, Y., Dincă, M.: Single-ion Li^+, Na^+, and Mg^{2+} solid electrolytes supported by a mesoporous anionic Cu–azolate metal–organic framework. J. Am. Chem. Soc. **139**, 13260–13263 (2017). https://doi.org/10.1021/jacs.7b06197
136. Wei, T., Wang, Z.M., Zhang, Q., et al.: Metal–organic framework-based solid-state electrolytes for all solid-state lithium metal batteries: a review. CrystEngComm **24**, 5014–5030 (2022). https://doi.org/10.1039/d2ce00663d
137. Ge, Z., Li, J., Liu, J.: Enhanced electrochemical performance of all-solid-state sodium-sulfur batteries by PEO–$NaCF_3SO_3$–MIL-53(Al) solid electrolyte. Ionics **26**, 1787–1795 (2020). https://doi.org/10.1007/s11581-020-03513-9
138. Svarfvar, B.L., Ekman, K.B., Sundell, M.J., et al.: Electron-beam graft-modified membranes with externally controlled flux. Polym. Adv. Technol. **7**, 839–846 (1996). https://doi.org/10.1002/(sici)1099-1581(199611)7:11839:aid-pat592%3e3.0.co;2-t
139. Bristi, A.A., Samson, A.J., Sivakumaran, A., et al.: Ionic conductivity, Na plating–stripping, and battery performance of solid polymer Na ion electrolyte based on poly(vinylidene fluoride) and poly(vinyl pyrrolidone). ACS Appl. Energy Mater. **5**, 8812–8822 (2022). https://doi.org/10.1021/acsaem.2c01296
140. Bag, S., Zhou, C.T., Reid, S., et al.: Electrochemical studies on symmetric solid-state Na-ion full cell using $Na_3V_2(PO_4)_3$ electrodes and polymer composite electrolyte. J. Power Sources **454**, 227954 (2020). https://doi.org/10.1016/j.jpowsour.2020.227954
141. Wang, X.E., Zhu, H.J., Greene, G.W., et al.: Enhancement of ion dynamics in organic ionic plastic crystal/PVDF composite electrolytes prepared by co-electrospinning. J. Mater. Chem. A **4**, 9873–9880 (2016). https://doi.org/10.1039/c6ta02817a
142. Makhlooghiazad, F., Nti, F., Sun, J., et al.: Composite electrolytes based on electrospun PVDF and ionic plastic crystal matrices for Na-metal battery applications. J. Phys. Mater. **4**, 034003 (2021). https://doi.org/10.1088/2515-7639/abeed2
143. Fang, R.Y., Li, Y.T., Wu, N., et al.: Ultra-thin single-particle-layer sodium beta-alumina-based composite polymer electrolyte membrane for sodium-metal batteries. Adv. Funct. Mater. **33**, 2211229 (2023). https://doi.org/10.1002/adfm.202211229
144. Shetty, S.K., Ismayil, Nasreen, et al.: Sodium ion conducting PVA/NaCMC bio poly-blend electrolyte films for energy storage device applications. Int. J. Polym. Anal. Charact. **26**, 411–424 (2021). https://doi.org/10.1080/1023666x.2021.1899685
145. Cyriac, V., Ismayil, Noor, I.S.B.M., et al.: Modification in the microstructure of sodium carboxymethylcellulose/polyvinyl alcohol polyblend films through the incorporation of $NaNO_3$ for energy storage applications. Int. J. Energy Res. **46**, 22845–22866 (2022). https://doi.org/10.1002/er.8588
146. Yu, X.W., Xue, L.G., Goodenough, J.B., et al.: All-solid-state sodium batteries with a polyethylene glycol diacrylate–$Na_3Zr_2Si_2PO_{12}$ composite electrolyte. Adv. Energy Sustain. Res. **2**, 2000061 (2021). https://doi.org/10.1002/aesr.202000061
147. Ren, Y.X., Hortance, N., McBride, J., et al.: Sodium-sulfur batteries enabled by a protected inorganic/organic hybrid solid electrolyte. ACS Energy Lett. **6**, 345–353 (2021). https://doi.org/10.1021/acsenergylett.0c02494
148. Batten, S.R., Champness, N.R., Chen, X.M., et al.: Terminology of metal–organic frameworks and coordination polymers (IUPAC Recommendations 2013). Pure Appl. Chem. **85**, 1715–1724 (2013). https://doi.org/10.1351/pac-rec-12-11-20
149. Gebert, F., Knott, J., Gorkin, R., et al.: Polymer electrolytes for sodium-ion batteries. Energy Storage Mater. **36**, 10–30 (2021). https://doi.org/10.1016/j.ensm.2020.11.030
150. Menisha, M., Senavirathna, S.L.N., Vignarooban, K., et al.: Synthesis, electrochemical and optical studies of poly(ethylene oxide) based gel-polymer electrolytes for sodium-ion secondary batteries. Solid State Ion. **371**, 115755 (2021). https://doi.org/10.1016/j.ssi.2021.115755
151. Feuillade, G., Perche, P.: Ion-conductive macromolecular gels and membranes for solid lithium cells. J. Appl. Electrochem. **5**, 63–69 (1975). https://doi.org/10.1007/BF00625960
152. Yu, Q.P., Lu, Q.W., Qi, X.G., et al.: Liquid electrolyte immobilized in compact polymer matrix for stable sodium metal anodes. Energy Storage Mater. **23**, 610–616 (2019). https://doi.org/10.1016/j.ensm.2019.03.011
153. Choi, N.S., Lee, Y.G., Park, J.K., et al.: Preparation and electrochemcial characteristics of plasticized polymer electrolytes based upon a P(VdF-co-HFP)/PVAc blend. Electrochim. Acta **46**, 1581–1586 (2001). https://doi.org/10.1016/S0013-4686(00)00756-8
154. Vo, D.T., Do, H.N., Nguyen, T.T., et al.: Sodium ion conducting gel polymer electrolyte using poly(vinylidene fluoride hexafluoropropylene). Mater. Sci. Eng. B **241**, 27–35 (2019). https://doi.org/10.1016/j.mseb.2019.02.007
155. Janakiraman, S., Agrawal, A., Biswal, R., et al.: An amorphous polyvinylidene fluoride-co-hexafluoropropylene based gel polymer electrolyte for sodium-ion cells. Appl. Surf. Sci. Adv. **6**, 100139 (2021). https://doi.org/10.1016/j.apsadv.2021.100139
156. Chauhan, A.K., Kumar, D., Mishra, K., et al.: Performance enhancement of Na^+ ion conducting porous gel polymer electrolyte using $NaAlO_2$ active filler. Mater. Today Commun. **26**, 101713 (2021). https://doi.org/10.1016/j.mtcomm.2020.101713
157. Kwon, D.S., Gong, S.H., Yun, S., et al.: Regulating Na electrodeposition by sodiophilic grafting onto porosity-gradient gel polymer electrolytes for dendrite-free sodium metal batteries. ACS Appl. Mater. Interfaces **14**, 47650–47658 (2022). https://doi.org/10.1021/acsami.2c12287
158. Zhao, C.D., Guo, J.Z., Gu, Z.Y., et al.: Flexible quasi-solid-state sodium-ion full battery with ultralong cycle life, high energy density and high-rate capability. Nano Res. **15**, 925–932 (2022). https://doi.org/10.1007/s12274-021-3577-7
159. Shubha, N., Prasanth, R., Hng, H.H., et al.: Study on effect of poly (ethylene oxide) addition and *in-situ* porosity generation on poly (vinylidene fluoride)-glass ceramic composite membranes for lithium polymer batteries. J. Power Sources **267**, 48–57 (2014). https://doi.org/10.1016/j.jpowsour.2014.05.074
160. Zhang, Y.G., Bakenov, Z., Tan, T.Z., et al.: Polyacrylonitrile-nanofiber-based gel polymer electrolyte for novel aqueous sodium-ion battery based on a $Na_4Mn_9O_{18}$ cathode and Zn metal anode. Polymers **10**, 853 (2018). https://doi.org/10.3390/polym10080853
161. Lonchakova, O.V., Semenikhin, O.A., Zakharkin, M.V., et al.: Efficient gel-polymer electrolyte for sodium-ion batteries based on poly(acrylonitrile-co-methyl acrylate). Electrochim. Acta **334**, 135512 (2020). https://doi.org/10.1016/j.electacta.2019.135512
162. Zhou, Y.N., Xiao, Z.C., Han, D.Z., et al.: Approaching practically accessible and environmentally adaptive sodium metal batteries with high loading cathodes through *in situ* interlock interface. Adv. Funct. Mater. **32**, 2111314 (2022). https://doi.org/10.1002/adfm.202111314
163. Shuai, Y., Lou, J., Pei, X.L., et al.: Constructing an *in situ* polymer electrolyte and a Na-rich artificial SEI layer toward practical

solid-state Na metal batteries. ACS Appl. Mater. Interfaces **14**, 45382–45391 (2022). https://doi.org/10.1021/acsami.2c12518
164. Gandini, A.: Polymers from renewable resources: a challenge for the future of macromolecular materials. Macromolecules **41**, 9491–9504 (2008). https://doi.org/10.1021/ma801735u
165. Mittal, N., Ojanguren, A., Cavasin, N., et al.: Transient rechargeable battery with a high lithium transport number cellulosic separator. Adv. Funct. Mater. **31**, 2101827 (2021). https://doi.org/10.1002/adfm.202101827
166. Mittal, N., Tien, S.A., Lizundia, E., et al.: Hierarchical nanocellulose-based gel polymer electrolytes for stable Na electrodeposition in sodium ion batteries. Small **18**, 2107183 (2022). https://doi.org/10.1002/smll.202107183
167. Yang, Z.G., Zhang, J.L., Kintner-Meyer, M.C.W., et al.: Electrochemical energy storage for green grid. Chem. Rev. **111**, 3577–3613 (2011). https://doi.org/10.1021/cr100290v
168. Simari, C., Tuccillo, M., Brutti, S., et al.: Sodiated Nafion membranes for sodium metal aprotic batteries. Electrochim. Acta **410**, 139936 (2022). https://doi.org/10.1016/j.electacta.2022.139936
169. Abouimrane, A., Whitfield, P.S., Niketic, S., et al.: Investigation of Li salt doped succinonitrile as potential solid electrolytes for lithium batteries. J. Power Sources **174**, 883–888 (2007). https://doi.org/10.1016/j.jpowsour.2007.06.103
170. Kim, S.H., Choi, K.H., Cho, S.J., et al.: A shape-deformable and thermally stable solid-state electrolyte based on a plastic crystal composite polymer electrolyte for flexible/safer lithium-ion batteries. J. Mater. Chem. A **2**, 10854–10861 (2014). https://doi.org/10.1039/c4ta00494a
171. Abu-Lebdeh, Y., Abouimrane, A., Alarco, P.J., et al.: Ambient temperature proton conducting plastic crystal electrolytes. Electrochem. Commun. **6**, 432–434 (2004). https://doi.org/10.1016/j.elecom.2004.02.015
172. Long, S.: Fast ion conduction in molecular plastic crystals. Solid State Ion. **161**, 105–112 (2003). https://doi.org/10.1016/s0167-2738(03)00208-x
173. Zhu, X.M., Zhao, R.R., Deng, W.W., et al.: An all-solid-state and all-organic sodium-ion battery based on redox-active polymers and plastic crystal electrolyte. Electrochim. Acta **178**, 55–59 (2015). https://doi.org/10.1016/j.electacta.2015.07.163
174. Yu, X.W., Xue, L.G., Goodenough, J.B., et al.: Ambient-temperature all-solid-state sodium batteries with a laminated composite electrolyte. Adv. Funct. Mater. **31**, 2002144 (2021). https://doi.org/10.1002/adfm.202002144
175. Makhlooghiazad, F., Gunzelmann, D., Hilder, M., et al.: Mixed phase solid-state plastic crystal electrolytes based on a phosphonium cation for sodium devices. Adv. Energy Mater. **7**, 1601272 (2017). https://doi.org/10.1002/aenm.201601272
176. Biernacka, K., Makhlooghiazad, F., Popov, I., et al.: Investigation of unusual conductivity behavior and ion dynamics in hexamethylguanidinium bis(fluorosulfonyl)imide-based electrolytes for sodium batteries. J. Phys. Chem. C **125**, 12518–12530 (2021). https://doi.org/10.1021/acs.jpcc.1c01777
177. Makhlooghiazad, F., Sharma, M., Zhang, Z.Z., et al.: Stable high-temperature cycling of Na metal batteries on $Na_3V_2(PO_4)_3$ and $Na_2FeP_2O_7$ cathodes in NaFSI-rich organic ionic plastic crystal electrolytes. J. Phys. Chem. Lett. **11**, 2092–2100 (2020). https://doi.org/10.1021/acs.jpclett.0c00149

Shuzhi Zhao is currently a Ph.D. student in chemical engineering at Shanghai Jiao Tong University, China. He received a Master's degree in Science at the University of Melbourne at 2019. He is pursuing his Ph.D. degree under the supervision of Prof. Zi-Feng Ma and Xiao-Zhen Liao, and his research is focusing on solid-state polymer electrolytes for sodium-ion battery application.

Haiying Che is currently the president of Zhejiang Natrium Energy Co., Ltd. She received her Ph.D. degree under the supervision of Prof. Zi-Feng Ma at Shanghai Jiao Tong University focusing on the optimization of electrolytes of sodium-ion batteries.

Suli Chen is currently an associate professor of chemical engineering at Jiangnan University. She received her Ph.D. degree under the supervision of Prof. Zi-Feng Ma at Shanghai Jiao Tong University. Her recent research focuses on solid polymer electrolytes for sodium-ion battery application.

Haixiang Tao is currently the director of the research department of Zhejiang Natrium Energy Co., Ltd. He received his Ph.D. degree in chemical engineering from East China University of Science and Technology in 2013. His current research focuses on cathode materials for sodium-ion batteries.

Jianping Liao is currently the Technical Director of Zhejiang Natrium Energy Co., Ltd. He received his Ph.D.degree of chemical engineering in 1994 from the University of Stuttgart. Currently he is focusing on process scale-up and commercialization of sodium-ion batteries.

Xiao-Zhen Liao is currently a professor of chemical engineering at Shanghai Jiao Tong University, China. Her current research interests focus on micro-/nanostructured functional materials for sodium-ion batteries and lithium-ion batteries. Dr. Liao has presided over three projects under the auspices of the National Natural Science Foundation of China (NSFC), participated in two Program 973 projects, presided over and participated in a number of projects under the Shanghai Science and Technology Commission and Enterprise Cooperation Projects.

Zi-Feng Ma is currently Chair Professor of Shanghai Jiao Tong University and the founding Director of the Shanghai Electrochemical Energy Devices Research Centre. He was appointed to be the Chief Scientist of the National Basic Research Program of China for the electrochemical energy system in 2007 and 2013, respectively. As the project leader, he presided over the completion of key national 863 Program projects and twice served as the chief scientist of national 973 Program projects. He is a 2016 recipient of the China Industry-University-Research Collaborative Award. Prof. Ma holds or has filed over 80 patents and patent applications and has over 320 publications.